



This is to certify that the
thesis entitled

COMPARISON OF UWB SHORT-PULSE AND STEPPED-
FREQUENCY SYSTEMS FOR IMAGING THROUGH
BARRIERS

presented by

Benjamin Reid Crowgey

has been accepted towards fulfillment
of the requirements for the

M.S. degree in Electrical Engineering


Major Professor's Signature

13 - November - 2009

Date

PLACE IN RETURN BOX to remove this checkout from your record.
TO AVOID FINES return on or before date due.
MAY BE RECALLED with earlier due date if requested.

DATE DUE	DATE DUE	DATE DUE

COMPARISON OF UWB SHORT-PULSE AND STEPPED-FREQUENCY
SYSTEMS FOR IMAGING THROUGH BARRIERS

By

Benjamin Reid Crowgey

A THESIS

Submitted to
Michigan State University
in partial fulfillment of the requirements
for the degree of

MASTER SCIENCE

Electrical Engineering

2009

ABSTRACT

COMPARISON OF UWB SHORT-PULSE AND STEPPED-FREQUENCY SYSTEMS FOR IMAGING THROUGH BARRIERS

By

Benjamin Reid Crowgey

Ultra-wideband radar is useful for generating images of objects behind barriers due to its penetrability and its capability to resolve small targets. Imaging systems may be constructed to work directly in the time domain by generating baseband or monocycle pulses and digitizing the received signal using a high-speed analog-to-digital converter, or in the frequency domain by using a stepped-frequency narrow-band transmitter and receiver. Each type of system has advantages and drawbacks. The time-domain method provides ultra-wideband data with a single measurement, but it requires high-speed A/D converters to provide sufficient resolution, and adequate signal-to-noise ratios may necessitate repetitive measurements. Stepped-frequency systems have high dynamic range, but often require long dwell times and are subject to aliasing effects.

A canonical problem is established that allows the affects of various radar parameters on radar performance to be studied. For simplicity, a two-dimensional problem is considered, consisting of a perfectly conducting strip located behind a lossy dielectric slab of infinite extent illuminated by line sources. To assess the impact of the parameters on system performance, images of the target are created using the reflected field computed at several positions in front of the barrier and adjacent to the sources. Specific parameters that are considered include sample rate, A/D bit length, pulse width, and SNR for a time-domain system, and sample rate, A/D bit length, bandwidth, and SNR for a frequency domain system. A time-domain laboratory system was constructed to investigate whether the image techniques used with simulated data in the parameter study can be replicated in practice.

For Grandad

ACKNOWLEDGMENTS

I would like to acknowledge my parents John and Martha Crowgey, who encouraged me to pursue my interests in engineering and helped me along the way. A special thanks to my mother, who calmed me down when I needed it and was always there to talk. I acknowledge my grandparents, Willard and Jenett Crowgey and Donald and Jean Moore for their thoughts and support. Thank you to my sisters Sarah and Julie Crowgey for their insight and encouragement.

I would like to thank Dr. Leo Kempel for taking a chance on me and showing me the fun of Electromagnetics. If it wasn't for the simple cell phone seminar six years ago, who knows if I would even be here today. Thank you to Dr. Shanker Balasubramaniam for your entertaining electromagnetic classes and support. Most importantly, I would like to acknowledge my advisor, Dr. Edward Rothwell. Thank you for all your help and support on this research. I know I wouldn't have made it through without your guidance and light humor. Even if you had some interesting comments on my writing techniques, I know you always had my best interests at heart.

I acknowledge Dr. Eric Mokole, head of the Surveillance Technology Branch, Radar Division, at the Naval Research Laboratory in Washington, D.C. for initiating the working relationship and providing the funding for this research effort.

A special thanks to Olukorede A Akinlabi-Oladimeji for spending extra time doing some very tedious measurements with me. Also, thank you to Collin Meierbachtol for your random help throughout my masters career. You have both become great friends.

I would like to acknowledge the Michigan State University Electromagnetics Research Group for providing assistance on all of the projects I have worked on at MSU. It has been an honor to work with so many talented people, many of whom will be

lifetime friends.

Most of all I would like to thank my girlfriend, Stacey Richardson, for all her help and support during these final months. You are a great friend and a terrific person. I am lucky to have found someone like you. You spent hours proofreading this thesis, and I know Dr. Rothwell and I both thank you.

Table of Contents

List of Tables	viii
List of Figures	xv
1 Introduction	1
1.1 Background	2
1.2 Research Overview	2
2 Canonical Problem Theory	4
2.1 Electric Fields impressed by a current source in the Presents of a Di- electric Slab	5
2.1.1 Current Source	6
2.1.2 Partial Differential Wave Equation Derivation	6
2.1.3 Ordinary Differential Equation Derivation	11
2.1.4 Relationship Between Vector Potentials and Fields	14
2.1.5 Solutions to ODE	15
2.1.6 Electric Field Derivation	25
2.2 Scattered Field from Conducting Strip	26
2.2.1 Integral Equation Derivation	27
2.2.2 A_{mn} Evaluation	31
2.2.2.1 U_{mn} Evaluation	33
2.2.2.2 V_{mn} Evaluation	37
2.2.3 Matrix Equation	40
3 Numerical Results	41
3.1 Computation of Incident and Scattered Fields	42
3.2 Imaging Analysis	44
3.2.1 Frequency to Time Domain Transformation	44
3.2.2 2D Image Construction	48
3.2.3 Image Quantification	51
4 Parameter Analysis	54
4.1 Time Domain Analysis	54
4.1.1 Pulse Width	54
4.1.2 Sampling Rate	65
4.1.3 Signal-to-Noise Ratio	76

4.1.4	Digitization	87
4.2	Frequency Domain Analysis	98
4.2.1	Bandwidth	99
4.2.2	Sampling Rate	109
4.2.3	Signal-to-Noise Ratio	116
4.2.4	Digitization	127
4.3	Two Conducting Strips	139
4.3.1	Pulse Width	141
4.3.2	Bandwidth	151
5	Experiment	163
5.1	Experiment Set up	164
5.2	Experiment Calibration	169
5.3	Experiment Results	173
6	Conclusion	175
6.1	Topics for further study	176
Appendix A: Fortran Code for Electric Scattered Field		178
Appendix B: Fortran Code for Electric Incident Field		201
Appendix C: Matlab Imaging Code		210
Bibliography		225

List of Tables

- 6.1 Minimum system requirements for a time domain radar system. . . . 176
- 6.2 Minimum system requirements for a frequency domain radar system. 176

List of Figures

2.1	Canonical problem geometry.	4
2.2	Partitioning of canonical problem geometry.	5
2.3	Conducting strip parameters.	27
3.1	Position of source/observation pairs.	41
3.2	Magnitude of the frequency domain scattered field at a position centered above the strip.	45
3.3	Magnitude of the frequency domain scattered field weighted with a GMC.	46
3.4	Time-domain scattered field at a point centered above the conductive strip.	47
3.5	Time-domain incident field at a point centered above the conducting strip.	48
3.6	Image of lossy dielectric slab and conducting strip..	50
3.7	Proportionally correct mage of lossy dielectric slab and conducting strip.	50
3.8	Area in which sharpness of conducting strip is determined.	52
3.9	Circle of radius equal to the image radius centered around the conducting strip with scale $\times 10^{11}$	53
4.1	Effect of pulse width on image radius.	55
4.2	Conducting strip image constructed using a pulse width of $\tau = 0.06$ ns.	56
4.3	Conducting strip image constructed using a pulse width of $\tau = 0.10$ ns.	57
4.4	Conducting strip image constructed using a pulse width of $\tau = 0.16$ ns.	58
4.5	Conducting strip image constructed using a pulse width of $\tau = 0.26$ ns.	59

4.6	Conducting strip image constructed using a pulse width of $\tau = 0.50$ ns.	60
4.7	Conducting strip image constructed using a pulse width of $\tau = 1.00$ ns.	61
4.8	Conducting strip image constructed using a pulse width of $\tau = 1.50$ ns.	62
4.9	Conducting strip image constructed using a pulse width of $\tau = 2.00$ ns.	63
4.10	Conducting strip image constructed using a pulse width of $\tau = 2.50$ ns.	64
4.11	Conducting strip image constructed using a pulse width of $\tau = 3.00$ ns.	65
4.12	Effect of sampling period on image radius.	66
4.13	Conducting strip image constructed using a sampling period of $\Delta t = 0.05$ ns.	67
4.14	Conducting strip image constructed using a sampling period of $\Delta t = 0.10$ ns.	68
4.15	Conducting strip image constructed using a sampling period of $\Delta t = 0.20$ ns.	69
4.16	Conducting strip image constructed using a sampling period of $\Delta t = 0.30$ ns.	70
4.17	Conducting strip image constructed using a sampling period of $\Delta t = 0.40$ ns.	71
4.18	Conducting strip image constructed using a sampling period of $\Delta t = 0.50$ ns.	72
4.19	Conducting strip image constructed using a sampling period of $\Delta t = 0.60$ ns.	73
4.20	Conducting strip image constructed using a sampling period of $\Delta t = 0.70$ ns.	74
4.21	Conducting strip image constructed using a sampling period of $\Delta t = 0.80$ ns.	75
4.22	Conducting strip image constructed using a sampling period of $\Delta t = 1.60$ ns.	76
4.23	Effect of noise on image radius.	77
4.24	Conducting strip image constructed using a SNR = 20 dB.	78

4.25	Conducting strip image constructed using a SNR = 18 dB.	79
4.26	Conducting strip image constructed using a SNR = 16 dB.	80
4.27	Conducting strip image constructed using a SNR = 14 dB.	81
4.28	Conducting strip image constructed using a SNR = 12 dB.	82
4.29	Conducting strip image constructed using a SNR = 10 dB.	83
4.30	Conducting strip image constructed using a SNR = 8 dB.	84
4.31	Conducting strip image constructed using a SNR = 6 dB.	85
4.32	Conducting strip image constructed using a SNR = 4 dB.	86
4.33	Conducting strip image constructed using a SNR = 2 dB.	87
4.34	Effect of digitization on image radius.	88
4.35	Conducting strip image constructed using the number of bits = 12. .	89
4.36	Conducting strip image constructed using the number of bits = 11. .	90
4.37	Conducting strip image constructed using the number of bits = 10. .	91
4.38	Conducting strip image constructed using the number of bits = 9. . .	92
4.39	Conducting strip image constructed using the number of bits = 8. . .	93
4.40	Conducting strip image constructed using the number of bits = 7. . .	94
4.41	Conducting strip image constructed using the number of bits = 6. . .	95
4.42	Conducting strip image constructed using the number of bits = 5. . .	96
4.43	Conducting strip image constructed using the number of bits = 4. . .	97
4.44	Conducting strip image constructed using the number of bits = 3. . .	98
4.45	Effect of digitization on image radius.	99
4.46	Conducting strip image constructed using a bandwidth = 110.38%. .	100
4.47	Conducting strip image constructed using a bandwidth = 36.75%. . .	101
4.48	Conducting strip image constructed using a bandwidth = 22.13%. . .	102
4.49	Conducting strip image constructed using a bandwidth = 15.76%. . .	103

4.50	Conducting strip image constructed using a bandwidth = 12.26%. . .	104
4.51	Conducting strip image constructed using a bandwidth = 10.03%. . .	105
4.52	Conducting strip image constructed using a bandwidth = 8.49%. . . .	106
4.53	Conducting strip image constructed using a bandwidth = 7.35%. . . .	107
4.54	Conducting strip image constructed using a bandwidth = 6.49%. . . .	108
4.55	Conducting strip image constructed using a bandwidth = 5.81%. . . .	109
4.56	Effect of sampling rate on image radius.	110
4.57	Conducting strip image constructed using a sampling rate of $\Delta f = 20$ MHz.	111
4.58	Conducting strip image constructed using a sampling rate of $\Delta f = 40$ MHz.	112
4.59	Conducting strip image constructed using a sampling rate of $\Delta f = 60$ MHz.	113
4.60	Conducting strip image constructed using a sampling rate of $\Delta f = 80$ MHz.	114
4.61	Conducting strip image constructed using a sampling rate of $\Delta f = 100$ MHz.	115
4.62	Conducting strip image constructed using a sampling rate of $\Delta f = 120$ MHz.	116
4.63	Effect of the SNR on image radius.	117
4.64	Conducting strip image constructed using a SNR = 44 dB.	118
4.65	Conducting strip image constructed using a SNR = 42 dB.	119
4.66	Conducting strip image constructed using a SNR = 40 dB.	120
4.67	Conducting strip image constructed using a SNR = 38 dB.	121
4.68	Conducting strip image constructed using a SNR = 36 dB.	122
4.69	Conducting strip image constructed using a SNR = 34 dB.	123
4.70	Conducting strip image constructed using a SNR = 32 dB.	124

4.71	Conducting strip image constructed using a SNR = 30 dB.	125
4.72	Conducting strip image constructed using a SNR = 28 dB.	126
4.73	Conducting strip image constructed using a SNR = 26 dB.	127
4.74	Effect of digitization on image radius.	128
4.75	Conducting strip image constructed using the number of bits = 12. . .	129
4.76	Conducting strip image constructed using the number of bits = 11. . .	130
4.77	Conducting strip image constructed using the number of bits = 10. . .	131
4.78	Conducting strip image constructed using the number of bits = 9. . .	132
4.79	Conducting strip image constructed using the number of bits = 8. . .	133
4.80	Conducting strip image constructed using the number of bits = 7. . .	134
4.81	Conducting strip image constructed using the number of bits = 6. . .	135
4.82	Conducting strip image constructed using the number of bits = 5. . .	136
4.83	Conducting strip image constructed using the number of bits = 4. . .	137
4.84	Conducting strip image constructed using the number of bits = 3. . .	138
4.85	Conducting strip image constructed using the number of Bits = 2. . .	139
4.86	Parameters of two conducting strip study	140
4.87	Effect of pulse width on image radius of two conducting strips.	141
4.88	Two conducting strip image constructed using a pulse width of $\tau =$ 0.05 ns	142
4.89	Two conducting strip image constructed using a pulse width of $\tau =$ 0.10 ns	143
4.90	Two conducting strip image constructed using a pulse width of $\tau =$ 0.15 ns	144
4.91	Two conducting strip image constructed using a pulse width of $\tau =$ 0.25 ns	145
4.92	Two conducting strip image constructed using a pulse width of $\tau =$ 0.50 ns	146

4.93	Two conducting strip image constructed using a pulse width of $\tau = 1.00$ ns	147
4.94	Two conducting strip image constructed using a pulse width of $\tau = 1.50$ ns	148
4.95	Two conducting strip image constructed using a pulse width of $\tau = 2.00$ ns	149
4.96	Two conducting strip image constructed using a pulse width of $\tau = 2.5$ ns	150
4.97	Two conducting strip image constructed using a pulse width of $\tau = 3.00$ ns	151
4.98	Effect of bandwidth on image radius of two conducting strips.	152
4.99	Two conducting strip image constructed using a bandwidth of 110.38%	153
4.100	Two conducting strip image constructed using a bandwidth of 36.75%	154
4.101	Two conducting strip image constructed using a bandwidth of 22.13%	155
4.102	Two conducting strip image constructed using a bandwidth of 15.76%	156
4.103	Two conducting strip image constructed using a bandwidth of 12.26%	157
4.104	Two conducting strip image constructed using a bandwidth of 10.03%	158
4.105	Two conducting strip image constructed using a bandwidth of 8.49%	159
4.106	Two conducting strip image constructed using a bandwidth of 7.38%	160
4.107	Two conducting strip image constructed using a bandwidth of 6.49%	161
4.108	Two conducting strip image constructed using a bandwidth of 5.81%	162
5.1	Geometry of arch-range scattering system at MSU.	164
5.2	Time domain scattering measurement configuration.	165
5.3	Pulse generated by the PSPL 5208-DC pulse generating network.	166
5.4	Spectrum of the generated pulse.	167
5.5	Location of transmitting and receiving antennas.	168

5.6	Experimental setup.	169
5.7	Block diagram model of measurement system.	170
5.8	Raw measured waveform for a conducting plate.	172
5.9	System transfer function.	173
5.10	Image of barrier and strip created using time-domain response at responses measured at 21 different transmitter/receiver positions.	174

Images in this thesis are presented in color

Chapter 1

Introduction

A comparison between ultra-wide band (UWB) short-pulse and stepped-frequency systems for imaging through a barrier is undertaken in this thesis. The penetration ability of UWB radar, and its capabilities for resolving small targets, makes this technology quite appealing for producing images of objects behind barriers. The concept of a UWB radar can be used to implement both time and frequency domain systems. A time-domain-system may be implemented by generating baseband or monocycle pulses and then digitizing the received signal with the use of a high-speed analog-to-digital (A/D) converter. In a frequency domain system, a stepped-frequency narrow-band transmitter and receiver may be used. With each type of system there are advantages and disadvantages. For the time-domain method the UWB signal provides data with a single measurement, but requires high-speed A/D converters to ensure sufficient resolution of the image. In addition, inadequate signal-to-noise ratio (SNR) may produce a need for repetitive measurements and averaging, increasing the acquisition time. In the frequency domain, long dwell time and aliasing effects are concerns, while high dynamic range is a significant advantage.

1.1 Background

A significant amount of research has been done to analyze scattering from objects located behind barriers [1]. In addition, various processing methods have been developed to obtain images of the scatterer [2]. This thesis focuses on the comparison between short-pulse and stepped-frequency systems for imaging through a barrier [3] [4] [5]. The UWB simulations or measurements are performed in a synthetic aperture radar (SAR) configuration [6] [7] [8] and then images are created using a simple scattering-center technique.

1.2 Research Overview

A two-dimensional canonical problem is established to study the affects of various parameters on the quality of the image produced by time-domain and stepped frequency UWB radar systems. This canonical problem consists of a line source located above a lossy dielectric slab representing a barrier. The interrogating cylindrical waves produced by the line source impinge on the barrier and interact with targets placed behind the barrier. The scattered field is computed in the frequency domain at specific discrete frequencies within a chosen band. This simulates the data that would be acquired by a UWB stepped-frequency system. An equivalent time-domain system is studied by using an inverse Fourier transform to convert the data into the time domain.

Images are constructed using a simple scattering-center technique to provide a means of assessing radar performance. Factors such as pulse width, sampling rate, number of bits, SNR, and time jitter are examined in the time domain to determine their affect on the quality of the image as measured in terms of the dispersion of localized scattering centers. Bandwidth, sampling rate, SNR, and number of bits are examined in the frequency domain.

In addition, a laboratory time-domain radar system was constructed using instrumentation to allow a validation of the simulation results. The laboratory system is not a dedicated radar, but rather uses standard instrumentation. The data was acquired using the Michigan State University (MSU) reflectivity arch range consisting of two horn antennas. A barrier was constructed to replicate the simulated canonical problem.

Chapter 2

Canonical Problem Theory

To investigate the different properties of ultra-wide band short pulse and step-frequency imaging radar systems, a simple canonical problem is considered. Using simulations instead of measured data allows the affects of important system parameters to be studied over a much broader range of values than is allowed through laboratory experimentation. The canonical problem, shown in Figure 2.1, consists of an infinite electric line source aligned along the x -direction located at a height $z = h$ above a lossy dielectric slab, which represents a barrier. This dielectric slab has a thickness t ,

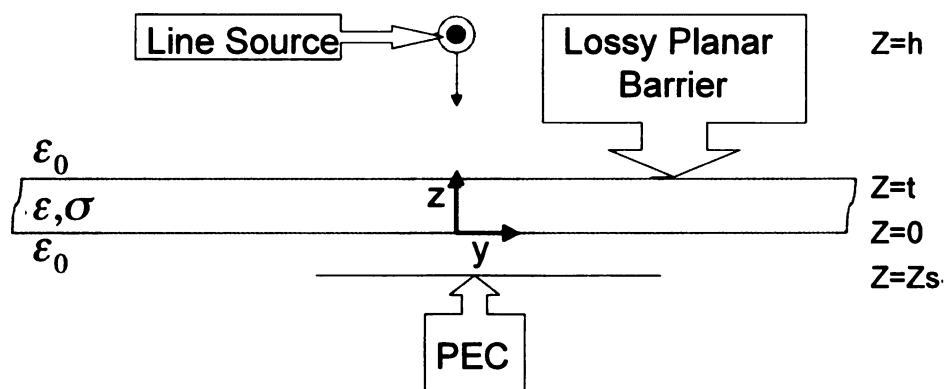


Figure 2.1: Canonical problem geometry.

and is infinite in the x - and y -directions. The slab has relative permittivity ϵ_r , con-

ductivity σ , and free-space permeability μ_0 . A target consisting of an infinitesimally thin perfectly-conducting (PEC) strip is located a distance $z = z_s$ behind the slab.

To solve for the electric fields for this canonical problem, the field incident on the conducting strip in the presence of the slab must first be determined. The boundary condition of zero total tangential electric field on the surface of the strip may then be employed to derive an integral equation for the surface current induced on the strip. This current is then used to compute the scattered field, and then the total field, which is what is measured in practice, is found by summing the incident and scattered fields.

2.1 Electric Fields impressed by a current source in the Presence of a Dielectric Slab

The fields incident on the conducting strip, in the presence of a dielectric slab, are derived by first considering Figure 2.2, where the problem is separated into 4 different regions. Regions 2 and 3 are chosen to be two separate regions because this results

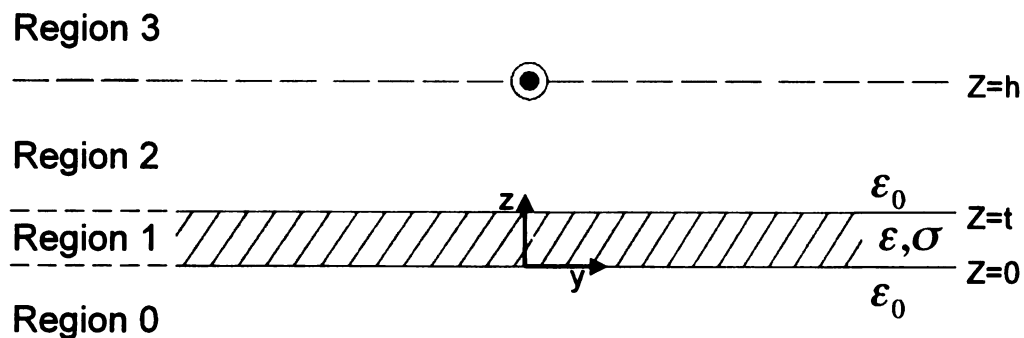


Figure 2.2: Partitioning of canonical problem geometry.

in source free regions with the line source located on an interface.

2.1.1 Current Source

The infinite line source is positioned at $z = h$ and $y = 0$; therefore the volume current density can be written as

$$\vec{J}(y, z) = \hat{x}I\delta(z - h)\delta(y). \quad (2.1)$$

The surface current density can be determined through the use of boundary conditions in this 2D canonical problem [9]. This current is given by

$$\vec{K}(y) = \lim_{\Delta \rightarrow 0} \int_{h-\Delta}^{h+\Delta} \vec{J}(y, z) dz. \quad (2.2)$$

Substituting the volume current density gives

$$\vec{K}(y) = \lim_{\Delta \rightarrow 0} \int_{h-\Delta}^{h+\Delta} \hat{x}I\delta(z - h)\delta(y) dz. \quad (2.3)$$

The surface current density for the infinite line source is thus

$$\vec{K}(y) = \hat{x}I\delta(y). \quad (2.4)$$

2.1.2 Partial Differential Wave Equation Derivation

The fields are represented in terms of potentials to facilitate their computation. The magnetic flux density vector, \vec{B} , is expressed as the curl of the magnetic vector potential, \vec{A} :

$$\vec{B} = \nabla \times \vec{A}. \quad (2.5)$$

Substituting (2.5) into the differential form of Faraday's law,

$$\nabla \times \vec{E} = -\frac{\partial \vec{B}}{\partial t}, \quad (2.6)$$

results in

$$\nabla \times \left(\vec{E} + \frac{\partial \vec{A}}{\partial t} \right) = 0. \quad (2.7)$$

The sum of the two vector quantities can thus be expressed as the gradient of the electric potential, ϕ :

$$\vec{E} + \frac{\partial \vec{A}}{\partial t} = -\nabla \phi. \quad (2.8)$$

Thus,

$$\vec{E} = -\nabla \phi - \frac{\partial \vec{A}}{\partial t}. \quad (2.9)$$

The differential form of Gauss's law is

$$\nabla \cdot D = \rho \quad (2.10)$$

or, from the constitutive relations assuming a homogeneous medium,

$$\nabla \cdot \vec{E} = \frac{\rho}{\epsilon}. \quad (2.11)$$

Substituting (2.9) into (2.11) results in

$$\nabla \cdot \left(-\nabla \phi - \frac{\partial \vec{A}}{\partial t} \right) = \frac{\rho}{\epsilon} \quad (2.12)$$

or

$$-\nabla^2 \phi - \frac{\partial}{\partial t} (\nabla \cdot \vec{A}) = \frac{\rho}{\epsilon}, \quad (2.13)$$

which is a differential equation for ϕ and \vec{A} .

Next, examine the differential form of Ampere's law,

$$\nabla \times \vec{H} = \vec{J} + \frac{\partial \vec{D}}{\partial t}. \quad (2.14)$$

The constitutive relation,

$$\vec{B} = \mu \vec{H}, \quad (2.15)$$

along with (2.5) is substituted into (2.14) to give

$$\nabla \times \nabla \times \vec{A} = \mu \vec{J} + \mu \frac{\partial \vec{D}}{\partial t}. \quad (2.16)$$

In a conducting medium, as seen in this canonical problem, the source field must be separated into two parts. The first is a causative impressed term \vec{J}_i which is independent of the produced fields. Also necessary is a secondary term \vec{J}_s which exists only as an effect of the sourced fields. For an isotropic conducting medium the effect of the sourced field is given by Ohm's law,

$$\vec{J}_s = \sigma \vec{E}. \quad (2.17)$$

Writing the total current as

$$\vec{J} = \vec{J}_i + \vec{J}_s, \quad (2.18)$$

(2.16) becomes,

$$\nabla \times \nabla \times \vec{A} = \mu \sigma \vec{E} + \mu \frac{\partial \vec{D}}{\partial t} + \vec{J}_i. \quad (2.19)$$

Then, using the constitutive relation

$$\vec{D} = \epsilon \vec{E}, \quad (2.20)$$

(2.19) is rewritten as

$$\nabla \times \nabla \times \vec{A} = \left(\mu\sigma + \mu\epsilon \frac{\partial}{\partial t} \right) \vec{E} + \vec{J}_i. \quad (2.21)$$

Substituting (2.9) into (2.21) yields

$$\nabla \times \nabla \times \vec{A} = \left(\mu\sigma + \mu\epsilon \frac{\partial}{\partial t} \right) \left(-\nabla\phi - \frac{\partial \vec{A}}{\partial t} \right) + \vec{J}_i, \quad (2.22)$$

or

$$\nabla \times \nabla \times \vec{A} = -\mu\sigma \nabla\phi - \mu\epsilon \frac{\partial}{\partial t} \nabla\phi - \mu\sigma \frac{\partial \vec{A}}{\partial t} - \mu\epsilon \frac{\partial^2 \vec{A}}{\partial t^2} + \vec{J}_i. \quad (2.23)$$

Recalling the vector identity

$$\nabla \times \nabla \times \vec{A} = \nabla \left(\nabla \cdot \vec{A} \right) - \nabla^2 \vec{A}, \quad (2.24)$$

(2.23) can be rewritten as

$$\nabla^2 \vec{A} = \nabla \left(\nabla \cdot \vec{A} + \mu\sigma\phi + \mu\epsilon \frac{\partial\phi}{\partial t} \right) + \mu\sigma \frac{\partial \vec{A}}{\partial t} + \mu\epsilon \frac{\partial^2 \vec{A}}{\partial t^2} - \vec{J}_i. \quad (2.25)$$

To simplify (2.25), the Lorentz condition for potentials

$$\nabla \cdot \vec{A} = -\frac{1}{\nu^2} \frac{\partial\phi}{\partial t} - \mu\sigma\phi \quad (2.26)$$

is used, where ν is given by

$$\nu = \frac{1}{\sqrt{\mu\epsilon}}. \quad (2.27)$$

This gives

$$\nabla \cdot \vec{A} = -\mu\epsilon \frac{\partial\phi}{\partial t} - \mu\sigma\phi. \quad (2.28)$$

Inserting (2.28) into (2.25), some terms on the right side of (2.25) vanish, thus giving

$$\nabla^2 \vec{A} = \mu\sigma \frac{\partial \vec{A}}{\partial t} + \mu\epsilon \frac{\partial^2 \vec{A}}{\partial t^2} - \vec{J}_i. \quad (2.29)$$

This is a time domain wave equation for the vector potential \vec{A} . By substituting (2.28) into (2.13) results in

$$-\nabla^2 \vec{\phi} - \mu\epsilon \frac{\partial^2 \vec{\phi}}{\partial t^2} - \mu\sigma \frac{\partial \vec{\phi}}{\partial t} = \frac{\rho}{\epsilon}, \quad (2.30)$$

which is a wave equation for the scalar potential.

The analysis performed in the remainder of this thesis will be undertaken in the frequency domain. Thus, a frequency domain wave equation is required. Transforming (2.29) into the frequency domain through the Fourier transform identity

$$\frac{\partial}{\partial t} \Leftrightarrow j\omega, \quad (2.31)$$

gives

$$\nabla^2 \vec{A} = \mu\sigma (j\omega) \vec{A} + \mu\epsilon (j^2\omega^2) \vec{A} - \vec{J}_i \quad (2.32)$$

or

$$\nabla^2 \vec{A} = (j\mu\sigma\omega - \mu\epsilon\omega^2) \vec{A} - \vec{J}_i. \quad (2.33)$$

All quantities are now frequency domain variables. Define the wavenumber as

$$k = \omega^2 \mu \epsilon^c, \quad (2.34)$$

where the complex permittivity is

$$\epsilon^c = \epsilon - j\frac{\sigma}{\omega}. \quad (2.35)$$

Then (2.33) reduces to

$$\nabla^2 \vec{A} + k^2 \vec{A} = -\vec{J}_i. \quad (2.36)$$

This is a partial differential equation for the vector potential, which is solved using in subsequent sections using spatial Fourier transform techniques.

As shown in Figure 2.2, the geometry is partitioned into 4 regions. Region 1, inside the dielectric slab, has the wavenumber, k , defined through

$$k^2 = \omega^2 \mu_0 \epsilon^c. \quad (2.37)$$

Since this is a source free region, (2.36) becomes

$$\nabla^2 \vec{A} + k^2 \vec{A} = 0. \quad (2.38)$$

In regions 0, 2, and 3 the wavenumber is given through

$$k_0^2 = \omega^2 \mu_0 \epsilon_0, \quad (2.39)$$

because these regions are free space. Also, these regions are source free. Therefore the partial differential wave equation (2.36) becomes

$$\nabla^2 \vec{A} + k_0^2 \vec{A} = 0. \quad (2.40)$$

2.1.3 Ordinary Differential Equation Derivation

An ordinary differential equation (ODE) is a relation that contains functions of only one independent variable. While a partial differential equation (PDE) is a relation which contains partial derivatives of several variables. Thus, ODEs are computationally easier to solve and are homogeneous, for this canonical problem, since the line

source lies on the interface between region 3 and region 2. To reduce the PDEs to ODEs, it is noticed the source and fields are invariant in the x -direction. Therefore a Fourier transform of the y variable is performed to reduce the PDE to an ODE. The definition of the Fourier transform pair is

$$\vec{A}(k_y, z) = \int_{-\infty}^{\infty} \vec{A}(y, z) e^{-jk_y y} dy \quad (2.41)$$

$$\vec{A}(y, z) = \frac{1}{2\pi} \int_{-\infty}^{\infty} \vec{A}(k_y, z) e^{jk_y y} dk_y. \quad (2.42)$$

Inserting (2.42) into the partial differential wave equation for region 1, (2.38), results in

$$\left(\nabla^2 + k^2\right) \frac{1}{2\pi} \int_{-\infty}^{\infty} \vec{A}(k_y, z) e^{jk_y y} dk_y = 0. \quad (2.43)$$

Since there is only a x component of the current seen in Figure 2.2, the vector magnetic potential \vec{A} only has a x component:

$$\vec{A}(k_y, z) = \hat{x} \tilde{A}_x(k_y, z). \quad (2.44)$$

Therefore (2.43) is rewritten as

$$\left(\nabla^2 + k^2\right) \frac{1}{2\pi} \int_{-\infty}^{\infty} \tilde{A}_x(k_y, z) e^{jk_y y} dk_y = 0. \quad (2.45)$$

or

$$\left(\frac{\partial^2}{\partial x^2} + \frac{\partial^2}{\partial y^2} + \frac{\partial^2}{\partial z^2} + k^2\right) \frac{1}{2\pi} \int_{-\infty}^{\infty} \tilde{A}_x(k_y, z) e^{jk_y y} dk_y = 0. \quad (2.46)$$

Since the integral is only dependent on y and z , the partial derivative with respect to x is zero. Performing the remaining derivatives results in

$$k^2 \frac{1}{2\pi} \int_{-\infty}^{\infty} \tilde{A}_x(k_y, z) e^{jk_y y} dk_y - \frac{1}{2\pi} \int_{-\infty}^{\infty} \tilde{A}_x(k_y, z) k_y^2 e^{jk_y y} dk_y + \frac{1}{2\pi} \int_{-\infty}^{\infty} \frac{\tilde{A}_x(k_y, z)}{\partial z^2} e^{jk_y y} dk_y = 0. \quad (2.47)$$

Factoring out the common variables from this expression, (2.47) reduces to

$$\frac{1}{2\pi} \int_{-\infty}^{\infty} \left(k^2 + \frac{\partial^2}{\partial z^2} - k_y^2 \right) \tilde{A}_x(k_y, z) e^{jk_y y} dk_y = 0. \quad (2.48)$$

The Fourier integral theorem then implies

$$\left(\frac{\partial^2}{\partial z^2} + p^2 \right) \tilde{A}_x(k_y, z) = 0, \quad (2.49)$$

with

$$p = \pm \sqrt{k_0^2 - k_y^2} \quad (2.50)$$

in regions 0, 2, and 3. For region 1, (2.48) requires

$$\left(\frac{\partial^2}{\partial z^2} + q^2 \right) \tilde{A}_x(k_y, z) = 0, \quad (2.51)$$

where

$$q = \pm \sqrt{k^2 - k_y^2}. \quad (2.52)$$

Note that the proper choice of signs on the radicals depends on the physics of the problem and is considered later.

2.1.4 Relationship Between Vector Potentials and Fields

The electric and magnetic fields can be found from the vector potentials once the ODEs (2.49) and (2.51) are solved. To find this relationship first recall the divergence of \vec{A} :

$$\nabla \cdot \vec{A} = \frac{\partial A_x}{\partial x} + \frac{\partial A_y}{\partial y} + \frac{\partial A_z}{\partial z}. \quad (2.53)$$

Since there is only an x component of \vec{A} , the divergence reduces to

$$\nabla \cdot \vec{A} = \frac{\partial A_x(y, z)}{\partial x}. \quad (2.54)$$

But A_x is only dependent on y and z , so

$$\nabla \cdot \vec{A} = 0. \quad (2.55)$$

Writing the Lorentz condition in the frequency domain and using (2.55) thus gives

$$\phi = 0. \quad (2.56)$$

The electric field is then, from (2.9),

$$\vec{E} = -j\omega\vec{A}. \quad (2.57)$$

Combining (2.5) and the constitutive relation (2.15), gives the magnetic field as

$$\vec{H} = \frac{1}{\mu} \nabla \times \vec{A}, \quad (2.58)$$

or from the definition of the curl,

$$\vec{H} = \frac{1}{\mu} \left(\hat{y} \frac{\partial A_x}{\partial z} - \hat{z} \frac{\partial A_x}{\partial y} \right). \quad (2.59)$$

The relations between the fields and the vector potentials are thus summarized as

$$E_x = -j\omega A_x \quad (2.60)$$

$$H_y = \frac{1}{\mu_0} \frac{\partial A_x}{\partial z} \quad (2.61)$$

$$H_z = -\frac{1}{\mu_0} \frac{\partial A_x}{\partial y} \quad (2.62)$$

2.1.5 Solutions to ODE

The ordinary differential equations (2.49) and (2.51) are each the harmonic differential equation. Thus both have solutions that are complex exponential or trigonometric functions. In region 3, $z > h$, there is only an upward propagating wave. Therefore

$$\tilde{A}_x(k_y, z) = C_1 e^{-j p z}, \quad (2.63)$$

where C_1 is a constant to be determined using appropriate boundary conditions. In region 2, $t \leq z < h$, there are both upwards and downwards propagating waves, requiring

$$\tilde{A}_x(k_y, z) = C_2 e^{j p z} + C_3 e^{-j p z}. \quad (2.64)$$

In region 1, $0 \leq z < t$, the potential can be written in terms of standing waves:

$$\tilde{A}_x(k_y, z) = C_4 \sin q z + C_5 \cos q z. \quad (2.65)$$

Region 0 has only a downwards propagating wave. Therefore

$$\tilde{A}_x(k_y, z) = C_6 e^{j p z}. \quad (2.66)$$

It is important that the appropriate sign on p and q from equations (2.50) and (2.52) be determined through the use of physical reasoning. In region 3, when $k_y^2 \leq k_0^2$, the

wave must propagate upwards. Therefore, the sign on expressions in the exponent of (2.63) must be negative. This requires

$$p = +\sqrt{k_0^2 - k_y^2}, \quad k_0^2 \leq k_y^2. \quad (2.67)$$

When $k_y^2 > k_0^2$, the wave must upward evanescent, again requiring the expression in the exponent to be negative. Thus,

$$p = -j\sqrt{k_y^2 - k_0^2}, \quad k_y^2 > k_0^2. \quad (2.68)$$

This is equivalent to requiring $\text{Re}\{p\} \geq 0$ and $\text{Im}\{p\} \leq 0$. Through this same type of physical reasoning, it can be determined that $\text{Re}\{q\} \geq 0$ and $\text{Im}\{q\} \leq 0$.

The boundary conditions of the field vectors at the interfaces of different media are necessary to solve electromagnetic canonical problems involving contiguous regions of different parameters. These boundary conditions are found by applying Maxwell's equations to a small region at the interface of two different media. From these derivations it is found that the tangential component of the electric field is continuous across an interface. In other words

$$\hat{n} \times (\vec{E}_1 - \vec{E}_2) = 0, \quad (2.69)$$

where \hat{n} is the normal vector pointing into region 1 from region 2, t designates the tangential component of \vec{E} field and the numbers designate the region on each side of the interface. The normal component of \vec{D} is discontinuous across an interface where a surface charge exists, with the amount of discontinuity being equal to the surface charge density:

$$\hat{n} \cdot (\vec{D}_1 - \vec{D}_2) = \rho_s. \quad (2.70)$$

In contrast, the normal component of \vec{B} is continuous across an interface and the

tangential component of \vec{H} is discontinuous across an interface where a free surface current exists. Thus,

$$\hat{n} \cdot (\vec{B}_1 - \vec{B}_2) = 0 \quad (2.71)$$

$$\hat{n} \times (\vec{H}_1 - \vec{H}_2) = J_s \quad (2.72)$$

With this set of boundary conditions, the constants in the solutions to the ODEs can be found. First, the respective \vec{E} fields are found from (2.60) and the boundary conditions between regions 0 and 1 are employed. Since (2.69) holds true at $z = 0$,

$$[C_4 \sin zq + C_5 \cos zq]_{z=0} = [C_6 e^{jPz}]_{z=0}, \quad (2.73)$$

and thus,

$$C_5 = C_6. \quad (2.74)$$

The tangential \vec{H} fields are examined next. Using (2.72) and (2.61) to derive \vec{H} from the potentials, and noting that there is no current source on the surface $z = 0$,

$$\left[\frac{1}{\mu_0} \frac{\partial}{\partial z} (C_4 \sin zq + C_5 \cos zq) \right]_{z=0} = \left[\frac{1}{\mu_0} \frac{\partial}{\partial z} (C_6 e^{jPz}) \right]_{z=0}. \quad (2.75)$$

Taking the derivative with respect to z and multiplying through by μ_0 gives

$$(C_4 q \cos zq - C_5 q \sin zq) \Big|_{z=0} = C_6 j p e^{jPz} \Big|_{z=0}. \quad (2.76)$$

Inserting $z = 0$ thus produces

$$C_4 = \frac{j p}{q} C_6. \quad (2.77)$$

On the boundary between regions 1 and 2 \vec{E} is continuous, resulting in

$$\left[-j\omega C_2 e^{jPz} - j\omega C_3 e^{-jPz} \right]_{z=t} = [-j\omega (C_4 \sin zq + C_5 \cos zq)]_{z=t}. \quad (2.78)$$

Substituting for C_4 and C_5 from (2.77) and (2.74), (2.78) becomes

$$\left[-j\omega C_2 e^{j p z} - j\omega C_3 e^{-j p z}\right]_{z=t} = \left[C_6 \left(\frac{p\omega}{q} \sin zq - j\omega \cos zq\right)\right]_{z=t}. \quad (2.79)$$

Thus,

$$C_2 e^{j p t} + C_3 e^{-j p t} = C_6 \left(\frac{j p}{q} \sin zt + \cos zt\right). \quad (2.80)$$

Next, the boundary conditions for the \vec{H} fields are employed at $z = t$. Using (2.72) gives

$$\left[\frac{1}{\mu_0} \frac{\partial}{\partial z} (C_2 e^{j p z} + C_3 e^{-j p z})\right]_{z=t} = \left[\frac{C_6}{\mu_0} \frac{\partial}{\partial z} \left(\frac{j p}{q} \sin zq + \cos zq\right)\right]_{z=t}. \quad (2.81)$$

Taking the derivatives with respect to z and substituting $z = t$ results in

$$j p C_2 e^{j p t} - j p C_3 e^{-j p t} = C_6 (j p \cos zt - q \sin qt). \quad (2.82)$$

Continuity of \vec{E} across the boundary between regions 2 and 3 requires

$$\left[-j\omega C_2 e^{j p z} - j\omega e^{-j p z}\right]_{z=h} = \left[-j\omega C_1 e^{-j p z}\right]_{z=h} \quad (2.83)$$

according to (2.69). Substituting $z = h$ then gives

$$C_2 e^{j p h} + e^{-j p h} = C_1 e^{-j p h}. \quad (2.84)$$

On the boundary between regions 2 and 3, the tangential \vec{H} field is discontinuous by the surface current, resulting in

$$\hat{z} \times (H_{3y} \hat{y} - H_{2y} \hat{y}) = \tilde{K}_x \hat{x}. \quad (2.85)$$

Where \tilde{K}_x is the transform domain surface current density given, using (2.4), as

$$\tilde{K}_x(k_y, z) = \int_{-\infty}^{\infty} I\delta(y)e^{-jk_y y} dk_y. \quad (2.86)$$

Integrating gives

$$\tilde{k}_x(k_y, z) = I. \quad (2.87)$$

With this, (2.85) becomes

$$\left[-\frac{\partial}{\partial z} \frac{1}{\mu_0} C_1 e^{-j p z} - \frac{\partial}{\partial z} \frac{1}{\mu_0} (-C_2 e^{j p z} - C_3 e^{-j p z}) \right]_{z=h} = I. \quad (2.88)$$

Differentiating and substituting $z = h$ yields

$$-j p C_1 e^{-j p h} - j p C_2 e^{j p h} + j p C_3 e^{-j p h} = -I \mu_0. \quad (2.89)$$

In summary, there are 6 equations and 6 unknowns,

$$C_5 = C_6 \quad (2.90)$$

$$C_4 = \frac{j p}{q} C_6 \quad (2.91)$$

$$C_2 e^{j p t} + C_3 e^{-j p t} = C_6 \left(\frac{j p}{q} \sin z t + \cos z t \right) \quad (2.92)$$

$$j p C_2 e^{j p t} - j p C_3 e^{-j p t} = C_6 (j p \cos z t - q \sin q t) \quad (2.93)$$

$$C_2 e^{j p h} + e^{-j p h} = C_1 e^{-j p h} \quad (2.94)$$

$$-j p C_1 e^{-j p h} - j p C_2 e^{j p h} + j p C_3 e^{-j p h} = -I \mu_0. \quad (2.95)$$

The 6 constants in (2.90)-(2.95) can be found using tedious standard linear algebra

techniques. First, (2.92) is multiplied by jp and added to (2.93), giving

$$2C_2 jpe^{jpt} = C_6 \left(-\frac{p^2}{q} \sin qt + 2jp \cos qt - q \sin qt \right), \quad (2.96)$$

or

$$C_2 = \frac{C_6}{2jpe^{jpt}} \left(-\frac{p^2}{q} \sin qt + 2jp \cos qt - q \sin qt \right). \quad (2.97)$$

Then the multiplication of (2.92) with jp is subtracted from (2.93), resulting in

$$2C_3 jpe^{-jpt} = C_6 \left(\frac{p^2}{q} \sin qt + q \sin qt \right), \quad (2.98)$$

or

$$C_3 = \frac{C_6}{2jpe^{-jpt}} \left(\frac{p^2}{q} \sin qt + q \sin qt \right). \quad (2.99)$$

Next, substitution of C_2 and C_3 from (2.97) and (2.99) into (2.94) gives

$$\begin{aligned} & \frac{C_6}{2jp} e^{jp(h-t)} \left(-\frac{p^2}{q} \sin qt + 2jp \cos qt - q \sin qt \right) + \\ & \frac{C_6}{2jp} e^{-jp(h-t)} \left(\frac{p^2}{q} \sin qt + q \sin qt \right) = C_1 e^{-jph}. \end{aligned} \quad (2.100)$$

Multiplying through by $2jp$ and factoring out C_6 , gives the equation

$$\begin{aligned} & C_6 \left[e^{jp(h-t)} \left(-\frac{p^2}{q} \sin qt + 2jp \cos qt - q \sin qt \right) + \right. \\ & \left. e^{-jp(h-t)} \left(\frac{p^2}{q} \sin qt + q \sin qt \right) \right] = 2C_1 jpe^{-jph}. \end{aligned} \quad (2.101)$$

To continue the procedure, C_2 and C_3 from (2.97) and (2.99), are substituted into

(2.95), yielding

$$\begin{aligned} & \frac{C_6}{2} e^{jp(h-t)} \left(-\frac{p^2}{q} \sin qt + 2jp \cos qt - q \sin qt \right) \\ & - \frac{C_6}{2} e^{-jp(h-t)} \left(\frac{p^2}{q} \sin qt + q \sin qt \right) = I\mu_0 - C_1 jpe^{jph}. \end{aligned} \quad (2.102)$$

Rearranging gives

$$\begin{aligned} & C_6 \left[e^{jp(h-t)} \left(-\frac{p^2}{q} \sin qt + 2jp \cos qt - q \sin qt \right) \right. \\ & \left. - e^{-jp(h-t)} \left(\frac{p^2}{q} \sin qt + q \sin qt \right) \right] = 2I\mu_0 - 2C_1 jpe^{jph}. \end{aligned} \quad (2.103)$$

To simplify notation, (2.101) is rewritten as

$$C_6 = \frac{2jpe^{-jph}}{[X]} C_1, \quad (2.104)$$

where

$$\begin{aligned} X = & \left[e^{jp(h-t)} \left(-\frac{p^2}{q} \sin qt + 2jp \cos qt - q \sin qt \right) + \right. \\ & \left. e^{-jp(h-t)} \left(\frac{p^2}{q} \sin qt + q \sin qt \right) \right]. \end{aligned} \quad (2.105)$$

Similarly, (2.103) is written as

$$C_6[Y] = -2I\mu_0 + 2C_1 jpe^{-jph}, \quad (2.106)$$

where

$$Y = \left[-e^{jp(h-t)} \left(-\frac{p^2}{q} \sin qt + 2jp \cos qt - q \sin qt \right) + e^{-jp(h-t)} \left(\frac{p^2}{q} \sin qt + q \sin qt \right) \right]. \quad (2.107)$$

Substituting (2.104) into (2.106) yields

$$[Y] \frac{2jpe^{-jph}}{[X]} C_1 = -2I\mu_0 + 2C_1 jpe^{-jph}, \quad (2.108)$$

or

$$\left([Y] \frac{2jpe^{-jph}}{[X]} - 2jpe^{-jph} \right) C_1 = -2I\mu_0. \quad (2.109)$$

Factoring out similar constants results in

$$C_1 2jpe^{-jph} \left(\frac{[Y] - [X]}{[X]} \right) = -2I\mu_0, \quad (2.110)$$

yielding

$$C_1 = \frac{I\mu_0}{jp} e^{jph} \left(\frac{[X]}{[Y] - [X]} \right). \quad (2.111)$$

As seen in (2.111), $[Y] - [X]$ must be computed. This results in the equation

$$Y - X = e^{jp(h-t)} \left(\frac{p^2}{q} \sin qt + \frac{p^2}{q} \sin qt - 2jp \cos qt - 2jp \cos qt + q \sin qt + q \sin qt \right) + e^{-jp(h-t)} \left(\frac{-p^2}{q} \sin qt + \frac{p^2}{q} \sin qt + q \sin qt - q \sin qt \right) \quad (2.112)$$

or, by subtracting out like terms,

$$Y - X = -2e^{jp(h-t)} \left(\frac{-p^2}{q} \sin qt + 2jp \cos qt - q \sin qt \right). \quad (2.113)$$

Therefore

$$\frac{[X]}{[Y - X]} = \left[e^{jp(h-t)} \left(-\frac{p^2}{q} \sin qt + 2jp \cos qt - q \sin qt \right) + e^{-jp(h-t)} \left(\frac{p^2}{q} \sin qt + q \sin qt \right) \right] \times \left[-2e^{jp(h-t)} \left(\frac{-p^2}{q} \sin qt + 2jp \cos qt - q \sin qt \right) \right]^{-1}. \quad (2.114)$$

Simplifying (2.114) yields

$$\frac{[X]}{[Y - X]} = -\frac{1}{2} - \frac{e^{-2jp(h-t)}}{2} \left(\frac{-\frac{p^2}{q} \sin qt + q \sin qt}{-\frac{p^2}{q} \sin qt + 2jp \cos qt - q \sin qt} \right). \quad (2.115)$$

Inserting (2.115), into (2.111) produces C_1 :

$$C_1 = \frac{I\mu_0}{2jp} e^{jph} + \frac{I\mu_0}{2jp} e^{-2jp(h-t)} e^{jph} \left(\frac{-\frac{p^2}{q} \sin qt + q \sin qt}{-\frac{p^2}{q} \sin qt + 2jp \cos qt - q \sin qt} \right). \quad (2.116)$$

The next constant to be solved for is C_6 . Substituting C_1 from (2.110) into (2.104), a simplified equation for C_6 results:

$$C_6 = \frac{-2I\mu_0}{[Y] - [X]}. \quad (2.117)$$

Inserting (2.113) gives C_6 :

$$C_6 = I\mu_0 \frac{e^{-jp(h-t)}}{-\frac{p^2}{q} \sin qt + 2jp \cos qt - q \sin qt}. \quad (2.118)$$

Substituting C_6 into (2.97) then gives C_2 :

$$C_2 = \frac{I\mu_0}{2jp} e^{-jp(h-t)} e^{-jpt} \frac{-\frac{p^2}{q} \sin qt + 2jp \cos qt - q \sin qt}{-\frac{p^2}{q} \sin qt + 2jp \cos qt - q \sin qt}. \quad (2.119)$$

This is simplified to give

$$C_2 = \frac{I\mu_0}{2jp} e^{-jph}. \quad (2.120)$$

Similarly, (2.118) is inserted into (2.99) producing C_3 :

$$C_3 = \frac{C_6}{2jp} e^{jpt} e^{-jp(h-t)} \frac{-\frac{p^2}{q} \sin qt + q \sin qt}{-\frac{p^2}{q} \sin qt + 2jp \cos qt - q \sin qt}. \quad (2.121)$$

The constants C_4 and C_5 can be found using a similar procedure. However, they are not needed to solve the canonical problem and thus are left undetermined. Therefore in summary,

$$C_1 = \frac{I\mu_0}{2jp} e^{jph} + \frac{I\mu_0}{2jp} e^{-2jp(h-t)} e^{jph} (R) \quad (2.122)$$

$$C_2 = \frac{I\mu_0}{2jp} e^{-jph} \quad (2.123)$$

$$C_3 = \frac{C_6}{2jp} e^{jpt} e^{-jp(h-t)} (R) \quad (2.124)$$

$$C_6 = I\mu_0 \frac{e^{-jp(h-t)}}{-\frac{p^2}{q} \sin qt + 2jp \cos qt - q \sin qt} \quad (2.125)$$

$$(2.126)$$

where

$$R = \frac{-\frac{p^2}{q} \sin qt + q \sin qt}{-\frac{p^2}{q} \sin qt + 2jp \cos qt - q \sin qt}. \quad (2.127)$$

2.1.6 Electric Field Derivation

With the constants now known, the fields on each side of the dielectric slab may be found. For the region above the slab, $z \geq t$, the solutions for the potential in regions 1 and 2 are combined as follows:

$$\tilde{A}_x(k_y, z) = \frac{I\mu_0}{2jp} e^{-jp|z-h|} + \frac{I\mu_0}{2jp} e^{-jp(z+h)} e^{2jpt} R. \quad (2.128)$$

Substituting (2.132) into the inverse Fourier transform wave equation, (2.42), gives

$$\begin{aligned} A_x(y, z) &= \frac{1}{2\pi} \int_{-\infty}^{\infty} \frac{I\mu_0}{2jp} e^{-jp|z-h|} e^{jk_y y} dk_y + \\ &\quad \frac{1}{2\pi} \int_{-\infty}^{\infty} \frac{I\mu_0}{2jp} e^{-jp(z+h)} e^{2jpt} R e^{jk_y y} dk_y, \end{aligned} \quad (2.129)$$

or

$$A_x(y, z) = \frac{I\mu_0}{4\pi j} \int_{-\infty}^{\infty} \left[\frac{e^{-jp|z-h|}}{p} e^{jk_y y} + \frac{e^{-jp(z+h-2t)} R}{p} e^{jk_y y} \right] dk_y. \quad (2.130)$$

The electric field above the slab, $z \geq t$, is then determined from (2.60) yielding

$$E_x(y, z) = \frac{-I\mu_0\omega}{4\pi} \int_{-\infty}^{\infty} \frac{e^{jk_y y}}{p} \left[e^{-jp|z-h|} + e^{-jp(z+h-2t)} R \right] dk_y. \quad (2.131)$$

When $z < 0$ the vector potential is determined by (2.66). Substituting (2.125) into (2.66) gives

$$\tilde{A}_x(k_y, z) = \frac{I\mu_0 e^{j p z} e^{-j p (h-t)}}{-\frac{p^2}{q} \sin qt + 2jp \cos qt - q \sin qt}, \quad (2.132)$$

or

$$\tilde{A}_x(k_y, z) = \frac{I\mu_0 e^{jp(z-h+t)}}{-\frac{p^2}{q} \sin qt + 2jp \cos qt - q \sin qt}. \quad (2.133)$$

Implementing the inverse Fourier transform, (2.42), results in

$$A_x(y, z) = \frac{I\mu_0}{2\pi} \int_{-\infty}^{\infty} \frac{I\mu_0 e^{jp(z-h+t)} e^{jk_y y}}{-\frac{p^2}{q} \sin qt + 2jp \cos qt - q \sin qt} dk_y. \quad (2.134)$$

Applying (2.60), the electric field for $z < 0$ is

$$E_x(y, z) = \frac{-j\omega I\mu_0}{2\pi} \int_{-\infty}^{\infty} \frac{I\mu_0 e^{jp(z-h+t)} e^{jk_y y}}{-\frac{p^2}{q} \sin qt + 2jp \cos qt - q \sin qt} dk_y. \quad (2.135)$$

In summary, for the canonical problem seen in Figure 2.2, the electric fields is found in the regions above and below the dielectric slab:

$$E_x(y, z) = \frac{-I\mu_0\omega}{4\pi} \int_{-\infty}^{\infty} \frac{e^{jk_y y}}{p} \left[e^{-jp|z-h|} + e^{-jp(z+h-2t)} R \right] dk_y, \quad z \geq t \quad (2.136)$$

$$E_x(y, z) = \frac{-j\omega I\mu_0}{2\pi} \int_{-\infty}^{\infty} \frac{e^{jp(z-h+t)} e^{k_y y}}{-\frac{p^2}{q} \sin qt + 2jp \cos qt - q \sin qt} dk_y \quad z < 0. \quad (2.137)$$

2.2 Scattered Field from Conducting Strip

With the impressed fields on either side of the dielectric slab determined, the current across the infinitesimally thin conducting strip can be found. From the current, the scattered field can be derived at a position above the slab.

2.2.1 Integral Equation Derivation

An integral equation is determined to obtain the current on the conducting strip [10]. Along the surface of the conducting strip the tangential electric field is equal to zero. Given that the tangential component of the electric field is zero, from Figure 2.3 it is

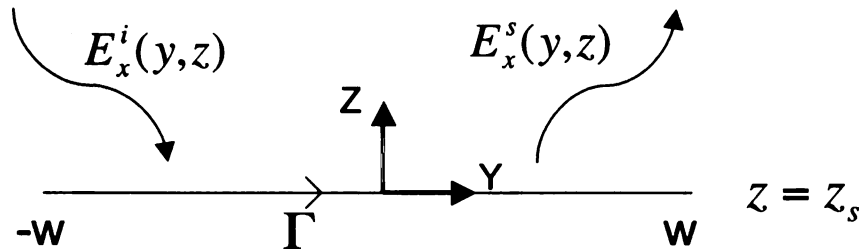


Figure 2.3: Conducting strip parameters.

determined

$$E_x^i(y, z) = -E_x^s(y, z). \quad (2.138)$$

The strip is assumed to be infinitesimally thin, therefore the currents on the top and bottom are nearly adjacent, which allows them to be summed together. The integral representation of the scattered electric field in terms of the two-dimensional Green's function is

$$E_x^s(y, z) = \int \int G_1(y', z' | y, z) J_x(y') dy' dz'. \quad (2.139)$$

The summed current, $J_x(y)$, is independent of the x direction, which makes it possible to write the surface current as a volume current density:

$$J_x(y, z) = J_{sx} \delta(z - z_s) \quad (2.140)$$

Substituting (2.140) into (2.139) yields

$$\int_{y'=-w}^w G_1(y', z_s|y, z_s) J_{sx}(y') dy' = -E_x^i(y, z_s). \quad (2.141)$$

The integral equation in (2.141) can be solved using the method of moments (MoM). This approach involves expanding the unknown current as a linear combination of basis functions:

$$J_{sx}(y) = \sum_{n=1}^N a_n f_n(y). \quad (2.142)$$

Substituting (2.142) into (2.141) gives

$$\sum_{n=1}^N a_n \int_{-w}^w G_1(y', z_s|y, z_s) f_n(y') dy' = -E_x^i(y, z_s). \quad (2.143)$$

For simplicity the basis functions f_n are chosen to be pulse functions:

$$f_n(y) = P_n(y) = \begin{cases} 1 & : y_n - \frac{\Delta}{2} \leq y' \leq y_n + \frac{\Delta}{2} \\ 0 & : \text{elsewhere.} \end{cases} \quad (2.144)$$

In (2.144),

$$y_n = -w + \left(n - \frac{1}{2}\right) \Delta, \quad (2.145)$$

and

$$\Delta = \frac{2w}{N}. \quad (2.146)$$

The quantity Δ is the width of the partitions, N is the total number of partitions used, and y_n is the center of a partition.

The method of collocation (or point matching) is used to convert the integral equation into a system of linear equations. By point matching at $y = y_m$, a set of

linear equations are obtained:

$$\sum_{n=1}^N a_n \int_{y_n - \frac{\Delta}{2}}^{y_n + \frac{\Delta}{2}} G_1(y', z_s | y_m, z_s) dy' = -E_x^i(y_m, z_s), \quad m = 1, 2, \dots, N, \quad (2.147)$$

or

$$\sum_{n=1}^N a_n A_{mn} = b_m. \quad (2.148)$$

The variable a_n in the matrix equation (2.148), represents the current on the conducting strip.

When a field impinges on an object, current is induced along the surface. Scattered fields are then produced from this induced current. For this canonical problem, the incident field on the conducting strip is the transmitted field from an electric line source above a lossy dielectric slab. Therefore giving,

$$b_m = \frac{-j\omega I \mu_0}{2\pi} \int_{-\infty}^{\infty} \frac{e^{jp(z-h+t)} e^{jk_y y_m}}{-\frac{p^2}{q} \sin qt + 2jp \cos qt - q \sin qt} dk_y. \quad (2.149)$$

The scattered field from the strip is actually the impressed field produced by an electric line source in the presence of a lossy slab. Thus yielding

$$G_1(y', z' | y_m, z) = \frac{-\mu_0 \omega}{4\pi} \int_{-\infty}^{\infty} \frac{e^{jk_y (y_m - y')}}{p} \left[e^{-jp|z-z'|} + \operatorname{Re} e^{jp(z+z'-2t)} \right] dk_y. \quad (2.150)$$

The source point in the equations for the impressed and transmitted fields derived in section 2.1.6 is in reference to the front of the dielectric slab. Therefore the source point in (2.149) and (2.150) also have to be referenced from the front of the slab. This results in $z' = t - z_s$. Since (2.148) is defined for all points on the surface of the

conductor, the observation point also results in $z = t - z_s$. Rewriting (2.147) yields

$$A_{mn} = \int_{y_n - \frac{\Delta}{2}}^{y_n + \frac{\Delta}{2}} \frac{-\mu_0 \omega}{4\pi} \int_{-\infty}^{\infty} \frac{e^{jk_y y m} e^{-jk_y y'}}{p} [1 + Re^{jp2z_s}] dk_y dy. \quad (2.151)$$

Rearranging (2.151) gives

$$A_{mn} = \frac{-\mu_0 \omega}{4\pi} \int_{-\infty}^{\infty} \frac{e^{jk_y y m}}{p} [1 + Re^{jp2z_s}] X dk_y, \quad (2.152)$$

where

$$X = \int_{y_n - \frac{\Delta}{2}}^{y_n + \frac{\Delta}{2}} e^{-jk_y y'} dy'. \quad (2.153)$$

Performing the integration in (2.153) yields

$$X = \left[-\frac{e^{-jk_y y'}}{jk_y} \right]_{y_n - \frac{\Delta}{2}}^{y_n + \frac{\Delta}{2}}. \quad (2.154)$$

Inserting the limits of integration for the variable y' gives,

$$X = \frac{-e^{-jk_y y_n} e^{jk_y \frac{\Delta}{2}} + e^{-jk_y y_n} e^{jk_y \frac{\Delta}{2}}}{jk_y}. \quad (2.155)$$

Simplifying further gives

$$X = e^{-jk_y y_n} \frac{e^{jk_y \frac{\Delta}{2}} - e^{-jk_y \frac{\Delta}{2}}}{jk_y}, \quad (2.156)$$

which can be reduced to

$$X = e^{-jk_y y_n} \frac{2j \sin k_y \frac{\Delta}{2}}{jk_y}, \quad (2.157)$$

or

$$X = e^{-jk_y y_n} \frac{\Delta \sin k_y \frac{\Delta}{2}}{k_y \frac{\Delta}{2}}. \quad (2.158)$$

Substituting (2.158) into (2.152) produces

$$A_{mn} = \frac{-\mu_0 \omega}{4\pi} \int_{-\infty}^{\infty} \frac{e^{-jk_y y_n} e^{jk_y y_m}}{p} [1 + Re^{jp2z_s}] \frac{\Delta \sin k_y \frac{\Delta}{2}}{k_y \frac{\Delta}{2}} dk_y. \quad (2.159)$$

2.2.2 A_{mn} Evaluation

The A_{mn} integral actually consist of two separate integrals:

$$A_{mn} = U_{mn} + V_{mn}, \quad (2.160)$$

where

$$U_{mn} = \frac{-\mu_0 \omega}{4\pi} \int_{-\infty}^{\infty} \frac{e^{-jk_y y_n} e^{jk_y y_m}}{p} \frac{\Delta \sin k_y \frac{\Delta}{2}}{k_y \frac{\Delta}{2}} dk_y, \quad (2.161)$$

and

$$V_{mn} = \frac{-\mu_0 \omega}{4\pi} \int_{-\infty}^{\infty} \frac{e^{-jk_y y_n} e^{jk_y y_m}}{p} \frac{\Delta \sin k_y \frac{\Delta}{2}}{k_y \frac{\Delta}{2}} Re^{jp2z_s} dk_y. \quad (2.162)$$

It is computationally expensive to integrate a function from negative infinity to positive infinity. Since portions of the integrand are even about it's axis, the integrations of U_{mn} and V_{mn} are simplified. First employing Euler's relation to (2.161) results

in

$$U_{mn} = \frac{-\mu_0\omega\Delta}{4\pi} \int_{-\infty}^{\infty} \frac{\cos k_y(m-n)\Delta}{p} \frac{\sin k_y \frac{\Delta}{2}}{k_y \frac{\Delta}{2}} + \frac{j \sin k_y(m-n)\Delta}{p} \frac{\sin k_y \frac{\Delta}{2}}{k_y \frac{\Delta}{2}} dk_y. \quad (2.163)$$

Given the definition of a sinc function, (2.163) is rewritten as

$$U_{mn} = \frac{-\mu_0\omega\Delta}{4\pi} \int_0^{\infty} \frac{\cos k_y(m-n)\Delta}{p} \operatorname{sinc} k_y \frac{\Delta}{2} + \frac{j \sin k_y(m-n)\Delta}{p} \operatorname{sinc} k_y \frac{\Delta}{2} dk_y. \quad (2.164)$$

In (2.164), the sinc and p functions are even about the vertical axis. When these functions are multiplied by a cos this results in an even integrand. While multiplying by a sin function results in an odd integrand. Therefore this yield

$$U_{mn} = \frac{-\mu_0\omega\Delta}{2\pi} \int_0^{\infty} \frac{\cos k_y(m-n)\Delta}{p} \operatorname{sinc} k_y \frac{\Delta}{2} dk_y, \quad (2.165)$$

or

$$U_{mn} = \frac{-\mu_0\omega\Delta}{2\pi} \int_0^{\infty} \frac{\cos k_y(m-n)\Delta}{p} \frac{\sin k_y \frac{\Delta}{2}}{k_y \frac{\Delta}{2}} dk_y. \quad (2.166)$$

Through the same reasoning (2.162) results in

$$V_{mn} = \frac{-\mu_0\omega\Delta}{2\pi} \int_0^{\infty} \frac{\cos k_y(m-n)\Delta}{p} \frac{\sin k_y \frac{\Delta}{2}}{k_y \frac{\Delta}{2}} \operatorname{Re} j p 2z_s dk_y. \quad (2.167)$$

2.2.2.1 U_{mn} Evaluation

The integrand in (2.166) has the form of

$$U_{mn} = \int_0^{\infty} \frac{\sin ax \cos bx}{x\sqrt{k^2 - x^2}} dx. \quad (2.168)$$

When $x = k$ the denominator of the integrand goes to zero, which is a singularity of the function. Therefore a numerical method [12] is considered which splits U_{mn} up into two parts, thus removing the singularity:

$$U_{mn} = \int_0^k \frac{f(x)}{\sqrt{k^2 - x^2}} dx + \int_k^{\infty} \frac{f(x)}{\sqrt{k^2 - x^2}} dx, \quad (2.169)$$

where

$$f(x) = \frac{\sin ax \cos bx}{x}. \quad (2.170)$$

Rewriting (2.169) gives,

$$U_{mn} = I_1^u + I_2^u. \quad (2.171)$$

Looking at I_1^u , the square root in the denominator can be factored giving

$$I_1^u = \int_0^k \frac{\left(\frac{f(x)}{\sqrt{k+x}} \right)}{\sqrt{k-x}} dx, \quad (2.172)$$

or

$$I_1^u = \int_0^k \frac{g(x)}{\sqrt{k-x}} dx. \quad (2.173)$$

Now, use the substitution

$$x = k - t^2 \quad (2.174)$$

or

$$t = \sqrt{k - x}, \quad (2.175)$$

with the differential

$$dx = -2t dt. \quad (2.176)$$

Inserting (2.175) and (2.176) into (2.173) and changing the limits of integration results

in

$$I_1^u = \int_{\sqrt{k}}^0 \frac{g(k - t^2)}{t} (-2t dt) \quad (2.177)$$

or

$$I_1^u = 2 \int_0^{\sqrt{k}} g(k - t^2) dt. \quad (2.178)$$

In the equation for I_2^u , x is always larger than k given the limits of integration.

Therefore,

$$I_2^u = \int_k^{\infty} \frac{f(x)}{-j\sqrt{x^2 - k^2}} dx, \quad (2.179)$$

or

$$I_2^u = j \int_k^{\infty} \frac{f(x)}{\sqrt{x^2 - k^2}} dx. \quad (2.180)$$

The sign on the square root function in the denominator of (2.179) is chosen because this function represents the variable p in the original equation. In (2.68) the sign on p is determined through physical reasoning.

The integrand in (2.180) oscillates substantially and only decays as $1/x^2$; thus it is difficult to integrate. Using Kummer's method [13],

$$I_2^u = j \int_k^{\infty} \left[\frac{f(x)}{\sqrt{x^2 - k^2}} - f_a(x) \right] dx + j \int_k^{\infty} f_a(x) dx, \quad (2.181)$$

where $f_a(x)$ is asymptotic expansion of $\frac{f(x)}{\sqrt{x^2-k^2}}$, the integration is easier to compute. This is useful only if the oscillations in the integral cancel out at high multiples of k , and the second term can be integrated in closed form. Further manipulations of (2.181) yields,

$$I_2^u = j \int_k^\infty \frac{f(x) - \sqrt{x^2 - k^2} f_a(x)}{\sqrt{x^2 - k^2}} dx + j \int_k^\infty f_a(x) dx. \quad (2.182)$$

Similarly to the simplification done for I_1^u , the square root function is split up:

$$I_2^u = j \int_k^\infty \frac{f(x) - \sqrt{x^2 - k^2} f_a(x)}{\frac{\sqrt{x+k}}{\sqrt{x-k}}} dx + j \int_k^\infty f_a(x) dx, \quad (2.183)$$

or

$$I_2^u = j \int_k^\infty \frac{\tilde{g}(x)}{\sqrt{x-k}} dx + j \int_k^\infty f_a(x) dx. \quad (2.184)$$

Next, use the substitution

$$x = k + k^2, \quad (2.185)$$

$$t = \sqrt{x-k}, \quad (2.186)$$

with the differential

$$dx = 2t dt. \quad (2.187)$$

By substituting (2.186) and (2.187) into (2.184) gives

$$I_2^u = j \int_k^\infty \frac{\tilde{g}(k+t^2)}{t} 2t dt + j \int_k^\infty f_a(x) dx, \quad (2.188)$$

or

$$I_2^u = 2j \int_k^\infty \tilde{g}(k+t^2) dt + j \int_k^\infty f_a(x) dx. \quad (2.189)$$

In a general form,

$$I_2^u = 2j \int_k^\infty \tilde{g}(k+t^2) dt + jI_A, \quad (2.190)$$

where

$$I_A = \int_k^\infty f_a(x) dx. \quad (2.191)$$

With the equation for I_2^u in manageable form the the asymptotic expansion $f_a(x)$ is chosen to achieve the requirements for the Kummer's method. By choosing,

$$f_a(x) = \frac{\sin ax \cos bx}{\beta^2 + x^2}, \quad (2.192)$$

and β to be arbitrary, I_A can be rewritten as

$$I_A = I_B - I_C, \quad (2.193)$$

where

$$I_B = \int_0^\infty \frac{\sin ax \cos bx}{\beta^2 + x^2} dx, \quad (2.194)$$

and

$$I_C = \int_0^k \frac{\sin ax \cos bx}{\beta^2 + x^2} dx. \quad (2.195)$$

The equation for I_C can be computed numerically. However I_B is more difficult. To calculate I_B , exponential integrals are used. Writing I_B in terms of exponential integrals yields

$$I_B = \frac{1}{4\beta} [E[(a-b)\beta] + E[(a+b)\beta]], \quad (2.196)$$

where

$$E(x) = e^{-x} E_i(x) - e^x E_i(-x) \quad (2.197)$$

and

$$E_i(x) = \int_{-\infty}^x \frac{e^{-t}}{t} dt. \quad (2.198)$$

2.2.2.2 V_{mn} Evaluation

When considering V_{mn} in (2.167), the upper integral limit is changed to a constant, A . This constant is chosen large enough in value so that the integrand has decayed close to zero and no longer significantly contributes to the integral. This results in

$$V_{mn} = \int_0^A \frac{f(k_y)}{\sqrt{k_0^2 - k_y^2}} dk_y. \quad (2.199)$$

The constant A must be larger than k_0 , since it is at $k_y = k_0$ that the integrand blows up and after where the integrand decays to close to zero. Therefore A , is chosen to be a multiplicative factor of k_0 .

A numerical method [12] is used to work around the singularity when $k_y = k_0$. Splitting the integral at k_0 , (2.199) becomes

$$V_{mn} = \int_0^{k_0} \frac{f(k_y)}{\sqrt{k_0^2 - k_y^2}} dk_y + \int_{k_0}^A \frac{f(k_y)}{\sqrt{k_0^2 - k_y^2}} dk_y, \quad (2.200)$$

or

$$V_{mn} = I_1^v + I_2^v. \quad (2.201)$$

Evaluating I_1^v by first factoring the square root in the denominator gives,

$$I_1^v = \int_0^{k_0} \frac{\left[\frac{f(k_y)}{\sqrt{k_0+k_y}} \right]}{\sqrt{k_0-k_y}} dk_y, \quad (2.202)$$

or

$$I_1^v = \int_0^{k_0} \frac{[g(k_y)]}{\sqrt{k_0-k_y}} dk_y, \quad (2.203)$$

for simplicity. Then by using substitution

$$k_y = k_0 - t^2 \quad (2.204)$$

or

$$t = \sqrt{k_0 - k_y}, \quad (2.205)$$

along with the differential

$$dk_y = -2t dt, \quad (2.206)$$

in (2.203) produces

$$I_1^v = \int_{\sqrt{k_0}}^0 \frac{g(k_0 - t^2)}{t} (-2t dt). \quad (2.207)$$

Simplifying further results in

$$I_1^v = 2 \int_0^{\sqrt{k_0}} g(k_0 - t^2) dt. \quad (2.208)$$

Knowing that the constant A is larger than k_0 , the second part of V_{mn} can be

rewritten as

$$I_2^v = \int_{k_0}^A \frac{f(k_y)}{-j\sqrt{k_y^2 - k_0^2}} dk_y. \quad (2.209)$$

Then, by factoring the square root in the denominator produces,

$$I_2^v = j \int_{k_0}^A \left[\frac{f(k_y)}{\sqrt{k_y - k_0}} \right] \frac{1}{\sqrt{k_y - k_0}} dk_y. \quad (2.210)$$

Using substitution

$$k_y = k_0 - t^2, \quad (2.211)$$

or

$$t = \sqrt{k_y - k_0}, \quad (2.212)$$

along with the differential

$$dk_y = 2t dt, \quad (2.213)$$

in (2.210) result in

$$I_2^v = j \int_0^{\sqrt{A-k_0}} \frac{g(k_0 + t^2)}{t} (2t dt). \quad (2.214)$$

Then with further simplification,

$$I_2^v = 2j \int_0^{\sqrt{A-k_0}} g(k_0 + t^2) dt. \quad (2.215)$$

2.2.3 Matrix Equation

With A_{mn} put into manageable form and

$$b_m = \frac{-j\omega I \mu_0}{2\pi} \int_{-\infty}^{\infty} \frac{e^{jp(z-h+t)} e^{jk_y y_m}}{-\frac{p^2}{q} \sin qt + 2jp \cos qt - q \sin qt} dk_y, \quad (2.216)$$

the current in the matrix equation of (2.148) can be derived. Thus the current at the center of each of the partition along the strip, a_n , is computed. These current values then can be treated as individual current sources with a width equal to that of the partition width of the conducting strip. The fields produced from an individual current source in the presence of a dielectric slab was derived in (2.137). Therefore the scattered field from strip can be computed by summing up the fields produced by each of the individual line sources. With this derivation the reflected and transmitted electric fields for the canonical problem seen in Figure 2.1 is solved for.

Chapter 3

Numerical Results

Computation of the fields scattered by the strip is carried out using the FORTRAN programming language. The position of the line source is set and represents the location of a transmitter. The scattered field is computed at an adjacent point, representing the position of a receiver. As seen in Figure 3.1, the transmit/receive pairs are moved parallel to the barrier and the fields computed from 20 MHz to 16 GHz at 20 MHz increments for each pair.

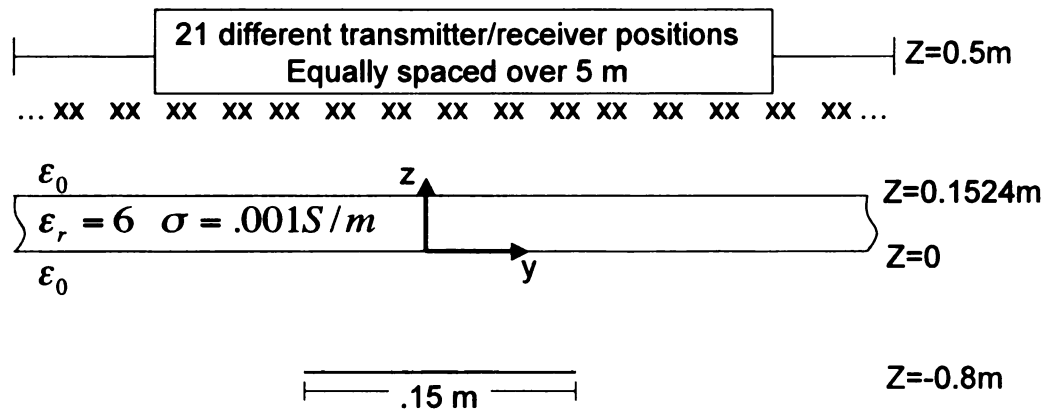


Figure 3.1: Position of source/observation pairs.

The total field is computed at 21 different transmitter/receiver locations in the frequency domain. At each of these positions, the frequency domain responses are

transformed into the time domain using the inverse Fourier transform. The time domain data fields from all 21 transmit/receive positions are used to construct an image of the target. An observation region is created using a 2-dimensional grid of points, and the propagation time for a wave propagating from each of the 21 different transmitter/receiver positions to that point is calculated. Given these propagation times, the intensity values from the time domain data are summed together creating an image of the target.

3.1 Computation of Incident and Scattered Fields

The permittivity, conductance, and thickness of the slab, as shown in Figure 3.1, are chosen to those of a concrete wall [14]. Multiple reflections from the conducting strip to the back of the dielectric slab will produce ghost images of the target. Therefore to decrease the merging of the ghosts and target responses, the strip is located sufficiently distant ($z = -0.8$ m) from the back of the dielectric slab. The width of the conducting strip is chosen to be relatively small at a width of 0.15 m., to test the ability of the image technique to resolve small targets.

The conducting strip is partitioned into narrower strips, with each of these strips having a constant current. The MoM technique is used to find the scattered field from the conducting strip. The number of partitions on the strip is set to 20 per wavelength, and is thus dependent on the frequency used. This number can be computed using the formula

$$N = 20 \frac{2wf}{c} \quad (3.1)$$

where $2w$ is the width of the strip, f is the frequency and c is the speed of light. The minimum number of partitions allowed is 10, regardless of frequency.

The integrals needed to find the incident and scattered fields are computed using the FORTRAN subroutine DQAG, which is part of the QUADPACK computational

package [15]. The computational package includes approximations to integrals of the form

$$\int_a^b f(x)w(x)dx. \quad (3.2)$$

The weight function w is used to incorporate known algebraic or logarithmic singularities, oscillations, or to indicate that a Cauchy principal value is desired. DQAG is a general purpose integration routine with a high efficiency and $w(x) = 1$ in (3.2).

The routine subdivides the interval $[a, b]$ and uses a $(2k + 1)$ -point Gauss-Kronrod rule to estimate the integral over that range [11]. The Gauss-Kronrod rule is an adaptive Gaussian quadrature method in which, for numerical integral routines, the error is estimated based on the evaluation at special points called Kronrod points. With this suitable point selection, the x -coordinate from previous iterations can be reused as data for the new set of points. A Gaussian quadrature would require a new x -coordinate at each of the iterations; this is important when a specified degree of accuracy is required but the number of points needed to achieve this accuracy is not known in advance.

The calling sequence for DQAG includes the function to integrate F , the lower limit a and upper limit b . The user defined absolute error ϵ is ERRABS, and the relative error ρ is ERRREL. The DQAG routine returns two numbers of interest: RESULT and ERREST, which are the approximate integral R and the error estimate E , respectively. The relation between these numbers are as follows:

$$\left| \int_a^b f(x)dx - R \right| \leq E \leq \max \left[\epsilon, \rho \left| \int_a^b f(x)dx \right| \right] \quad (3.3)$$

In these simulations, the absolute accuracy is 10^{-200} and the relative accuracy is chosen as 18 decimal places. Since the limits of integration are infinite, it is necessary to find a point to truncate the integrals that provides a desired accuracy, hence

determining a and b . Since the integrands of (2.136) and (2.137) are even about k_y , the lower limit of the integral can be set to 0 and the result multiplied by 2. The integrand decays rapidly once $k_y > k_0$. When $k_y > k_0$, values of p become imaginary in (2.50) producing an exponential decay in the integrand. Therefore, a good means for determining the integration truncation point is a multiple of k_0 . In these simulations the multiple is chosen to be 10.

The scattered field from the conducting strip is found by first solving the matrix equation (2.148). As described previously, A_{mn} is separated into two integrals. Using the DQAG integral routine, b_{mn} and V_{mn} are computed for the specified degree of accuracy. In addition, U_{mn} requires two more subroutines to evaluate $E_1(x)$ and $E_2(x)$, the exponential integrals found in the evaluation of U_{mn} . The matrix equation is of the simple form $Ax = b$, which is solved using another subroutine called SOLVEC using the decomposed matrix from the routine DCOMP. The solution is the complex current at each partition on the conducting strip. Finally, the field is determined at the receiver position by computing the scattered field from the known current on the conducting strip.

3.2 Imaging Analysis

3.2.1 Frequency to Time Domain Transformation

The field is computed at 21 positions above the slab between -2.5 m to 2.5 m with a spacing of 0.25 m, as seen in Figure 3.1. At each of these locations, the incident and scattered field is computed in the frequency domain between 20 MHz and 16 GHz, at a step size of 20 MHz. The incident and scattered fields are computed separately, and the frequency domain responses are transformed into the time domain using the visual basic program WaveCalc (supplied by John Ross and Associates). An example of the frequency domain field is shown in Figure 3.2 for the transmit/receive pair

centered above the conducting strip.

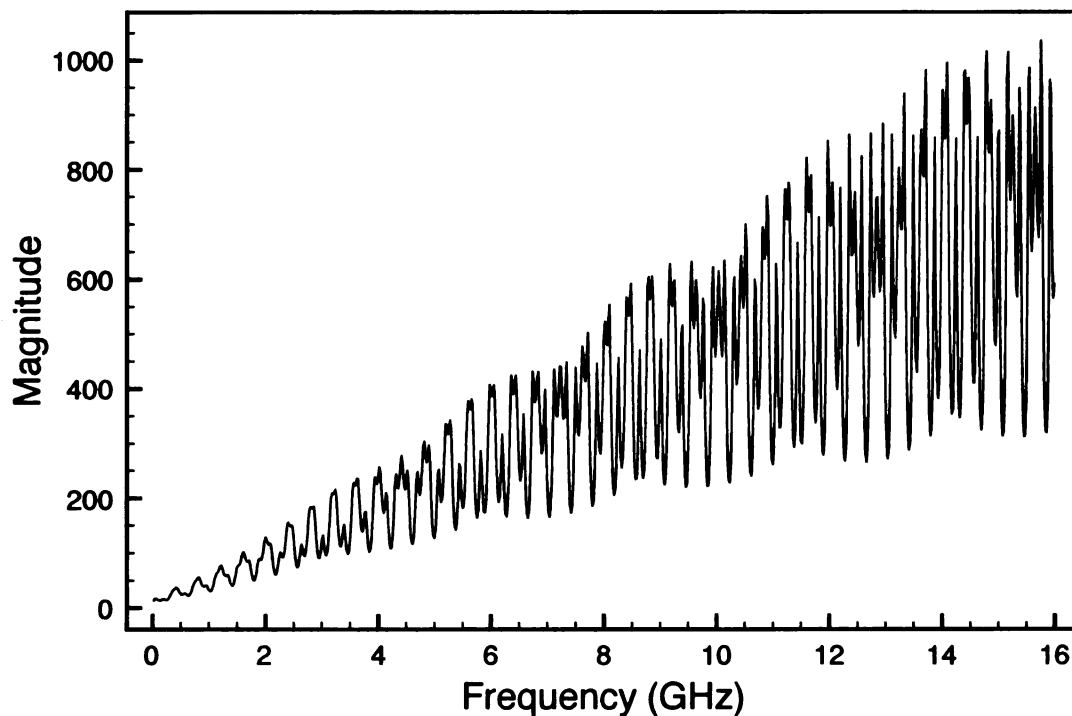


Figure 3.2: Magnitude of the frequency domain scattered field at a position centered above the strip.

Computing the fields over a certain frequency range is equivalent to evaluating the total fields over frequencies ranging from zero to infinity and truncating them using a rectangular function. Therefore, when the data is transformed into the time domain, the rectangular function is transformed into a sinc function, producing an abundance of oscillations on the edges. To eliminate some of these oscillations, the data is windowed in the frequency domain using a Gaussian modulated cosine (GMC) instead of a rectangular function. This allows for a steady roll off of the data, so that there are no abrupt changes, which results in few oscillations in the time domain. For these simulations, the GMC is centered at zero frequency with an equivalent pulse width of 0.12 ns. Figure 3.3 shows the weighted frequency domain data.

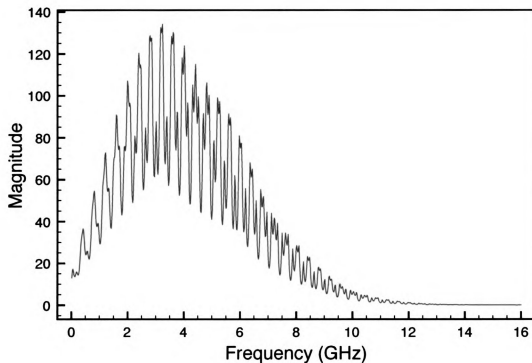


Figure 3.3: Magnitude of the frequency domain scattered field weighted with a GMC.

Finally, the weighted frequency domain data is zero padded and WaveCalc is used to transform the data into the time domain. Zero padding adds additional points at high frequencies and results in a finer sampling in the time domain. The final time domain response is shown in Figure 3.4.

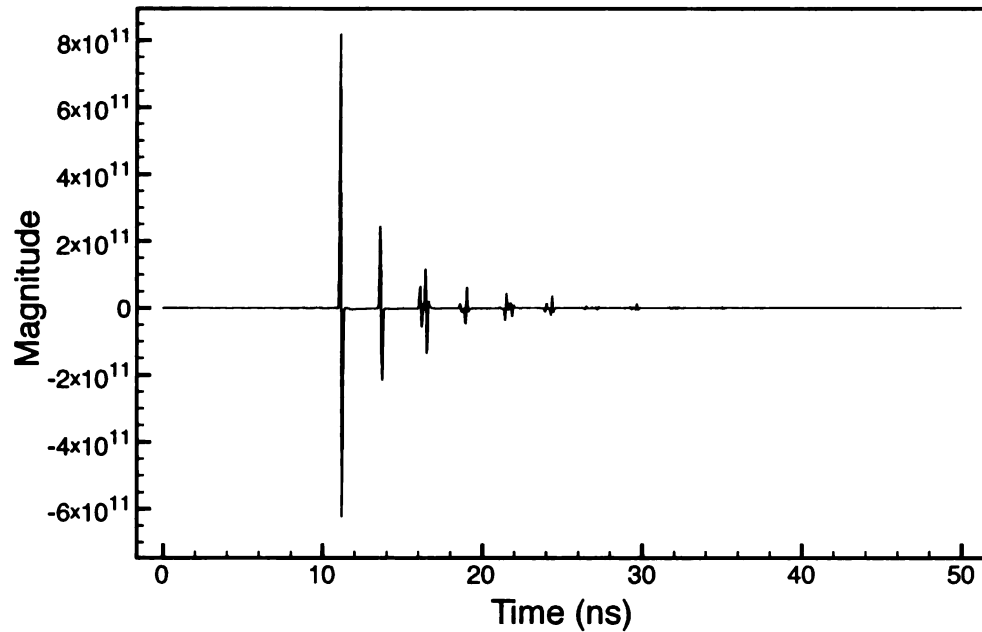


Figure 3.4: Time-domain scattered field at a point centered above the conductive strip.

The first event seen in Figure 3.4 represents the first wave interaction with the conducting strip. The following spikes are multiple reflections between the dielectric slab and the strip. Note that Figure 3.4 does not include the incident field. This field, shown in Figure 3.5, is computed separately and shows much stronger spikes representing the field reflected by the slab (the flash).

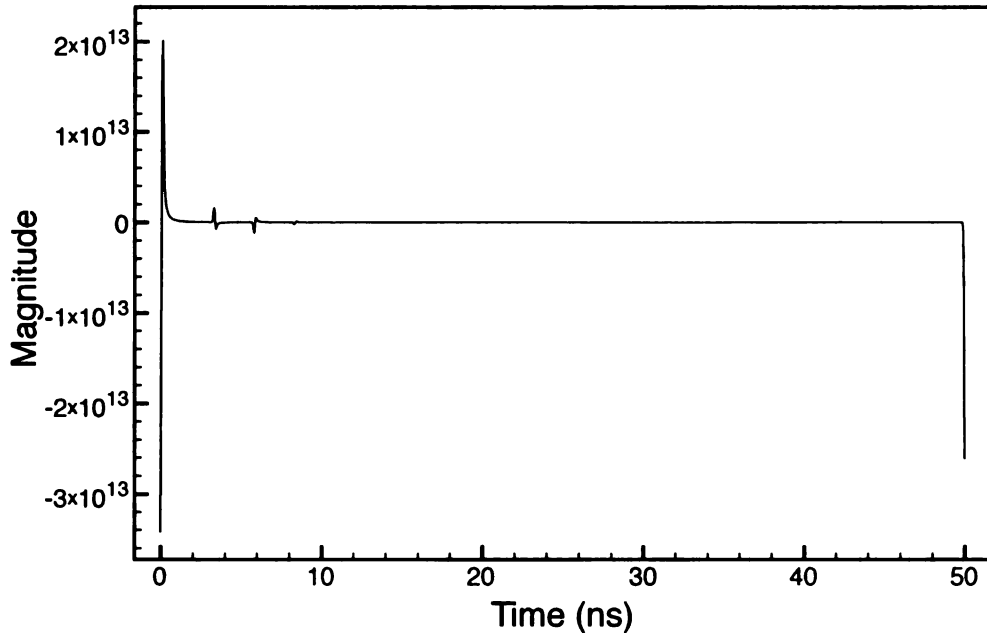


Figure 3.5: Time-domain incident field at a point centered above the conducting strip.

3.2.2 2D Image Construction

The time domain data fields from all 21 transmit/receive positions are used to construct an image of the target. An observation region is created using a 2-dimensional grid of points, and the propagation time for a wave propagating from each of the 21 different transmitter/receiver positions to that point is calculated. Given this distance between the transmit/receive position and the grid point, the approximate propagation time is

$$\tau = \frac{d}{c} \sqrt{\epsilon_r}. \quad (3.4)$$

Where τ is the travel time, d is the distance from the transmitter/receiver position to a particular point on the grid, c is the speed of light and ϵ_r is the relative permittivity of the material through which the wave travels. The actual travel time is somewhat difficult to compute since a ray entering the lossy slab undergoes refraction, and thus

doesn't follow the straight line path between the transmit/receive point and the grid point. However, since the slab is thin, the straight line path gives very accurate results. For the portions of the path in free space, ϵ_r is unity, while for the portions inside the slab ϵ_r is taken to be the real part of the complex permittivity of the slab: $\epsilon_r = 6$.

Using the computed travel time, the value of the total (incident plus scattered) field is found from each time domain waveform, and the results for all 21 transmit/receive positions are added to determine the image intensity at this particular grid point. The image intensity is highest at points corresponding to places of strong reflection, such as the front of the slab and the target. Thus, strong image intensity indicates a scatterer. Sometimes this is called a scattering center approach since it localizes the points on the scatterer that produce the largest reflections.

Figures 3.6 and 3.7 display the two-dimensional intensity image within a box that includes a portion of the dielectric slab and the conducting strip, using the time-domain data from 21 transmit/receive pairs. The axes of these two figures are distance in meters.

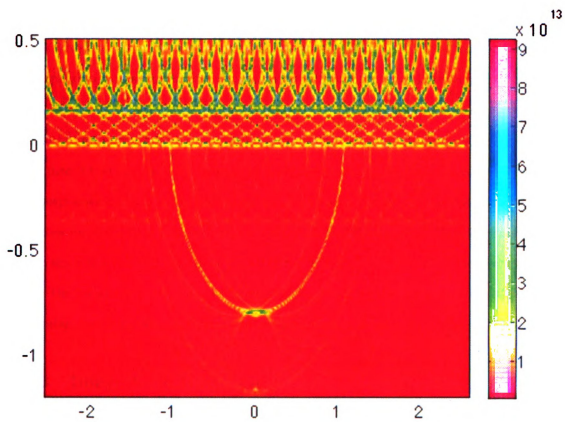


Figure 3.6: Image of lossy dielectric slab and conducting strip..

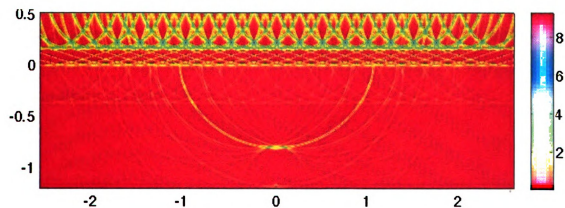


Figure 3.7: Proportionally correct mage of lossy dielectric slab and conducting strip with scale $\times 10^{13}$.

Figure 3.6 shows a compressed aspect ratio resulting in a square figure, while Figure 3.6 shows the proper aspect ratio. As seen in Figure 3.1, the back of the lossy dielectric slab is positioned at $z=0$ m, while the front is at $z=0.1524$ m and the strip is at $z=-0.8$ m. Comparing this figure to Figure 3.6 visually shows the correct positions of the objects analyzed.

Figure 3.6 shows how the image of the target and the slab are built up from the time responses at each of the transmit/receive pairs. A strong peak in a time response produces an arc in the image. These arcs overlap at points where a scattering center exists, since the reflection from the scattering center appears in all of the observations. Thus, the brightest spots in the image correspond to the strongest scatterers. In particular, the conducting strip target can be clearly seen.

3.2.3 Image Quantification

The sharpness of the target image depends on the parameters of the simulated radar system, including sampling rate, pulse width, etc. To determine the effects on the image of altering certain parameters, a way of quantifying the sharpness of the conducting strip image is needed. To do this, an image radius is defined, which is the radius of an equivalent circle that has an area equal to the region that contains the majority of the image intensity. An observation box is centered on the conducting strip as shown in Figure 3.8.

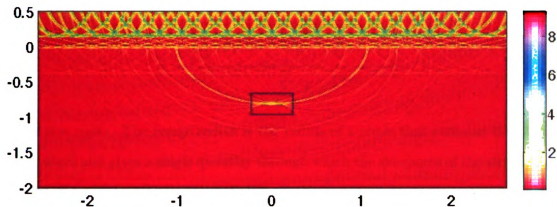


Figure 3.8: Area in which sharpness of conducting strip is determined with scale $\times 10^{13}$.

The size of the box is arbitrary, but it should completely contain the strip and should not be too large so that other artifacts in the image are excluded. In this research, a box size of 0.3 by 0.46 m is chosen. Inside this box the position of the center of pixel intensity is determined. This approach is much like the formula for finding the center of mass of an object. The coordinates of the center are given by

$$y_0 = \frac{\sum_{i=0}^{n_y} f_i y_i}{\sum_{i=1}^{n_y} f_i} \quad (3.5)$$

$$z_0 = \frac{\sum_{i=0}^{n_z} f_i z_i}{\sum_{i=1}^{n_z} f_i}. \quad (3.6)$$

In these equations y and z are the pixel positions, n_y and n_z are the number of pixels in the y and z direction respectively, and f represents that particular pixel intensity.

The radius of intensity, R , is found by considering only pixels with intensities above 0.5 times the maximum intensities of all pixels within the box, which are used

in the formula

$$R = \frac{\sum_{i=1}^n f_i \sqrt{(y_i - y_0)^2 + (z_i - z_0)^2}}{\sum_{i=1}^n f_i}. \quad (3.7)$$

where $n = n_y n_z$. The image radius is the radius of a circle that contains the higher pixel values and gives a single quantity through which the sharpness of the strip image may be described. A large image radius corresponds to a blurry image and a small radius to a sharper image. An example of an image radius is shown in Figure 3.9 for a relatively large pulse width of 2.0 ns.

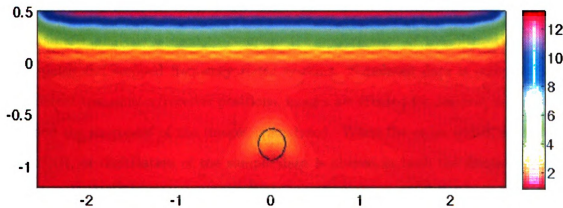


Figure 3.9: Circle of radius equal to the image radius centered around the conducting strip with scale $\times 10^{11}$.

Chapter 4

Parameter Analysis

A parameter analysis is used to compare the performance of the ultra-wide band short-pulse and stepped frequency radar systems. Simulated data is computed at 21 different transmitter/receiver positions, images are created for different parameter sets and the sharpness of the images is analyzed. When the pulse width, sampling rate, SNR, or digitization of the sample data is altered in both the frequency and time domain, the image radius changes allowing for optimization of these parameters in an actual prototype.

4.1 Time Domain Analysis

The significant parameters that are investigated during simulations of the time-domain system are the incident pulse width, sample rate, SNR, and digitization. Each of these is considered here in turn.

4.1.1 Pulse Width

The pulse width in the time domain is the duration of the pulse emitted from the transmitter of a UWB radar system. Longer durations of the pulse width cause the

image of the conducting strip to become blurred. Additionally, during transmitting the receiver is non-active to prevent cross coupling of the transmitted pulse. If the duration of the pulse is longer than it takes for the start of the pulse to reflect from an object and return to the receiver, this signal is not received, producing false results. To simulate this type of parameter change, the width of the Gaussian modulated cosine window function is altered in the frequency domain. With the geometry parameters of Figure 3.1, values of the computed image radius are shown in Figure (4.1).

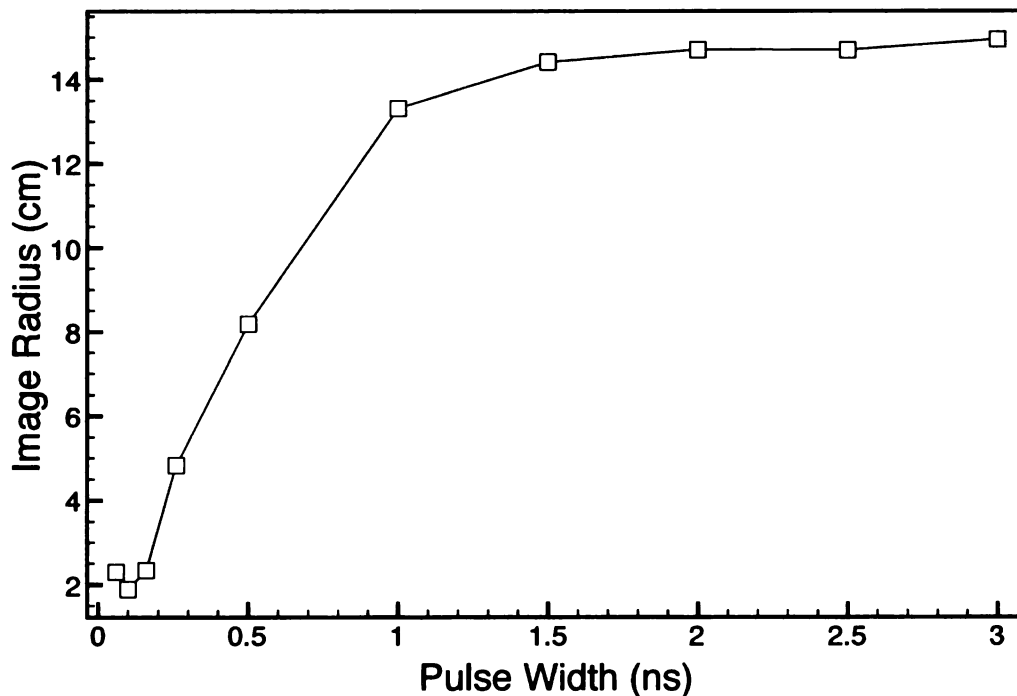


Figure 4.1: Effect of pulse width on image radius.

This figure demonstrates that increasing the pulse width enlarges the image radius which corresponds to an increase in the blurring of the strip. Between 0.06 ns and 0.10 ns the image radius unexpectedly decreases; this probably is because the threshold value of the pixel intensity used to compute the radius is set too low.

It is helpful to visually associate the reduction of image quality as the pulse width increases with the increase of image radius. The images are displayed in Figure 4.2-

4.11. When the pulse width reaches 1.5 ns, Figure 4.8, the conducting strip nearly fades into the background. In Figure 4.11, where the pulse width is 3.0 ns, the image of the conducting strip appears to have moved away from the actual position of the strip. The size, position, intensity, and shape of the strip can not be determined when the pulse width is too large.

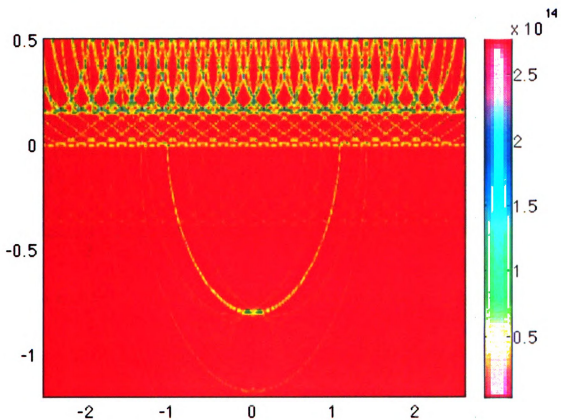


Figure 4.2: Conducting strip image constructed using a pulse width of $\tau = 0.06$ ns.

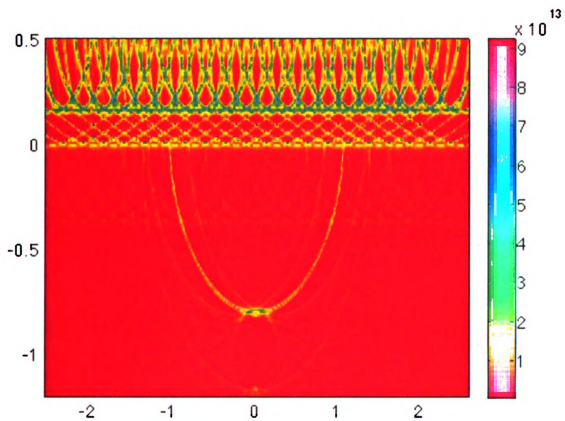


Figure 4.3: Conducting strip image constructed using a pulse width of $\tau = 0.10$ ns.

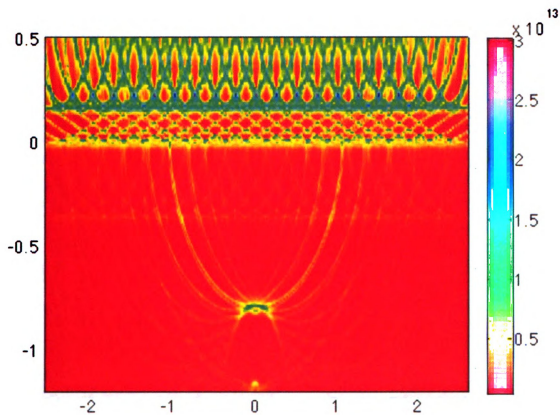


Figure 4.4: Conducting strip image constructed using a pulse width of $\tau = 0.16$ ns.

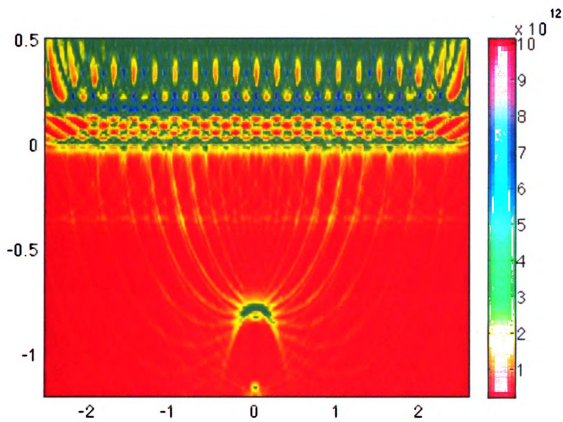


Figure 4.5: Conducting strip image constructed using a pulse width of $\tau = 0.26$ ns.

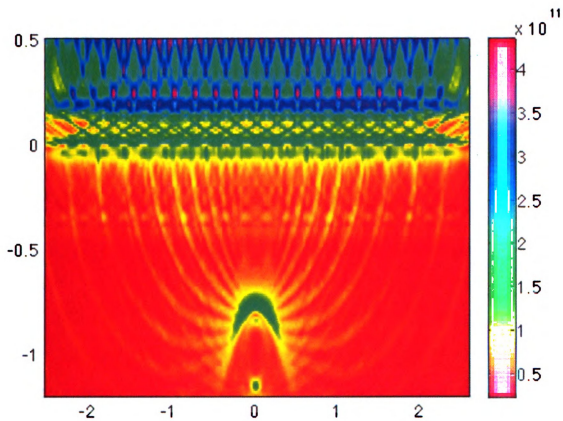


Figure 4.6: Conducting strip image constructed using a pulse width of $\tau = 0.50$ ns.

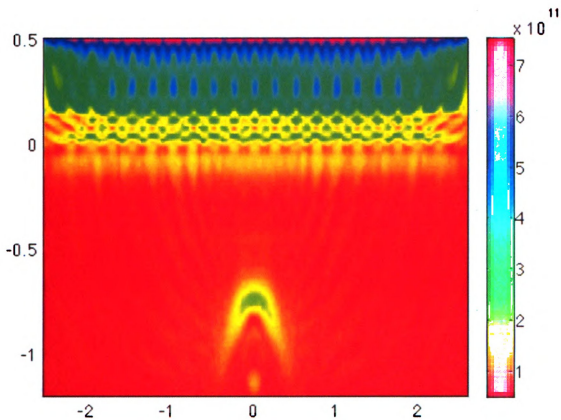


Figure 4.7: Conducting strip image constructed using a pulse width of $\tau = 1.00$ ns.

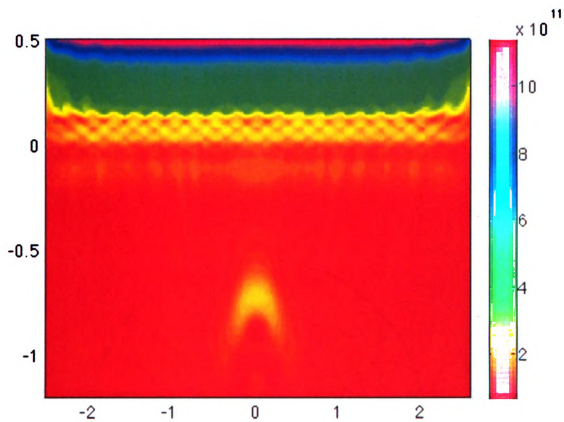


Figure 4.8: Conducting strip image constructed using a pulse width of $\tau = 1.50$ ns.

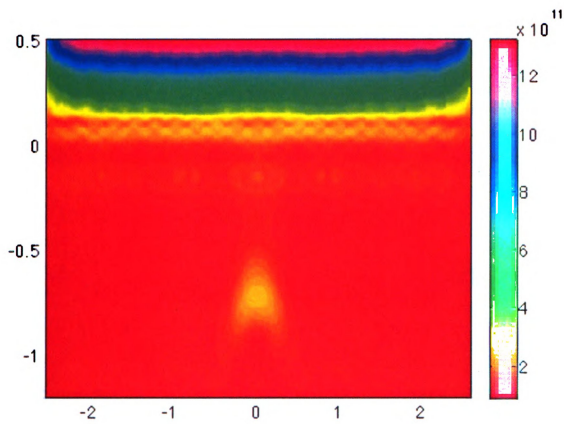


Figure 4.9: Conducting strip image constructed using a pulse width of $\tau = 2.00$ ns.

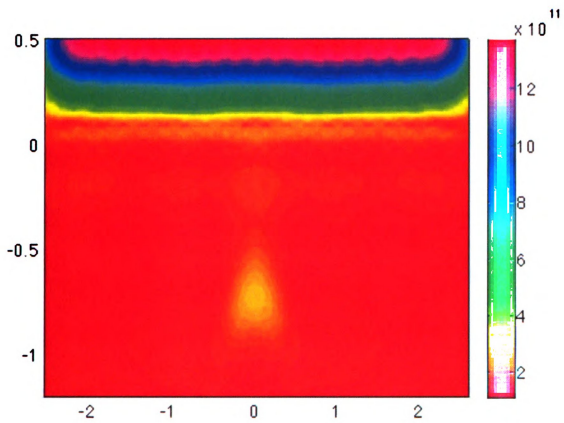


Figure 4.10: Conducting strip image constructed using a pulse width of $\tau = 2.50$ ns.

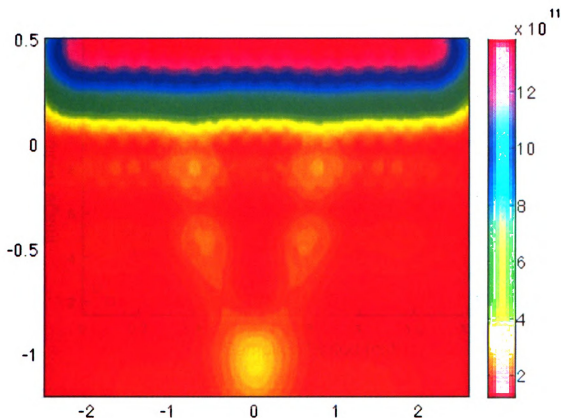


Figure 4.11: Conducting strip image constructed using a pulse width of $\tau = 3.00$ ns.

4.1.2 Sampling Rate

The sample rate in the time domain represents the number of samples taken per second from a continuous signal to form a discrete signal (also described in terms of the sampling period, which is the time between samples). The simulated data is computed at a high sampling rate, and the affect of lower sampling rates is easily determined by discarding data points. Figure 4.12 shows the dependence of image radius on sampling rate. As the number of samples per second decreases, the image radius increases and the conducting strip becomes blurrier.

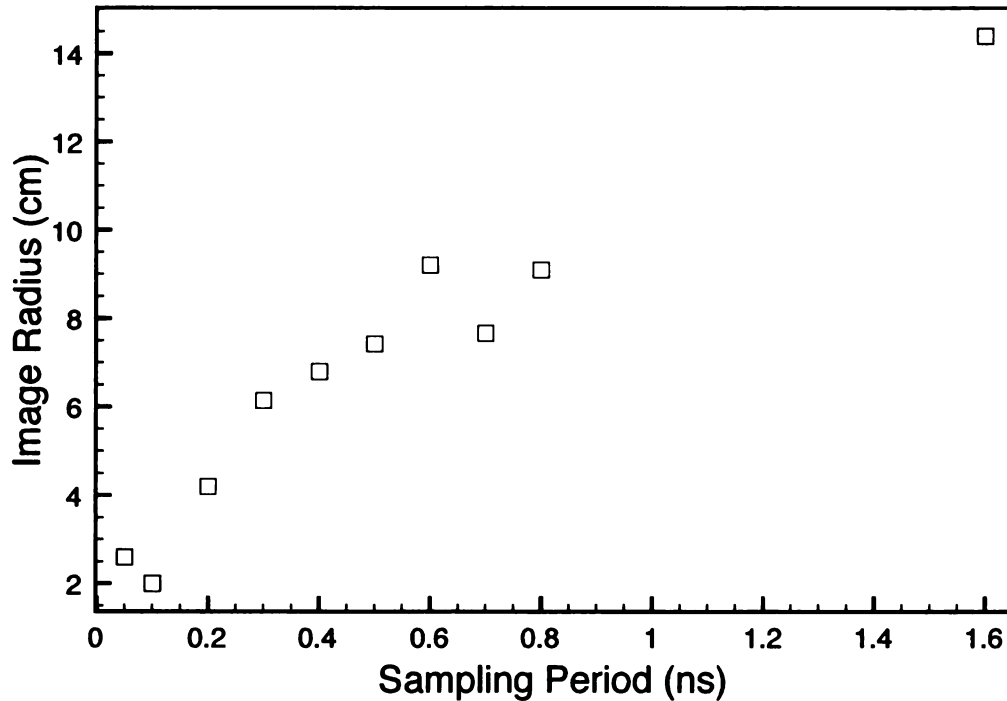


Figure 4.12: Effect of sampling period on image radius.

As seen with the affect of pulse width, the smallest value of sampling period does not produce the smallest image radius. This is again a result of the difficulty in choosing an appropriate threshold for selecting which pixel intensities are to be used in computing the radius. For visual inspection, Figures 4.13 - 4.22 show the images for each of the sample rates shown in Figure 4.12. As seen in Figure 4.17, when the sample period reaches 0.40 ns the image of the conducting strip is so unclear that an accurate detection cannot be produced.

In addition to blurriness, another concern is the existence of ghost images of the conducting strip. With the time-domain system, ghosting is due to multiple reflections within the barrier or between the target and the barrier, which produce additional peaks in the scattered field signal. These peaks add when constructing the image, producing ghost images at regular intervals behind the actual image. In Figure 4.17

it is seen that for a large sample period (0.40 ns, which is a sampling rate of 2.5 GHz), the intensity of the ghost image is larger than the actual conducting strip, which would result in an incorrect location of the object behind the slab. When the sampling period reaches 1.60 ns, Figure 4.22, the conducting strip is not visible and no analysis is possible.

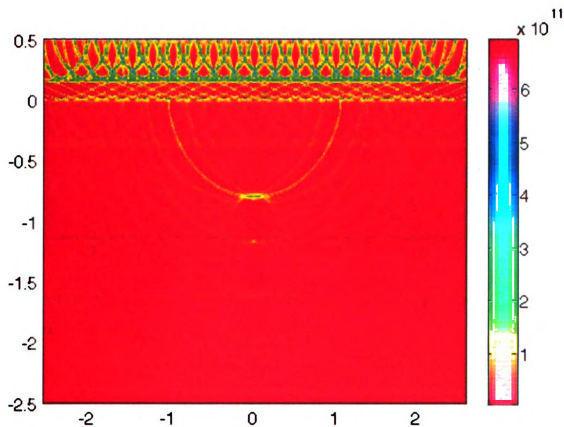


Figure 4.13: Conducting strip image constructed using a sampling period of $\Delta t = 0.05$ ns.

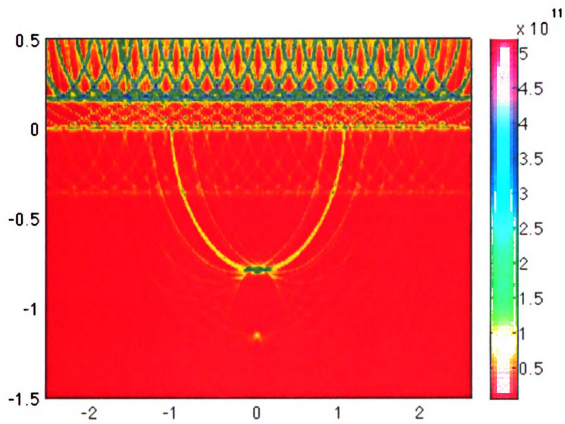


Figure 4.14: Conducting strip image constructed using a sampling period of $\Delta t = 0.10$ ns.

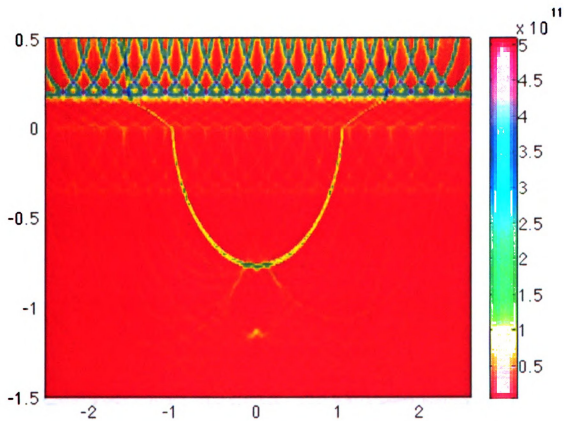


Figure 4.15: Conducting strip image constructed using a sampling period of $\Delta t = 0.20$ ns.

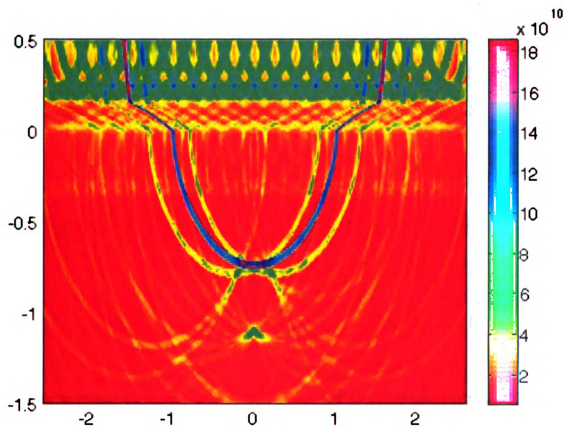


Figure 4.16: Conducting strip image constructed using a sampling period of $\Delta t = 0.30$ ns.

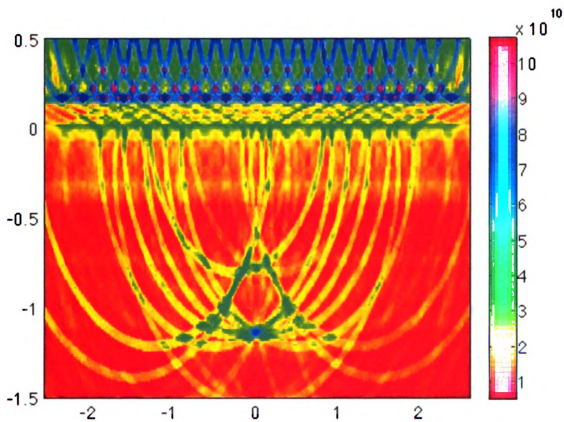


Figure 4.17: Conducting strip image constructed using a sampling period of $\Delta t = 0.40$ ns.

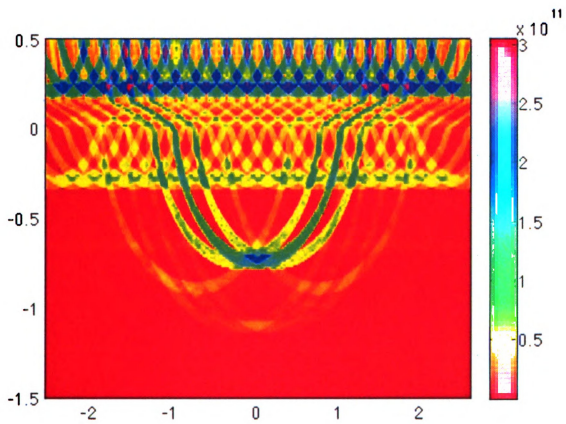


Figure 4.18: Conducting strip image constructed using a sampling period of $\Delta t = 0.50$ ns.

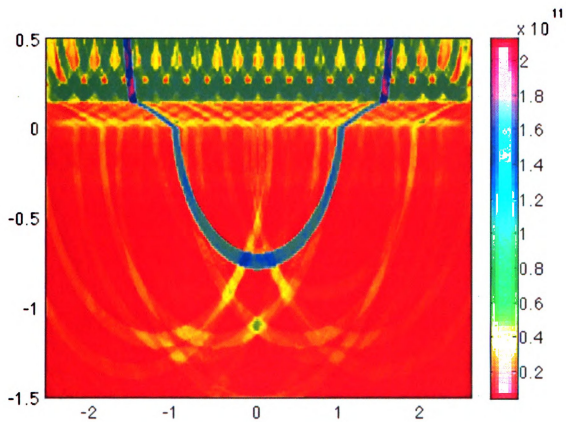


Figure 4.19: Conducting strip image constructed using a sampling period of $\Delta t = 0.60$ ns.

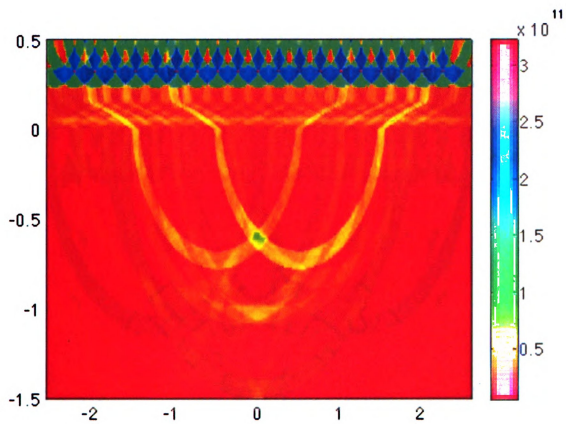


Figure 4.20: Conducting strip image constructed using a sampling period of $\Delta t = 0.70$ ns.

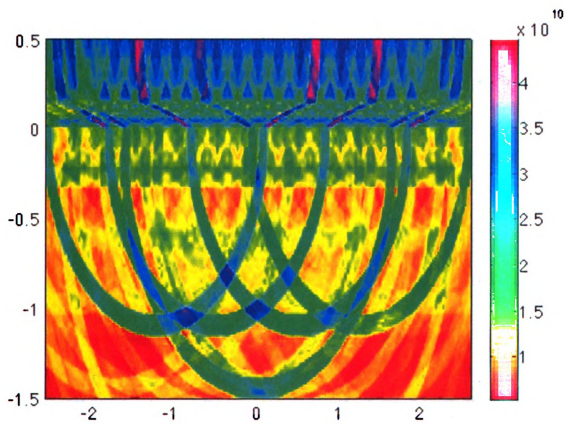


Figure 4.21: Conducting strip image constructed using a sampling period of $\Delta t = 0.80$ ns.

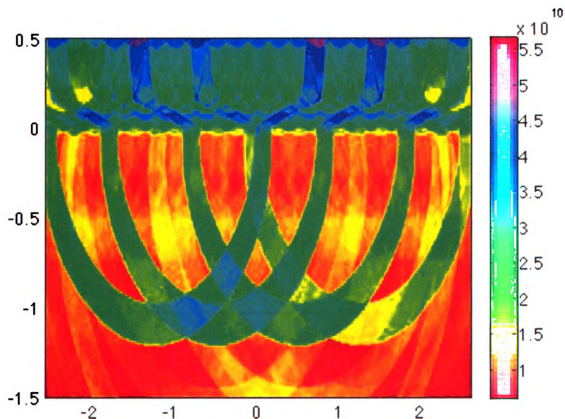


Figure 4.22: Conducting strip image constructed using a sampling period of $\Delta t = 1.60$ ns.

4.1.3 Signal-to-Noise Ratio

An essential consideration in any radar system is the signal-to-noise ratio (SNR) appearing at the receiver. As the SNR is reduced, it is anticipated that the target image will become less distinct. To examine this effect, random Gaussian noise is added to the simulated time-domain data using the program WavCalc. The noise level is relative to the largest peak in the waveform (which is the flash from the barrier), and thus the SNR values described here represent the decibels (dB) down from the peak value of the time signal. The relationship of image radius to SNR is shown in Figure 4.23.

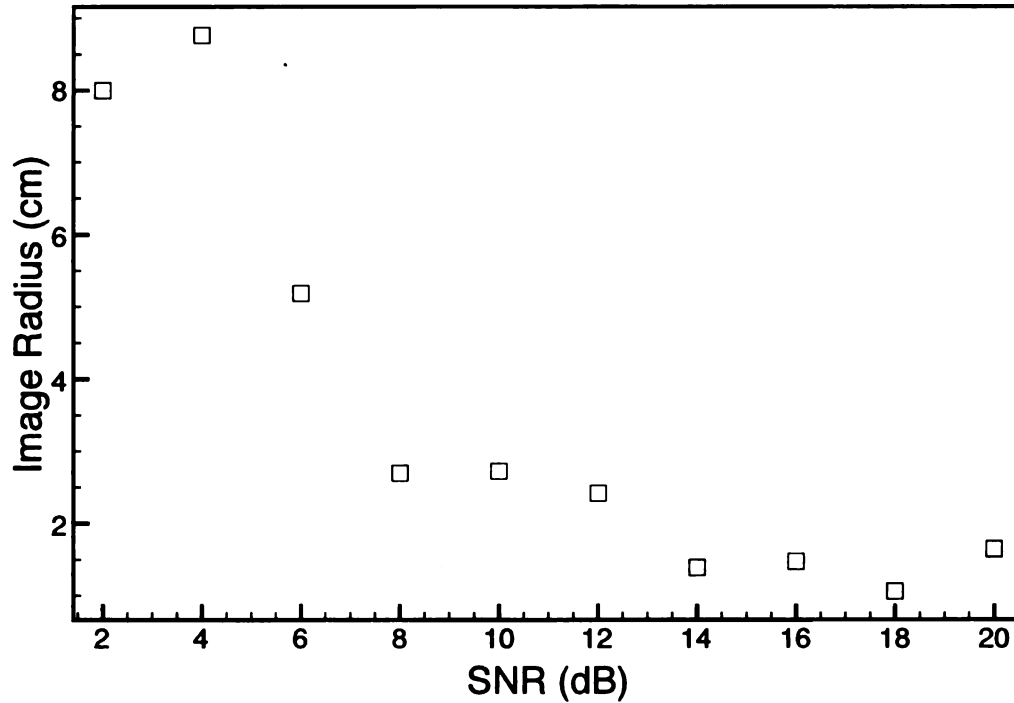


Figure 4.23: Effect of noise on image radius.

While the sharpness of the image is dependent on SNR, it is seen that the noise must be around $\text{SNR} = 10$ dB before image degradation occurs. This is because reflection from the target is quite large, and the time-domain peak extends above the noise until the noise level becomes as large as the reflection.

The target images as a function of SNR are shown in Figures 4.24-4.33. Though the image radius at $\text{SNR} = 4$ dB is not as large compared to the radii produced by high sample periods and pulse widths, at the low SNR the conducting strip still blends into the background, as seen in Figure 4.32. As the noise increases, the background becomes uniform and no images can be discerned.

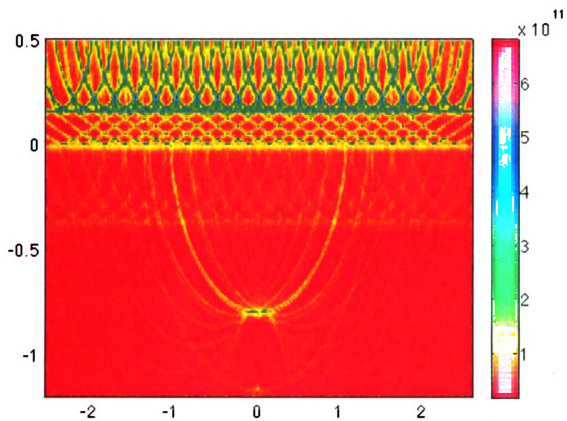


Figure 4.24: Conducting strip image constructed using a SNR = 20 dB.

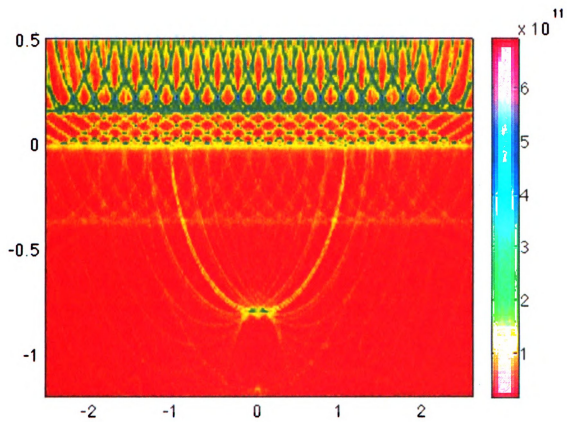


Figure 4.25: Conducting strip image constructed using a SNR = 18 dB.

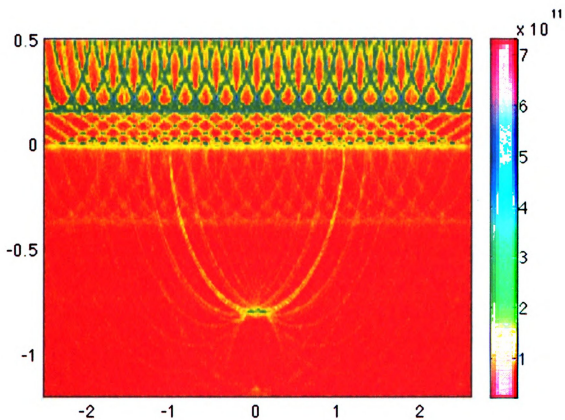


Figure 4.26: Conducting strip image constructed using a SNR = 16 dB.

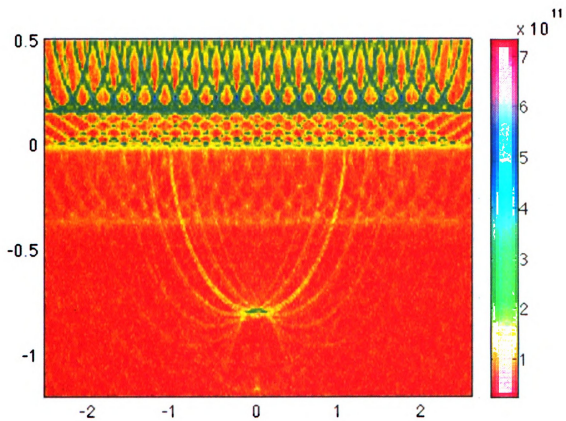


Figure 4.27: Conducting strip image constructed using a SNR = 14 dB.

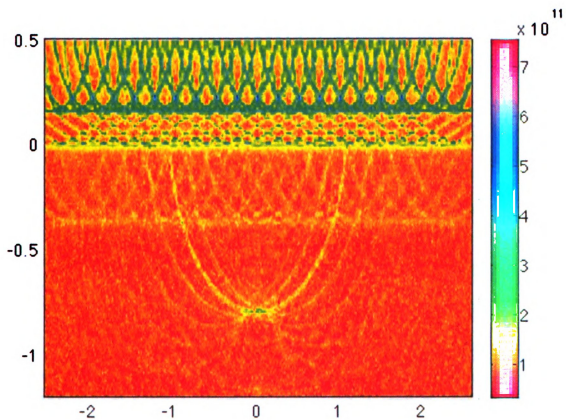


Figure 4.28: Conducting strip image constructed using a SNR = 12 dB.

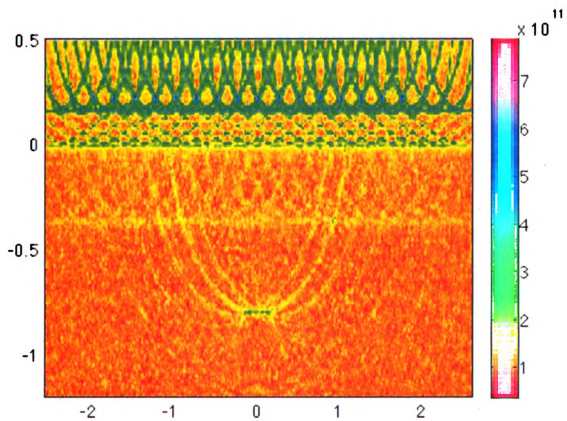


Figure 4.29: Conducting strip image constructed using a SNR = 10 dB.

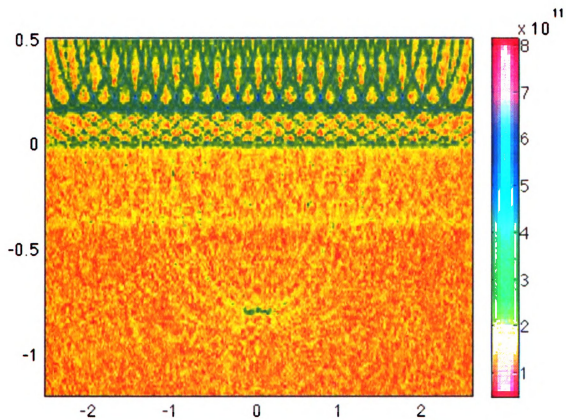


Figure 4.30: Conducting strip image constructed using a SNR = 8 dB.

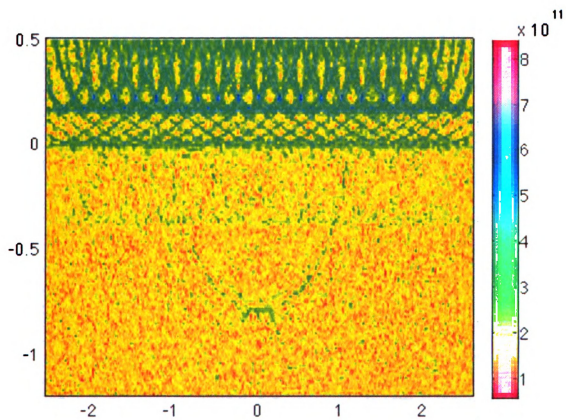


Figure 4.31: Conducting strip image constructed using a SNR = 6 dB.

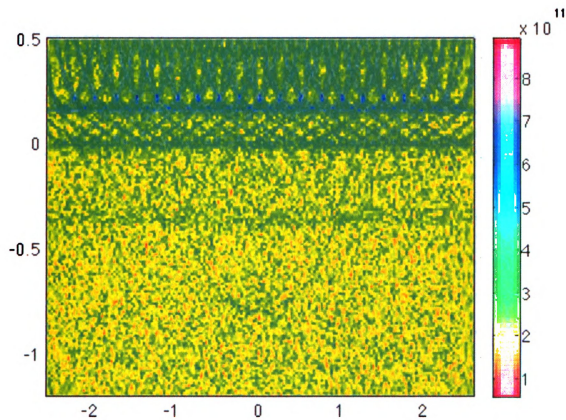


Figure 4.32: Conducting strip image constructed using a SNR = 4 dB.

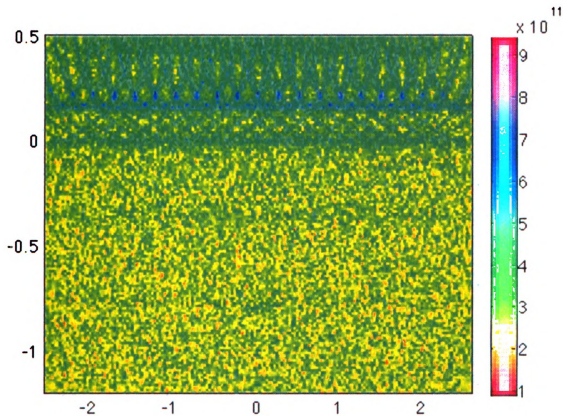


Figure 4.33: Conducting strip image constructed using a SNR = 2 dB.

4.1.4 Digitization

In a time-domain radar system a fast A/D converter is used to sample the time signal, digitizing the sample using a certain number of bits. Using a low number of bits results in losing smaller signals by rounding, and poor accuracy in larger signals. It is anticipated that dependence of the sharpness of the image on the number of bits used in the A/D converter will be fairly consistent until the number of bits becomes too small. At that point the image should degrade rapidly.

In order to implement the digitization process, the simulated time data is dis-

cretized into bins of size d based on the number of A/D bits, according to the formula

$$d = \frac{R}{2^N - 1}. \quad (4.1)$$

Here R represents the range of the intensity and N the number of bits. Every point in the time data must be put into a bin. This is done using the equation

$$bin = y_{min} + \text{round} \left[\frac{y - y_{min}}{d} \right] d \quad (4.2)$$

With this digitized version of the time data, images are created using different numbers of bits. The images are shown in Figures 4.35-4.44. Figure 4.34 shows how the image radius depends on the number of bits used.

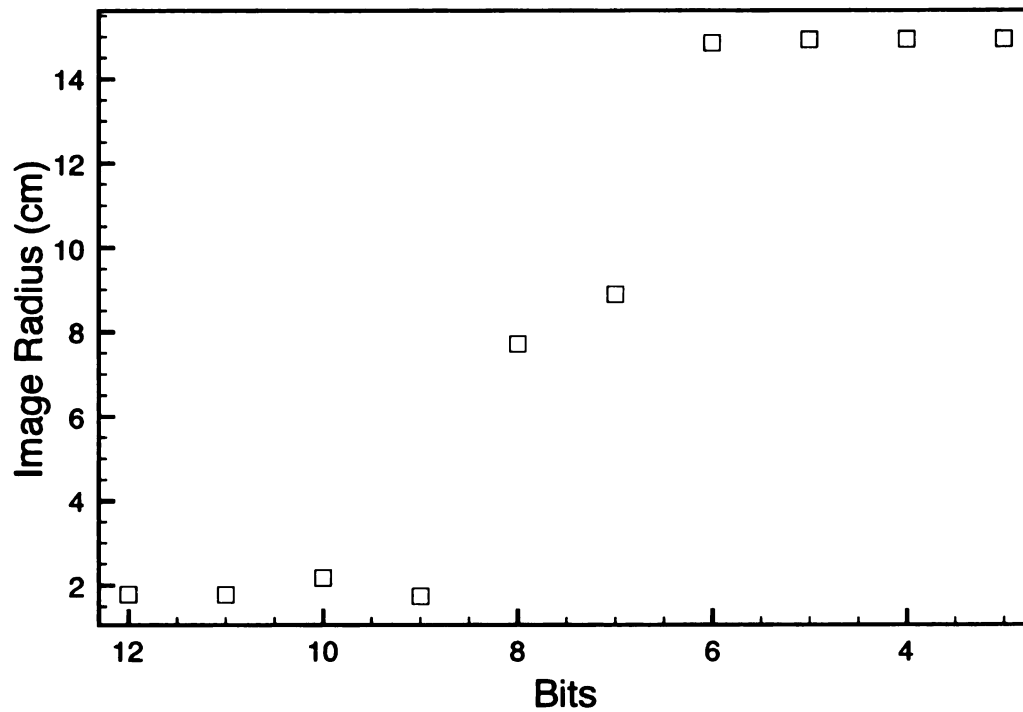


Figure 4.34: Effect of digitization on image radius.

As seen in the figure there are two jumps in image radius. From 12 to 9 bits

the constant image radius results from the conducting strip peak intensity values not being effected by the rounding into bins. The jumps between 9 and 8 bits, and 7 and 6 bits result from a threshold bit value where the peak values now round poorly into large bin sizes. From 7 to 2 bits the image radius is so high that decreasing the bits can not decrease the image quality anymore. The subtle changes in intensity become lost and soon, as seen in Figure 4.44, the strip completely disappears into the background. This results from having too few bits to differentiate between the strip intensity and the background. However, it is interesting to note that the ghost images of the strip are actually removed from the image with decreasing bit numbers since these weaker artifacts fall into the first bin.

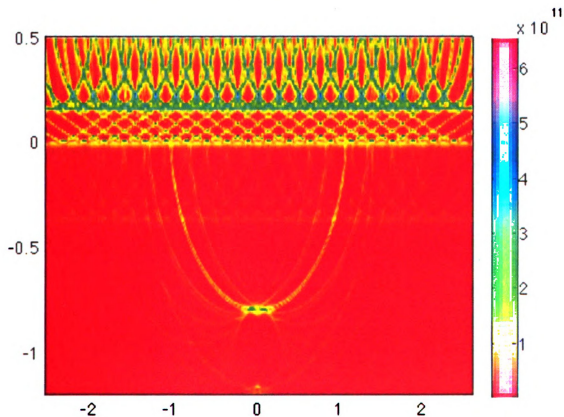


Figure 4.35: Conducting strip image constructed using the number of bits = 12.

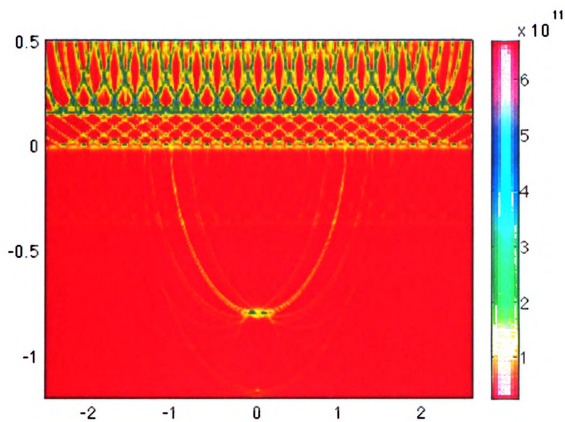


Figure 4.36: Conducting strip image constructed using the number of bits = 11.

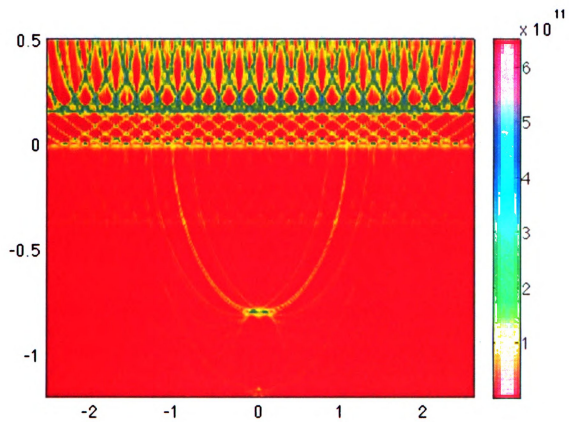


Figure 4.37: Conducting strip image constructed using the number of bits = 10.

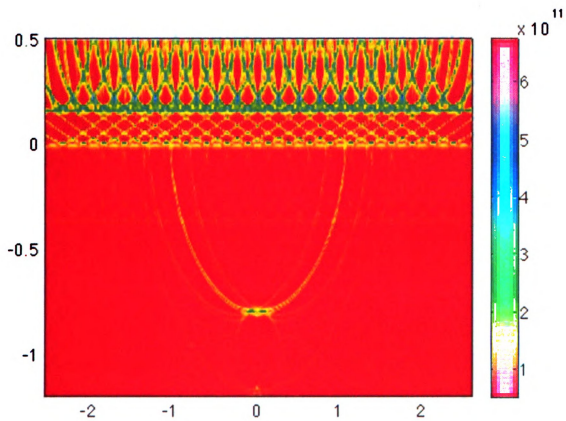


Figure 4.38: Conducting strip image constructed using the number of bits = 9.

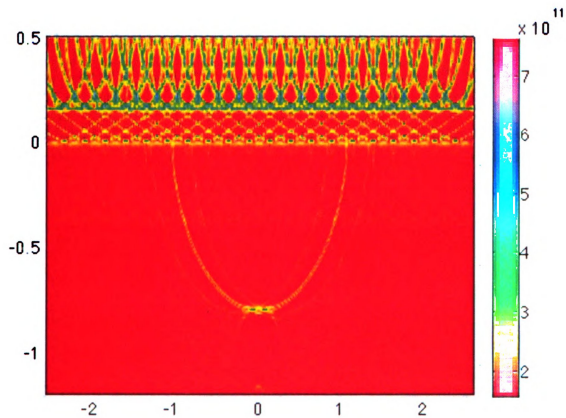


Figure 4.39: Conducting strip image constructed using the number of bits = 8.

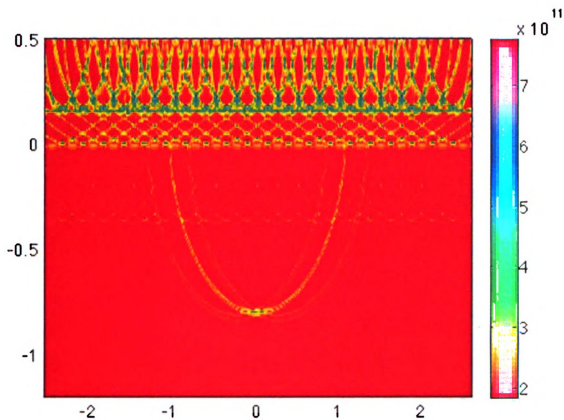


Figure 4.40: Conducting strip image constructed using the number of bits = 7.

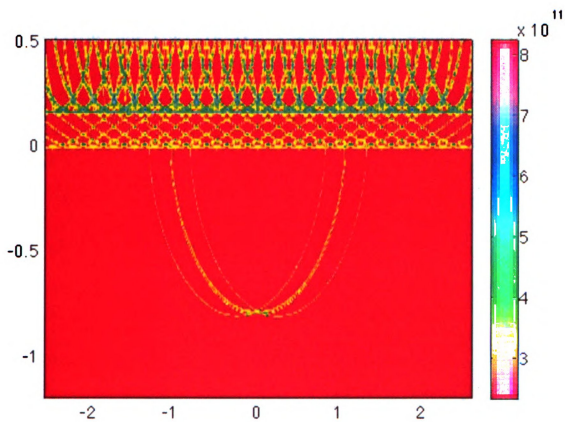


Figure 4.41: Conducting strip image constructed using the number of bits = 6.

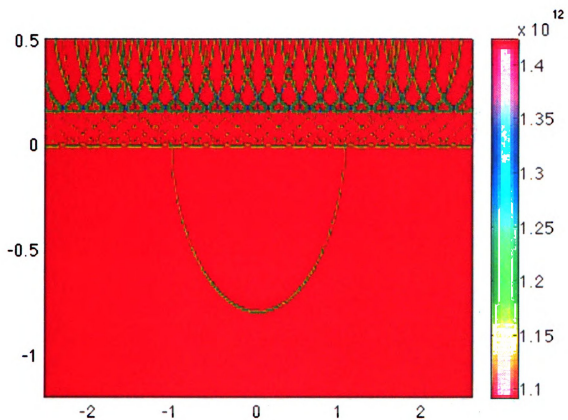


Figure 4.42: Conducting strip image constructed using the number of bits = 5.

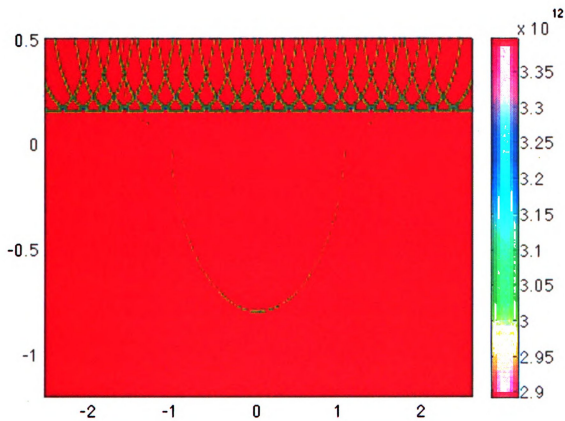


Figure 4.43: Conducting strip image constructed using the number of bits = 4.

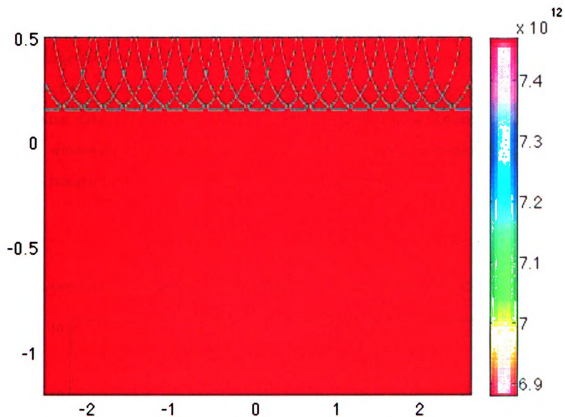


Figure 4.44: Conducting strip image constructed using the number of bits = 3.

4.2 Frequency Domain Analysis

The important parameters concerning the frequency domain radar system are bandwidth (equivalent to pulse width in the time domain system), sample rate, SNR, and digitization. The effect of these parameters on image quality is investigated by manipulating the simulated frequency domain data before the inverse Fourier transform is taken.

4.2.1 Bandwidth

Increasing the bandwidth of a stepped-frequency radar system increases the resolution of the images generated by the system. To investigate this effect with the simulated data, the frequency domain data is multiplied by a Gaussian modulated cosine windowing function centered on 8 GHz. The equivalent frequency pulse width, τ , is changed to determine the bandwidth, Ω , as given by

$$\Omega = \frac{1}{\pi\tau} 4 \ln 2. \quad (4.3)$$

The dependence of image radius on bandwidth is shown in Figure 4.45.

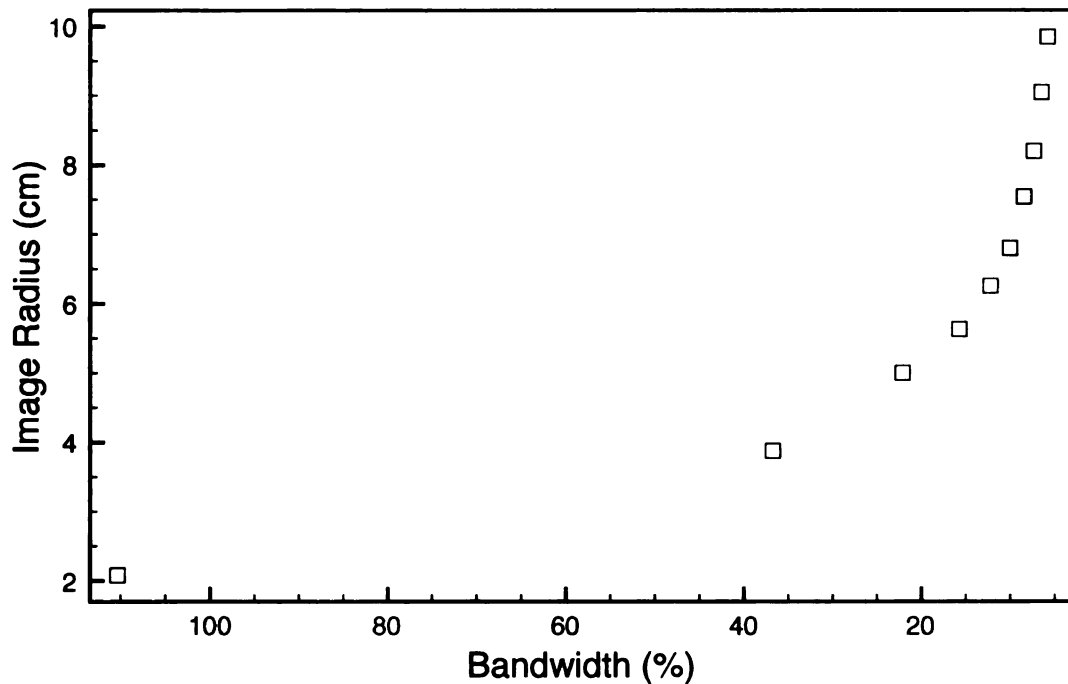


Figure 4.45: Effect of digitization on image radius.

The following figures show the decrease in image quality as the bandwidth increases. Following the progression through each of the images, the conducting strip and the lossy dielectric slab become progressively unclear. When the bandwidth is

at 5.81%, as seen in Figure 4.55, the conducting strip is nearly indiscernible from the background; this makes locating the object behind the lossy dielectric slab almost impossible.

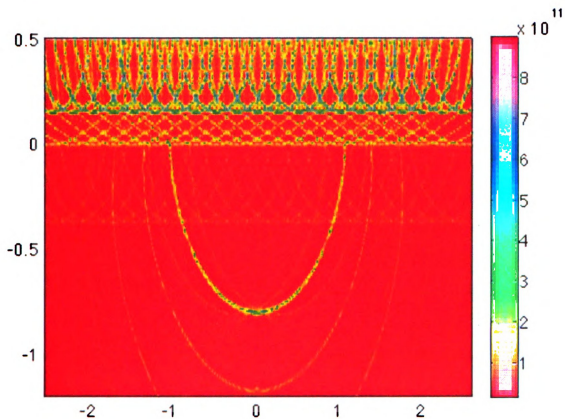


Figure 4.46: Conducting strip image constructed using a bandwidth = 110.38%.

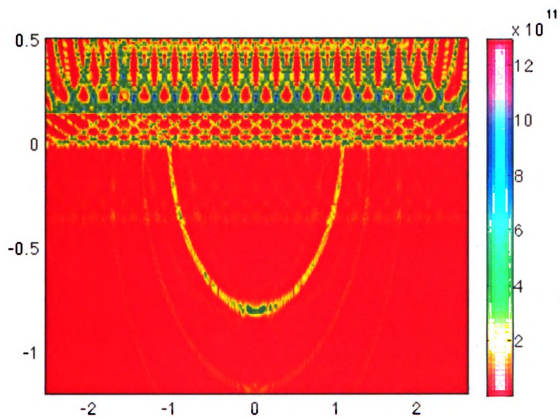


Figure 4.47: Conducting strip image constructed using a bandwidth = 36.75%.

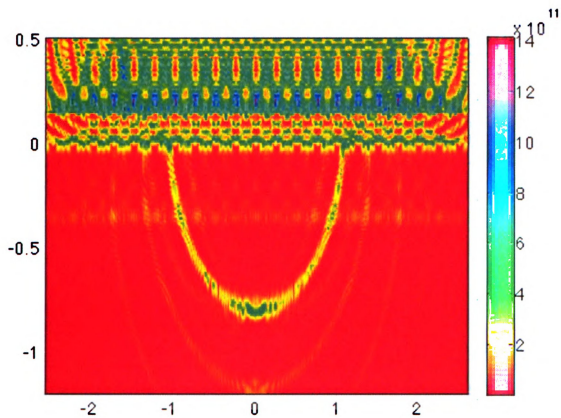


Figure 4.48: Conducting strip image constructed using a bandwidth = 22.13%.

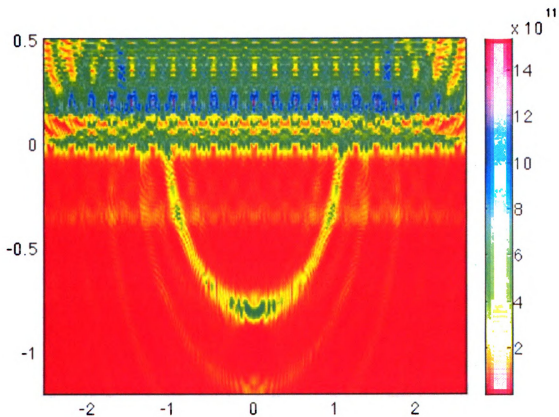


Figure 4.49: Conducting strip image constructed using a bandwidth = 15.76%.

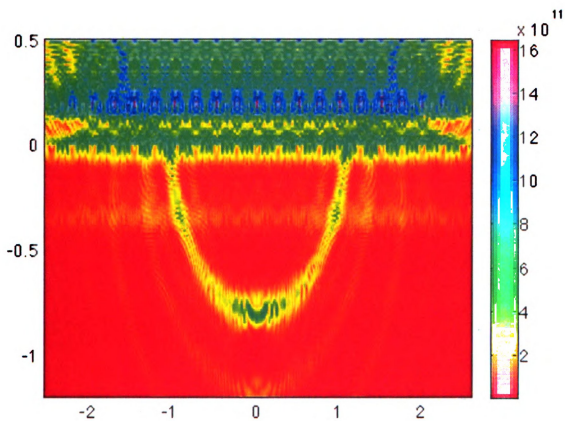


Figure 4.50: Conducting strip image constructed using a bandwidth = 12.26%.

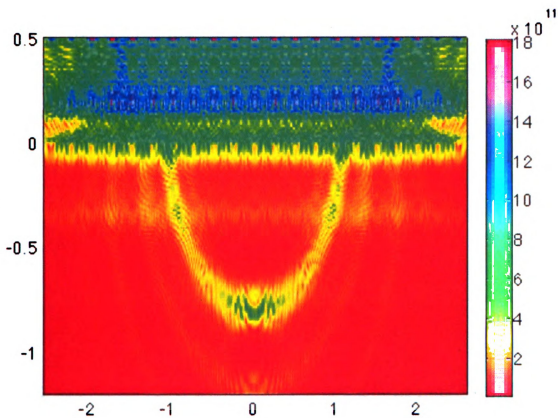


Figure 4.51: Conducting strip image constructed using a bandwidth = 10.03%.

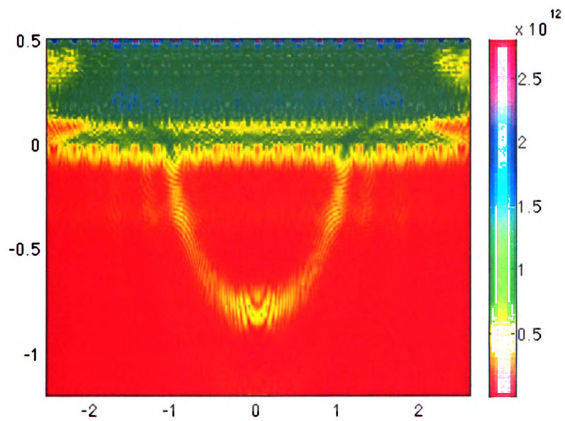


Figure 4.52: Conducting strip image constructed using a bandwidth = 8.49%.

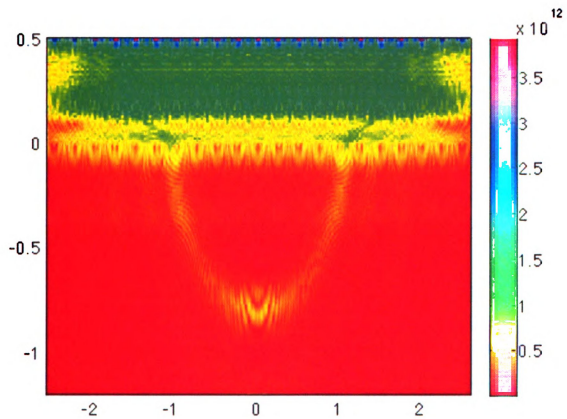


Figure 4.53: Conducting strip image constructed using a bandwidth = 7.35%.

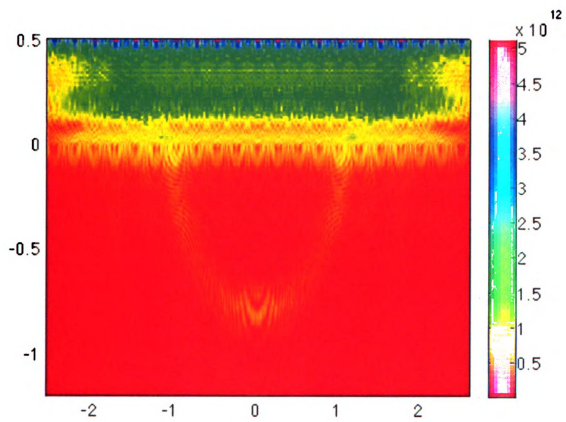


Figure 4.54: Conducting strip image constructed using a bandwidth = 6.49%.

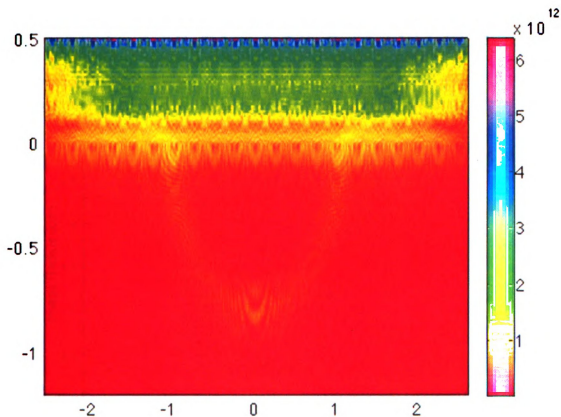


Figure 4.55: Conducting strip image constructed using a bandwidth = 5.81%.

4.2.2 Sampling Rate

In a frequency domain system, inadequate sample rate is the main cause of aliasing. When the data is sampled at too large a frequency step size, the transformed time domain data wraps around such that later events overlap with earlier events. This effect produces an image with scattering centers that should be separated in space, but instead overlap. To investigate the affect of aliasing on image quality, the frequency step size of the simulated data is increased and the images are formed. The start and stop frequency, 20 MHz to 16 GHz, remains the same in every case, but the number of data points within this band is changed. The resulting images are shown in Figures 4.57-4.62, and the computed image radius is shown in Figure 4.56. As the frequency

step size increases, the image radius widens and the image becomes blurrier. At a step size of 160 MHz (100 samples) the conducting strip is lost completely and therefore no image radius is available.

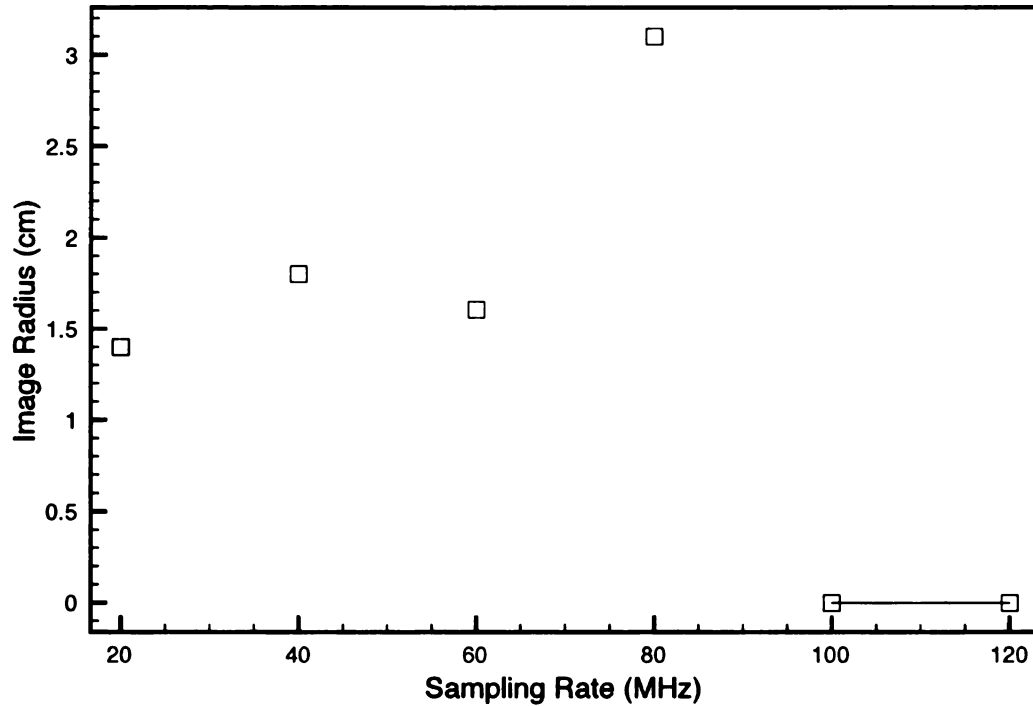


Figure 4.56: Effect of sampling rate on image radius.

As seen in the figures, artifacts become more prominent as the sample step size is increased. In Figure 4.58 the ghost of the strip is brighter, which could result in false identification of another conducting strip. Figure 4.60 shows multiple artifacts around the conducting strip creating background noise and producing a larger image radius. The conducting strip is completely blends into the background in Figures 4.61 and 4.62.

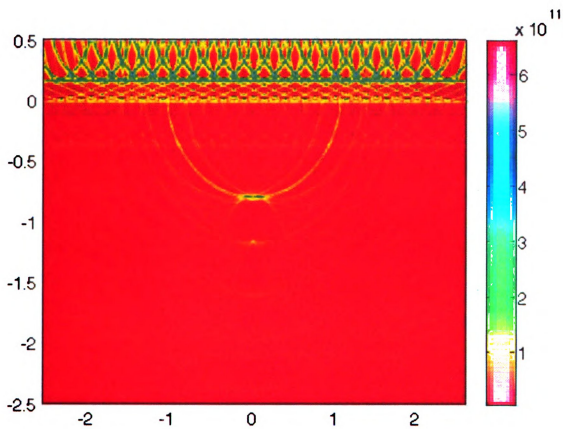


Figure 4.57: Conducting strip image constructed using a sampling rate of $\Delta f = 20$ MHz.

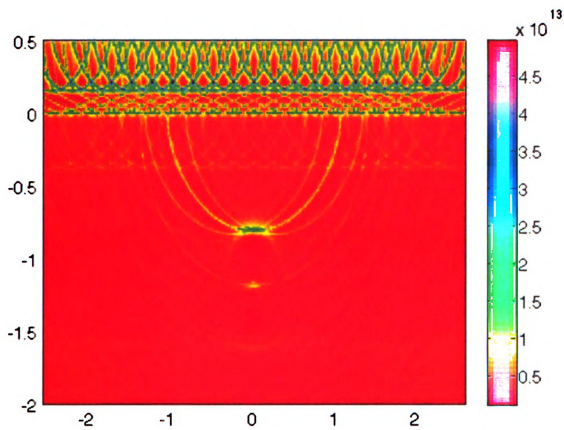


Figure 4.58: Conducting strip image constructed using a sampling rate of $\Delta f = 40$ MHz.

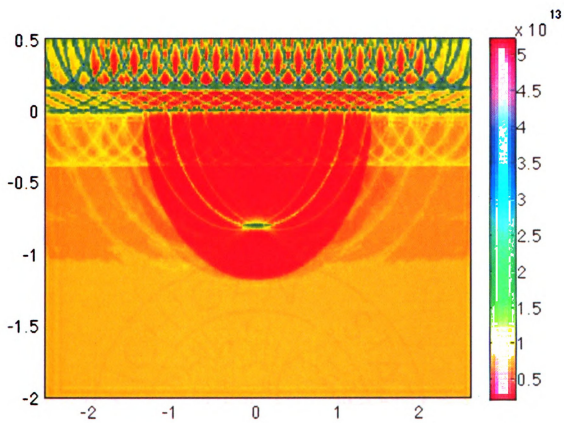


Figure 4.59: Conducting strip image constructed using a sampling rate of $\Delta f = 60$ MHz.

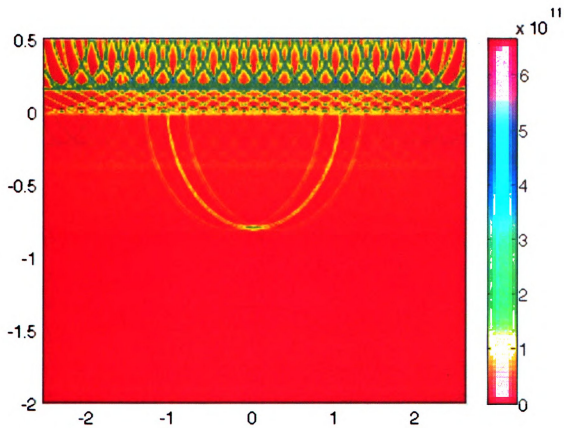


Figure 4.60: Conducting strip image constructed using a sampling rate of $\Delta f = 80$ MHz.

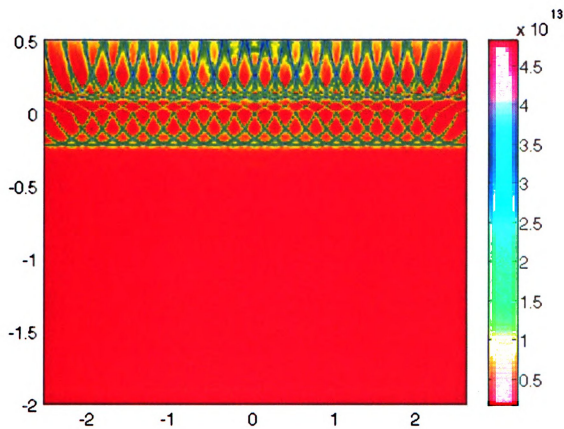


Figure 4.61: Conducting strip image constructed using a sampling rate of $\Delta f = 100$ MHz.

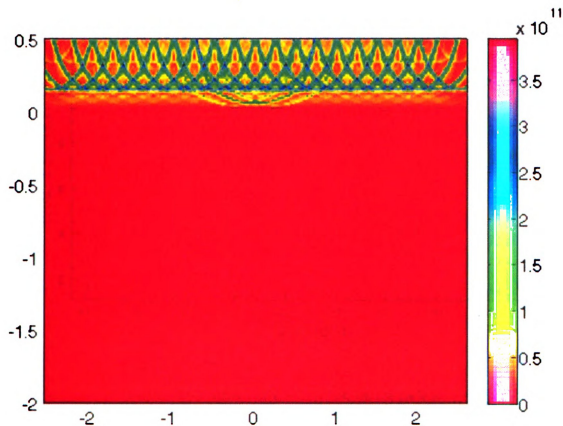


Figure 4.62: Conducting strip image constructed using a sampling rate of $\Delta f = 120$ MHz.

4.2.3 Signal-to-Noise Ratio

The same SNR issues seen with time domain data can occur in the frequency domain. To investigate the effect of SNR on images created using frequency-domain data, white Gaussian noise was added directly in the frequency domain using the program WaveCalc. In this case, the SNR is defined as the ratio of signal power to noise power (as opposed to a ratio of amplitudes as in the time domain). Figure 4.63 shows the dependence of image radius on SNR.

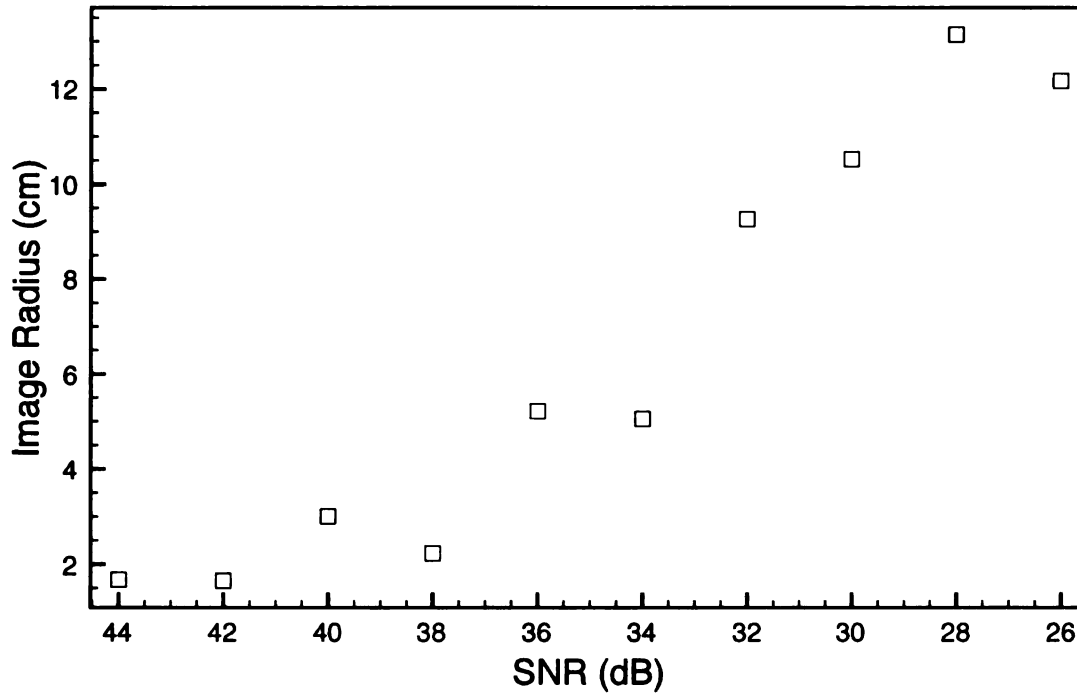


Figure 4.63: Effect of the SNR on image radius.

This graph shows that image radius increases with decreasing SNR. Some discrepancies exist wherein the image radius decreases with the decrease of SNR. This may result from a wrong threshold value or a rogue peak of intensity showing up in the noise. Figures 4.64 - 4.73 show the images created with various values of SNR. As expected, the presence of noise makes it difficult to locate the strip.

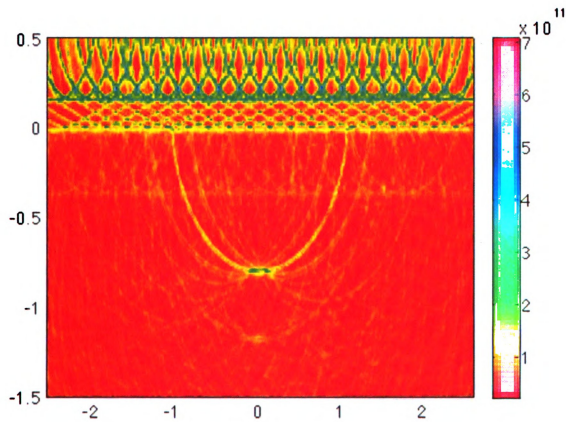


Figure 4.64: Conducting strip image constructed using a SNR = 44 dB.

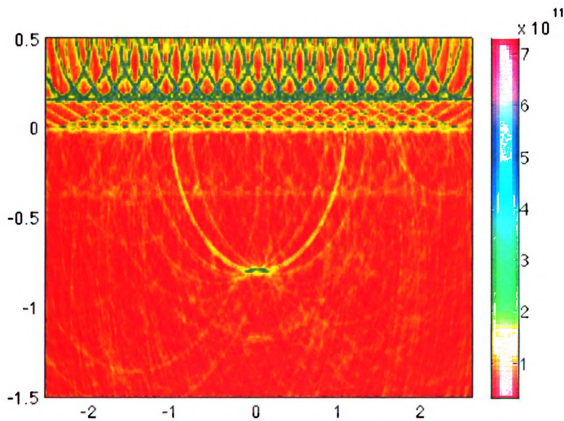


Figure 4.65: Conducting strip image constructed using a SNR = 42 dB.

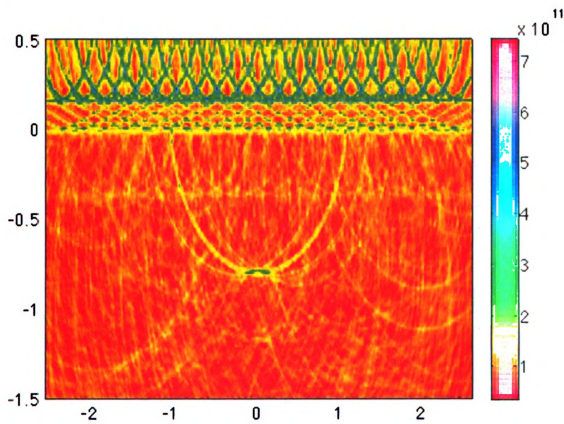


Figure 4.66: Conducting strip image constructed using a SNR = 40 dB.

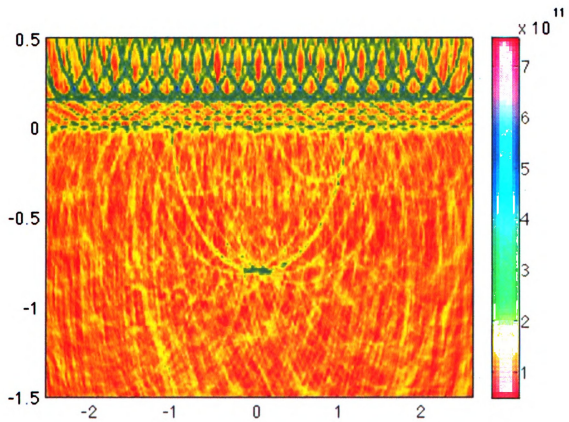


Figure 4.67: Conducting strip image constructed using a SNR = 38 dB.

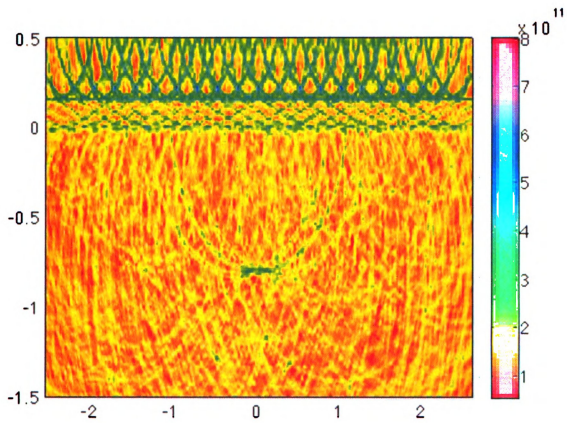


Figure 4.68: Conducting strip image constructed using a SNR = 36 dB.

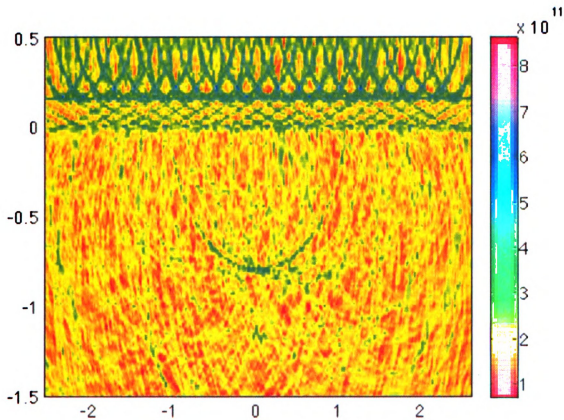


Figure 4.69: Conducting strip image constructed using a SNR = 34 dB.

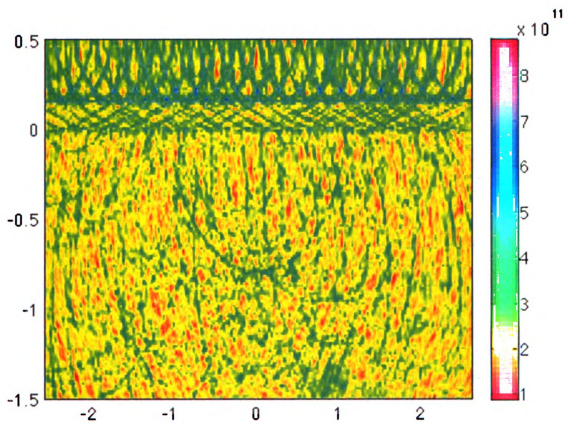


Figure 4.70: Conducting strip image constructed using a SNR = 32 dB.

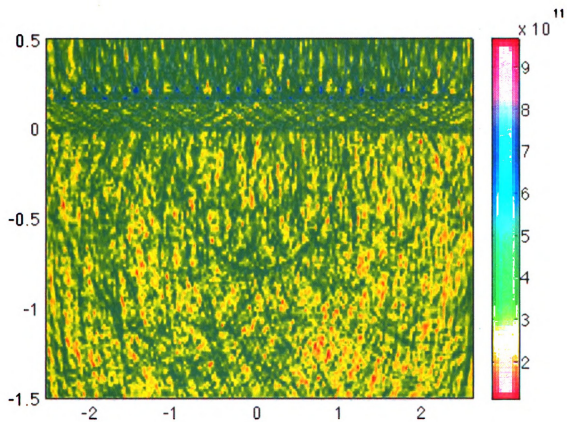


Figure 4.71: Conducting strip image constructed using a SNR = 30 dB.

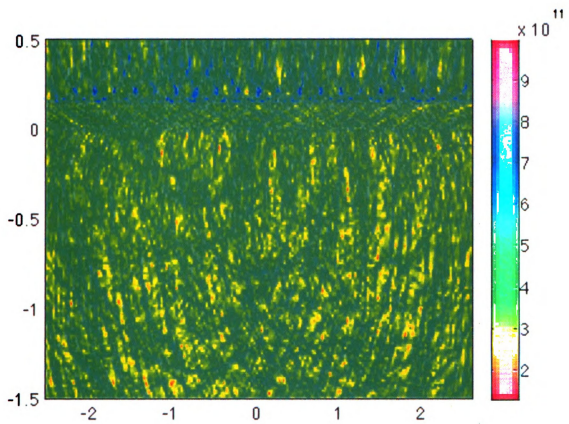


Figure 4.72: Conducting strip image constructed using a SNR = 28 dB.

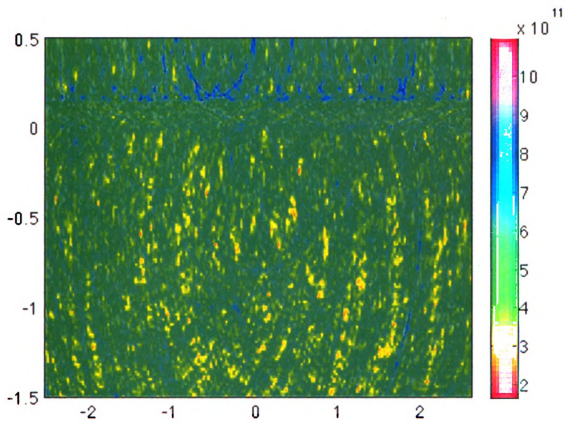


Figure 4.73: Conducting strip image constructed using a SNR = 26 dB.

4.2.4 Digitization

Digitization in a frequency domain system takes place directly in the frequency domain. To construct the images, the data is transformed into the time domain. An important consideration is that in a frequency domain system, the reflection from the target cannot be separated from the flash in the front of the barrier, as it can in a time domain system (by using a time window). Thus, the target signal may have a larger discretization error than with the time domain system.

Digitizing is done exactly as in the time domain, by assigning data to discrete bins. The signals are moved into bins depending on the bin size described in (4.2), and digitized based on (4.1). Figure 4.74 shows the image radius as a function of the

number of bits used to represent the data. Figures 4.75 - 4.85 show the images for various numbers of bits used.

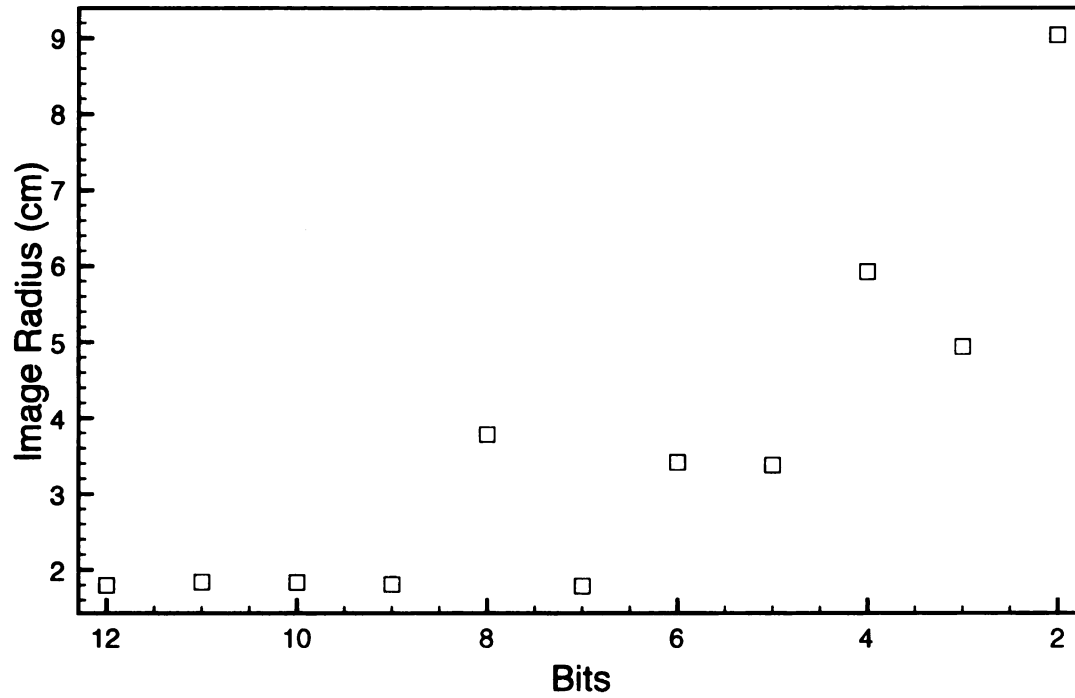


Figure 4.74: Effect of digitization on image radius.

A different type of blurring is seen than was observed with the digitization of the time-domain data, and the target can just barely be distinguished with a discretization of 4 bits.

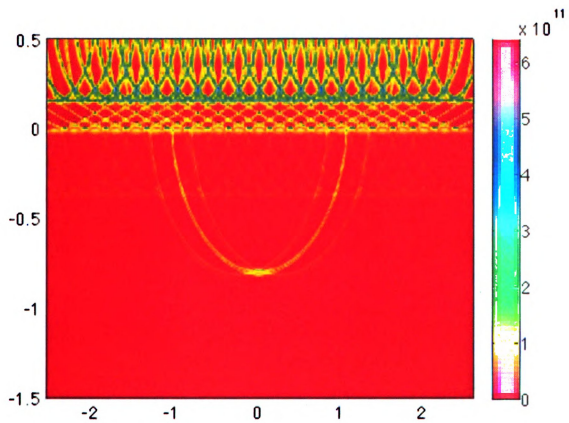


Figure 4.75: Conducting strip image constructed using the number of bits = 12.

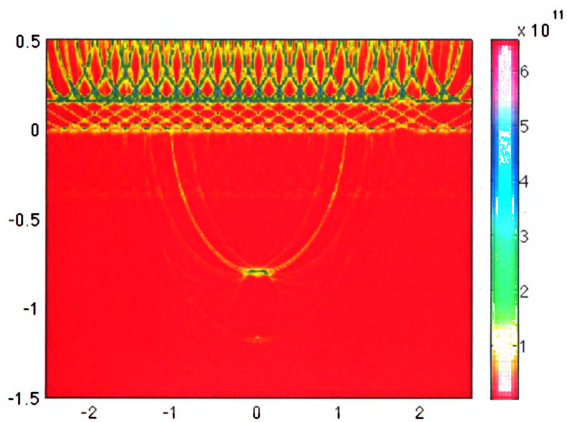


Figure 4.76: Conducting strip image constructed using the number of bits = 11.

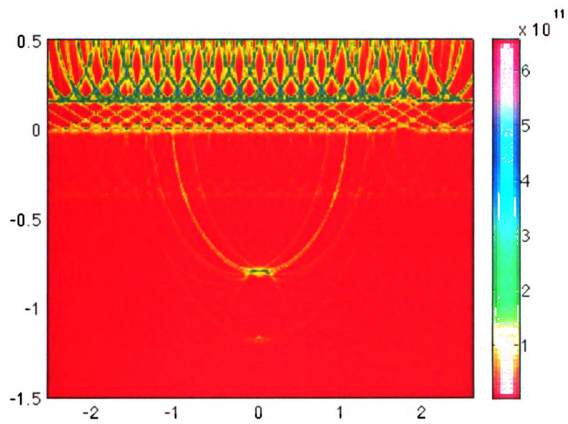


Figure 4.77: Conducting strip image constructed using the number of bits = 10.

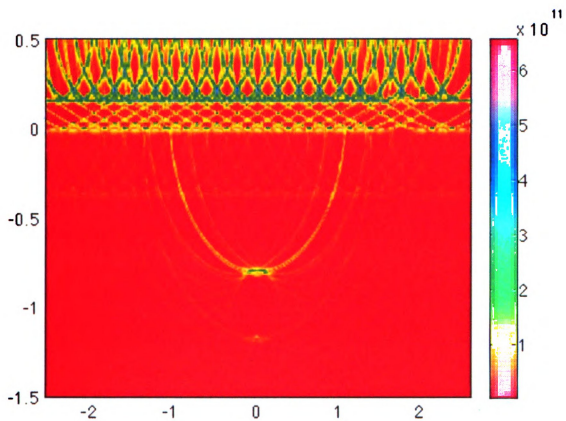


Figure 4.78: Conducting strip image constructed using the number of bits = 9.

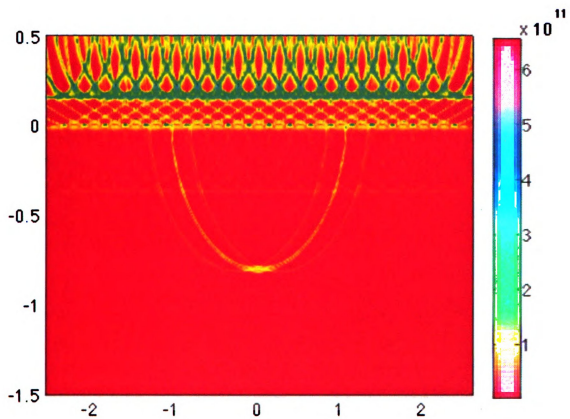


Figure 4.79: Conducting strip image constructed using the number of bits = 8.

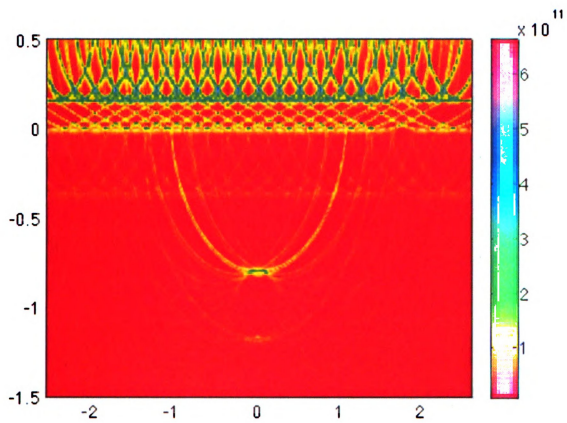


Figure 4.80: Conducting strip image constructed using the number of bits = 7.

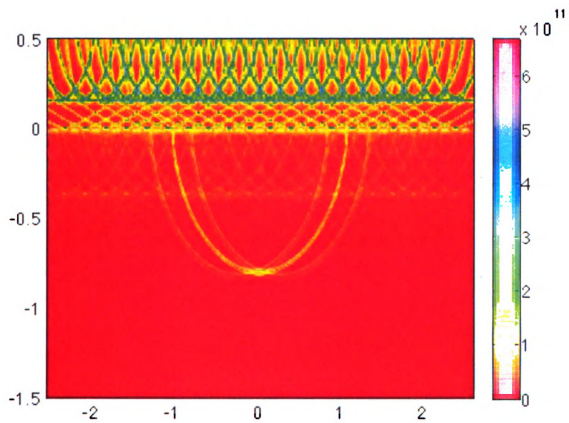


Figure 4.81: Conducting strip image constructed using the number of bits = 6.

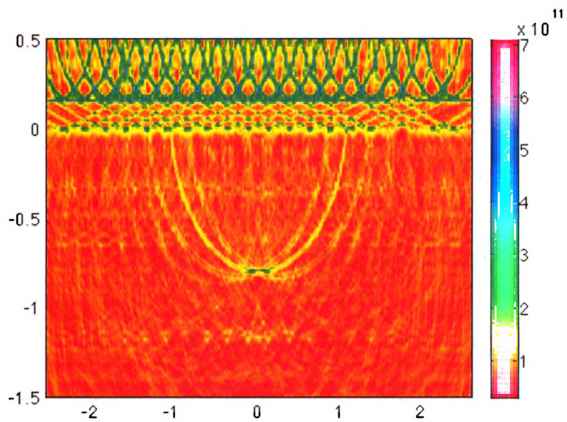


Figure 4.82: Conducting strip image constructed using the number of bits = 5.

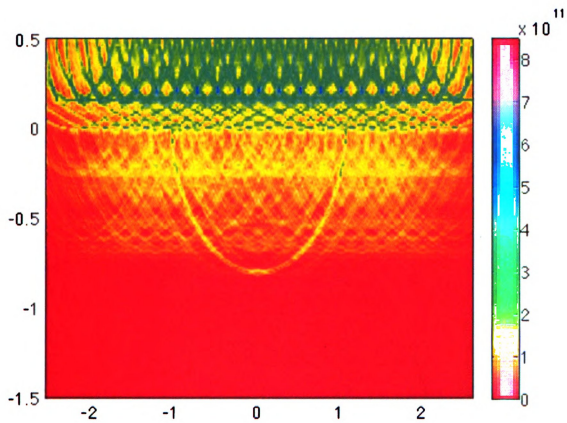


Figure 4.83: Conducting strip image constructed using the number of bits = 4.

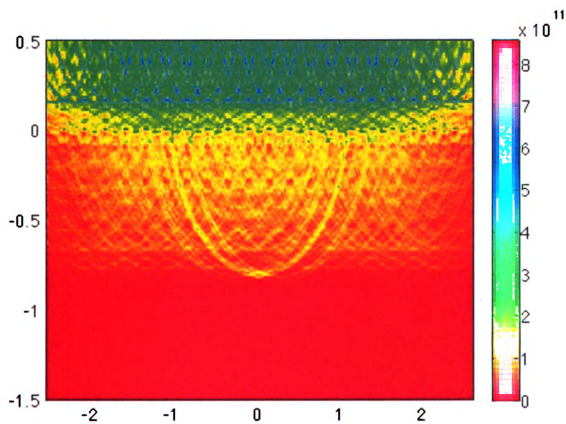


Figure 4.84: Conducting strip image constructed using the number of bits = 3.

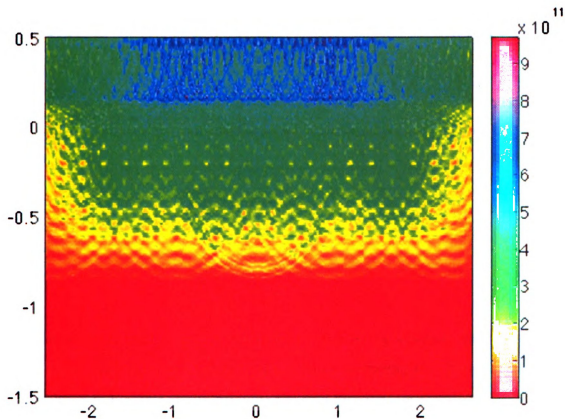


Figure 4.85: Conducting strip image constructed using the number of Bits = 2.

4.3 Two Conducting Strips

The parameter analysis is continued to compare the performance of the ultra-wide band short-pulse and stepped frequency radar systems when imaging multiple targets. Simulated data is computed at 21 different transmitter/receiver positions, images are created for different parameter sets and the sharpness of each image is analyzed. As seen in Figure 4.86, the multiple targets used are two conducting strips.

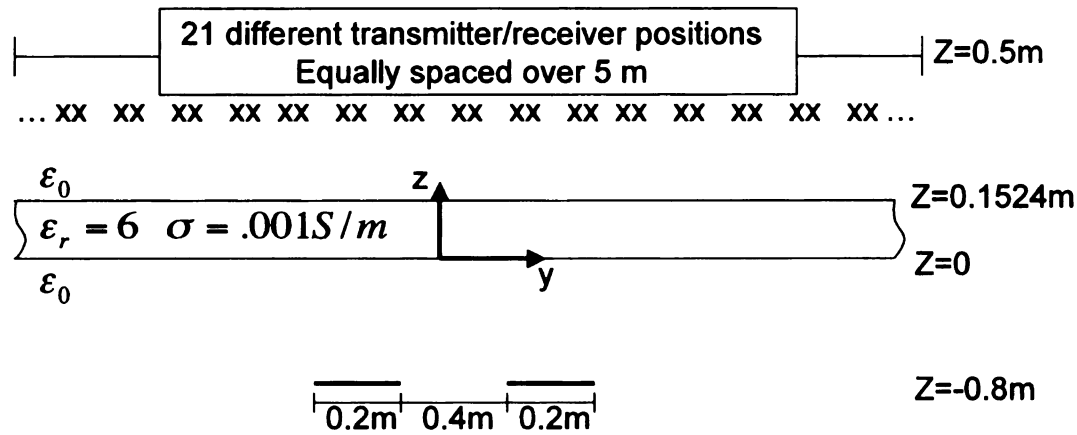


Figure 4.86: Parameters of two conducting strip study

The program used to compute the field scattered by a single conducting strip needs to be modified only slightly to accommodate scattering by the two conducting strips shown in Figure 4.86. To compute the field scattered by the two strips, a large conducting strip of 0.80 m is first used to fill the A_{mn} and b_{mn} matrices of equations (2.159) and (2.149). Then the entries corresponding to the 0.4 m gap between the two strips are removed from these two matrices by replacing the stored values with zeros. This models two strips of 0.2 m in length, separated by a gap of 0.4 m .

The scattered field from the two conducting strips is found by first solving the matrix equation (2.148). The solution is the complex current at each partition on the two conducting strips. The total field is then determined at the receiver positions by adding the scattered field from the known current on the conducting strips to the incident field.

When the pulse width is altered in both the frequency and time domain, the image radius changes for both conducting strips allowing for optimization of these parameters in an actual prototype. Only the pulse width in the time domain and the bandwidth in the frequency domain is examined in this section for multiple targets.

4.3.1 Pulse Width

With the geometry parameters of Figure 4.86, values of the computed image radii are shown in Figure 4.87.

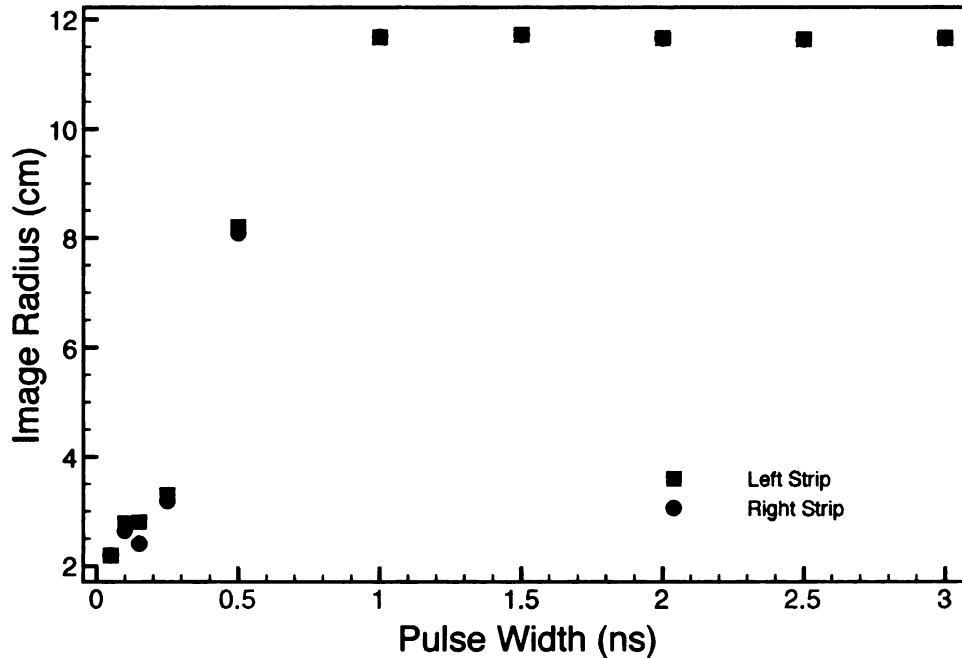


Figure 4.87: Effect of pulse width on image radius of two conducting strips.

This figure demonstrates that increasing the pulse width enlarges the image radii which corresponds to an increase in the blurring of the strips. The left and right strips both increase with similar tendencies as the pulse width expands. The images of the different pulse widths are displayed in Figures 4.88- 4.97. When the pulse width reaches 0.5 ns, shown in Figure 4.92, the conducting strips blend together becoming one large conducting strip. Thus, a pulse width of less than 0.5 ns is needed to resolve these multiple targets. In Figure 4.94, where the pulse width is 1.5 ns, the image of the conducting strips start to blur into the background. The size, position, intensity, and shape of the strips cannot be determined when the pulse width is larger than 1.5 ns.

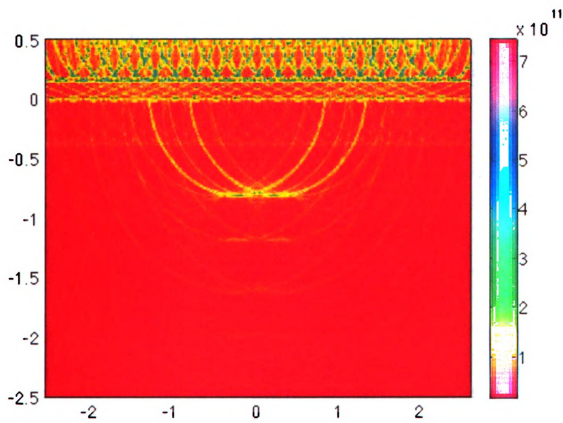


Figure 4.88: Two conducting strip image constructed using a pulse width of $\tau = 0.05$ ns

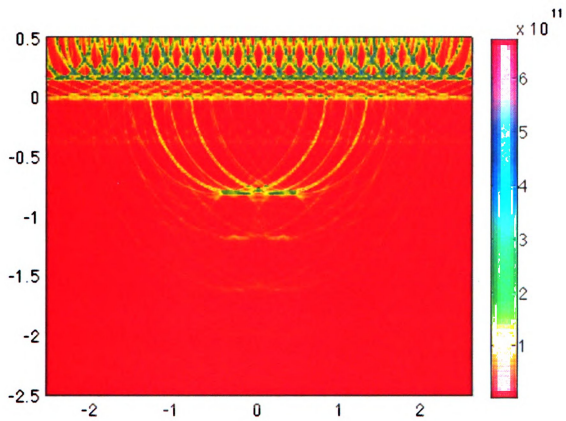


Figure 4.89: Two conducting strip image constructed using a pulse width of $\tau = 0.10$ ns

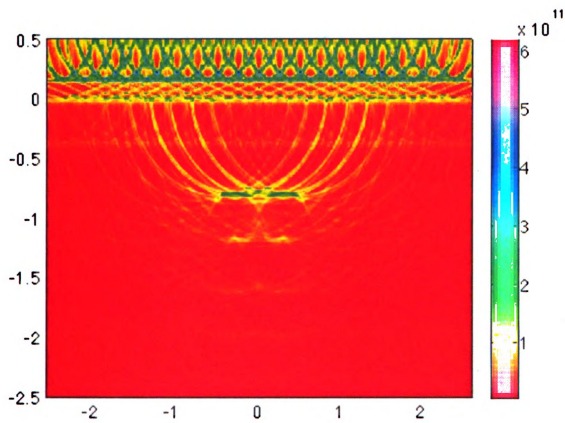


Figure 4.90: Two conducting strip image constructed using a pulse width of $\tau = 0.15$ ns

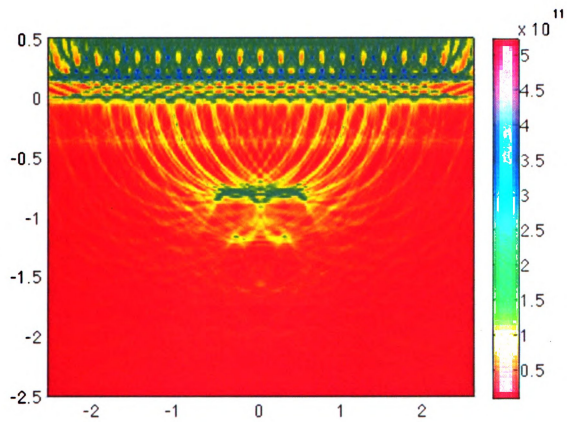


Figure 4.91: Two conducting strip image constructed using a pulse width of $\tau = 0.25$ ns

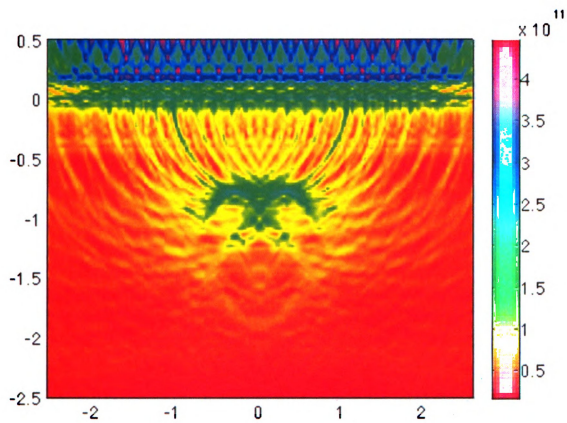


Figure 4.92: Two conducting strip image constructed using a pulse width of $\tau = 0.50$ ns

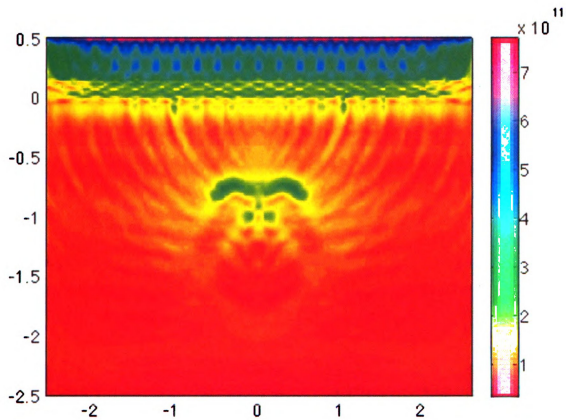


Figure 4.93: Two conducting strip image constructed using a pulse width of $\tau = 1.00$ ns

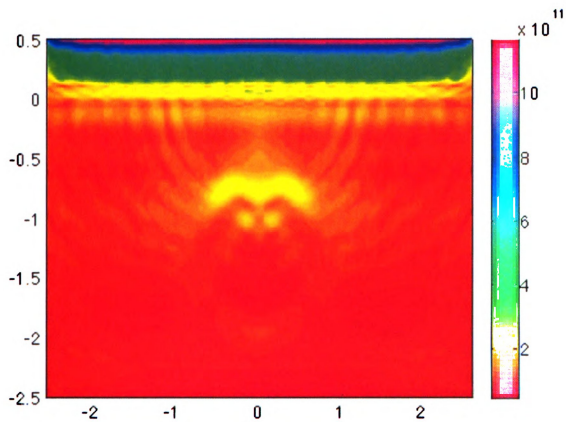


Figure 4.94: Two conducting strip image constructed using a pulse width of $\tau = 1.50$ ns

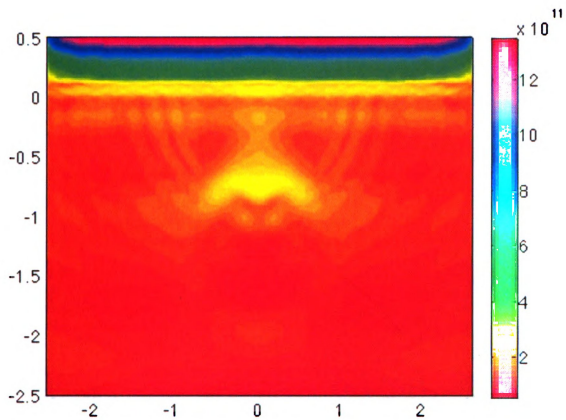


Figure 4.95: Two conducting strip image constructed using a pulse width of $\tau = 2.00$ ns

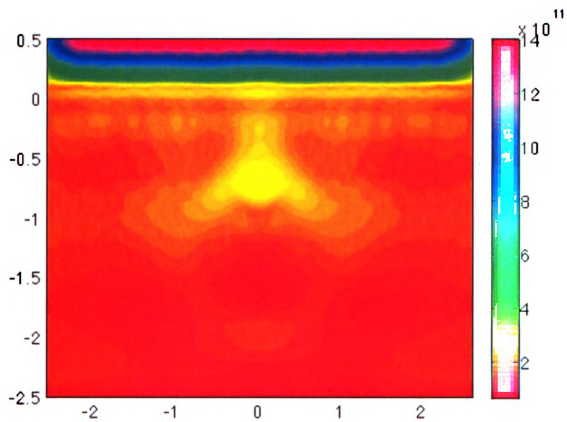


Figure 4.96: Two conducting strip image constructed using a pulse width of $\tau = 2.5$ ns

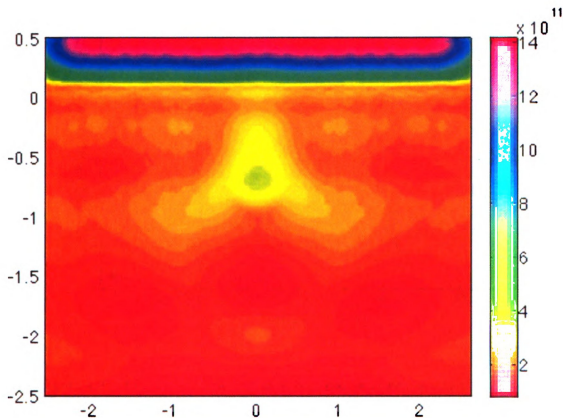


Figure 4.97: Two conducting strip image constructed using a pulse width of $\tau = 3.00$ ns

4.3.2 Bandwidth

As stated before, increasing the bandwidth of a stepped-frequency radar system increases the resolution of the generated images. The dependence of image radii on bandwidth for the two conducting strips is shown in Figure 4.98. Since the conducting strips are positioned symmetrically about the z -axis, the image radii seen in Figure 4.98 increase almost at the same rate. As the bandwidth gets smaller the image radius increases causing blurriness for the targets.

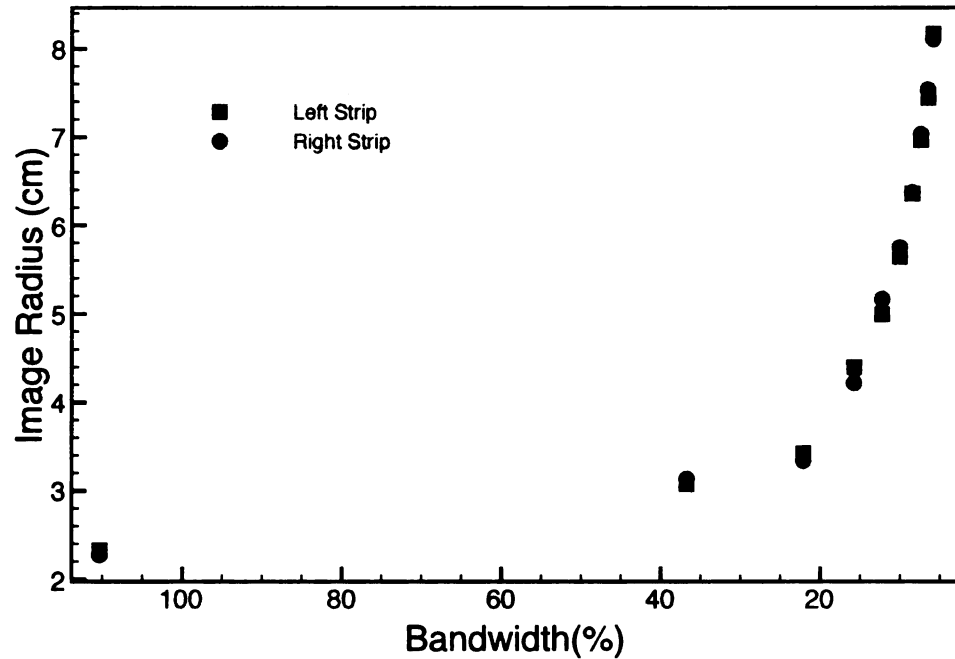


Figure 4.98: Effect of bandwidth on image radius of two conducting strips.

Figures 4.99 - 4.108 show the decrease in image quality as the bandwidth increases. Following the progression through each of the images, the conducting strips and the barrier become progressively unclear. When the bandwidth is at 22.13%, as seen in Figure 4.101, the conducting strips are nearly indiscernible from one another; this makes locating the separate objects almost impossible. At a bandwidth of 8.81%, as shown in Figure 4.108, the two conducting strips have almost completely blended into the background.

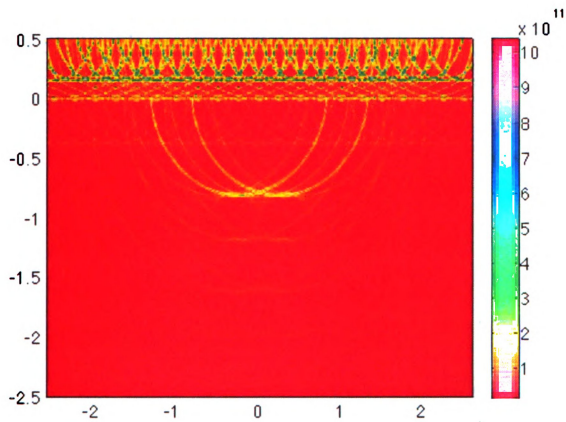


Figure 4.99: Two conducting strip image constructed using a bandwidth of 110.38%

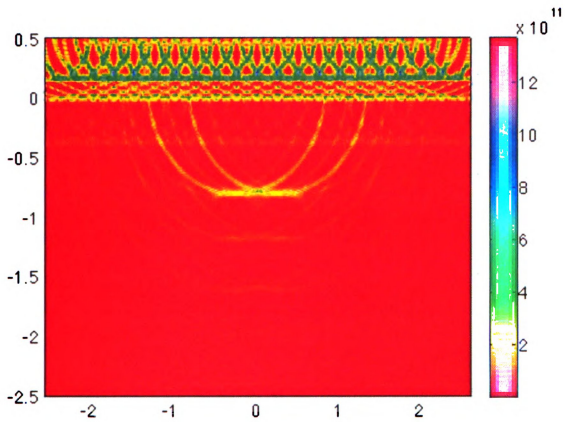


Figure 4.100: Two conducting strip image constructed using a bandwidth of 36.75%

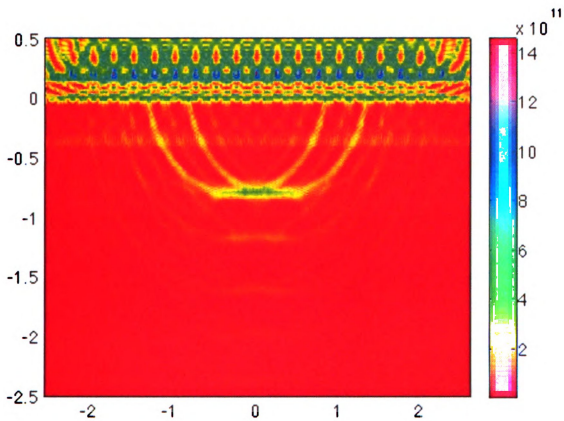


Figure 4.101: Two conducting strip image constructed using a bandwidth of 22.13%

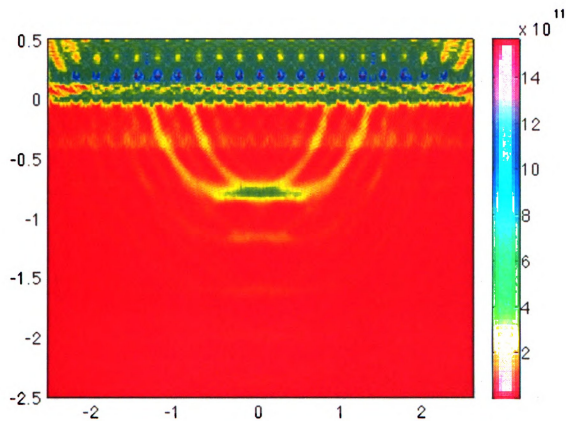


Figure 4.102: Two conducting strip image constructed using a bandwidth of 15.76%

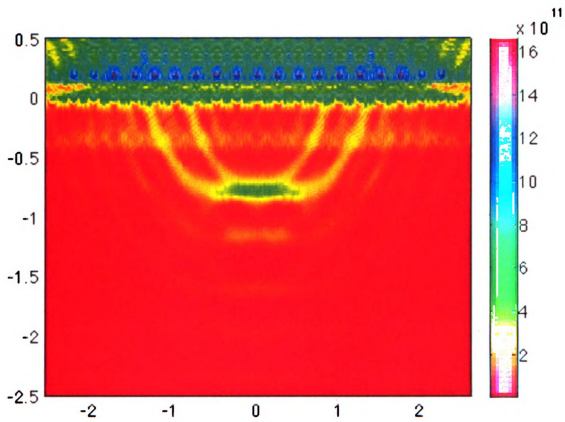


Figure 4.103: Two conducting strip image constructed using a bandwidth of 12.26%

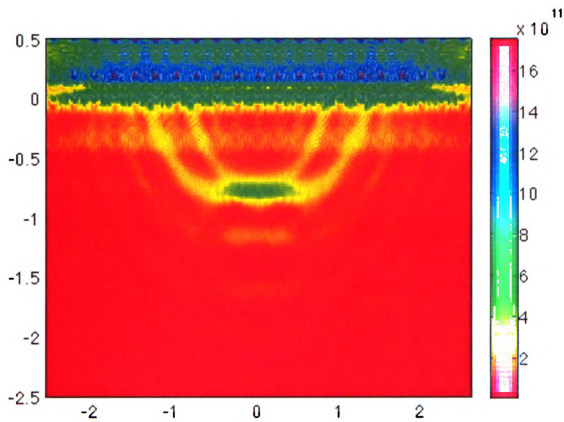


Figure 4.104: Two conducting strip image constructed using a bandwidth of 10.03%

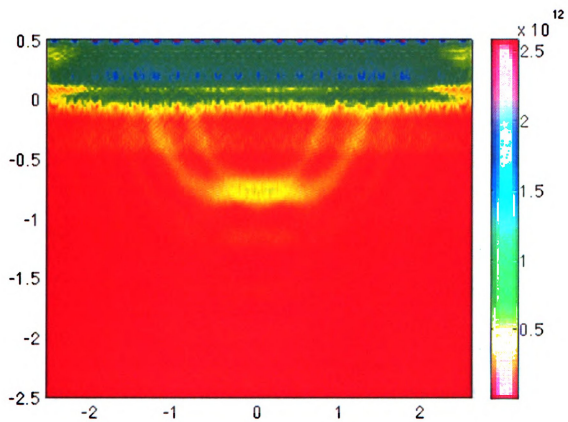


Figure 4.105: Two conducting strip image constructed using a bandwidth of 8.49%

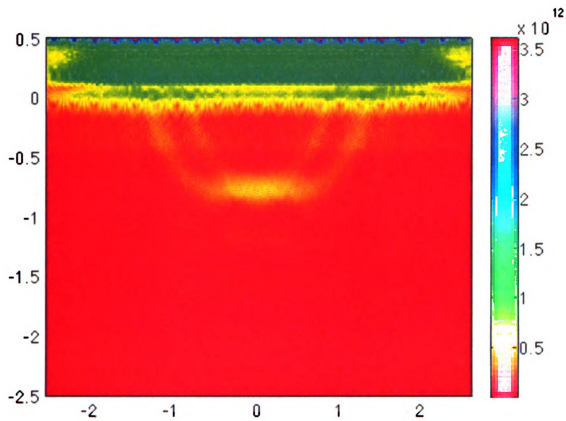


Figure 4.106: Two conducting strip image constructed using a bandwidth of 7.38%

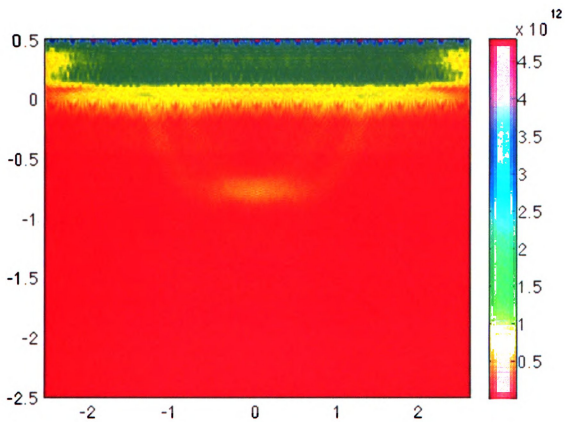


Figure 4.107: Two conducting strip image constructed using a bandwidth of 6.49%

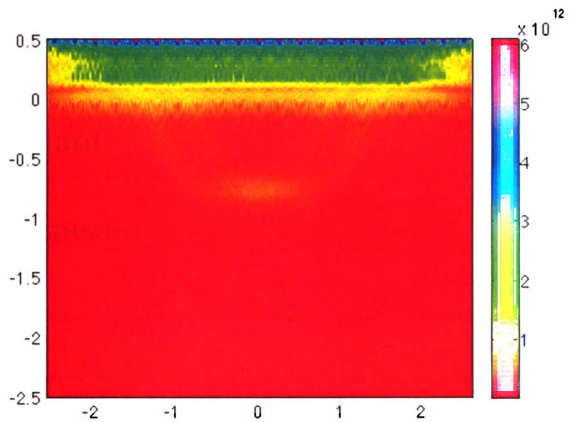


Figure 4.108: Two conducting strip image constructed using a bandwidth of 5.81%

Chapter 5

Experiment

A time-domain laboratory system [16] was constructed to investigate whether the image techniques used with simulated data in the parameter study can be replicated in practice. The laboratory system is not a dedicated radar, but rather uses standard instrumentation .

This time-domain data was acquired using the MSU reflectivity arch range. This arch range consists of two horn antennas, which can be arbitrarily located on an arch of 20 ft in diameter. As seen in Figure 5.1, the transmitting and receiving wideband TEM-horn antennas remain stationary while the barrier and strip target are moved, providing equivalent results to moving the transmit/receive antenna pairs, as done with the simulated data, and thereby simulating a rail SAR. The transmitting and receiving antennas are American Electronic Laboratories H-1498 TEM horns each with a bandwidth of 2 to 18 GHz.

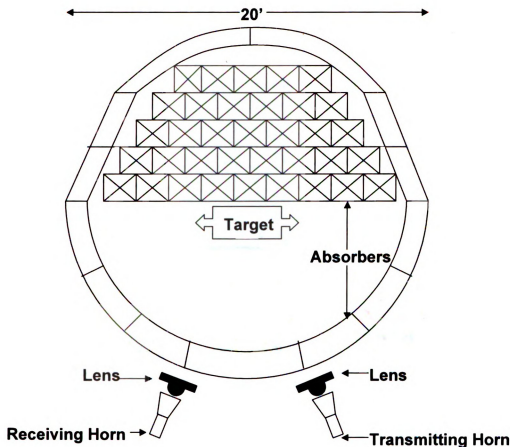


Figure 5.1: Geometry of arch-range scattering system at MSU.

5.1 Experiment Set up

A 4 ft by 8 ft barrier was constructed using 1/2 inch construction drywall mounted on pine wood of dimensions 2 inches by 4 inches. The barrier is able to roll by using small caster wheels. A conducting strip was constructed using a 2 in by 8 ft segment of aluminum tape applied to a low-density styrofoam column supported 2 ft behind the barrier. The time domain response is measured using a Hewlett Packard digital sampling oscilloscope (DSO) model HP54750A. As seen in Figure 5.2, this device has a time-domain-reflectometer/time-domain-transmission (TDR/TDT) plug-in module,

model HP54753A, which provides 20 GHz and 18 GHz channels for the oscilloscope.

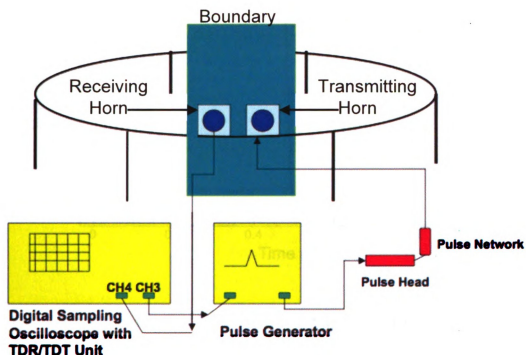


Figure 5.2: Time domain scattering measurement configuration.

This TDR/TDT device has an integrated step generator, which sends steps from channel 3 with a rise time of 45 ps and an amplitude of 200 mV. This unit triggers a step generator made by Picosecond Pulse Labs (PSPL), part number 4015B. A remote pulse head (PSPL 4015RPH) follows the pulse generator and creates another step. The step signal is sent into a PSPL 5208-DC pulse-generating network where a pseudo-Gaussian pulse signal is generated. This pulse, shown in Figure 5.3, is applied to the transmitting antenna.

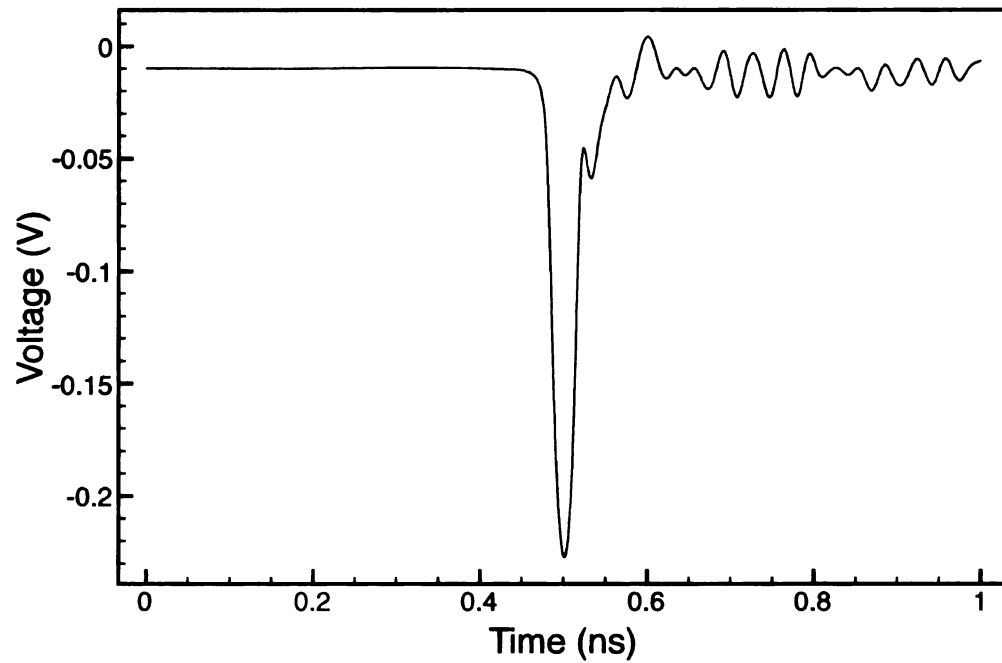


Figure 5.3: Pulse generated by the PSPL 5208-DC pulse generating network.

The frequency spectrum of the generated pulse can be determined by examining its Fourier transform, which is shown in Figure 5.4. It is seen that the pulse has a bandwidth of approximately 20 GHz.

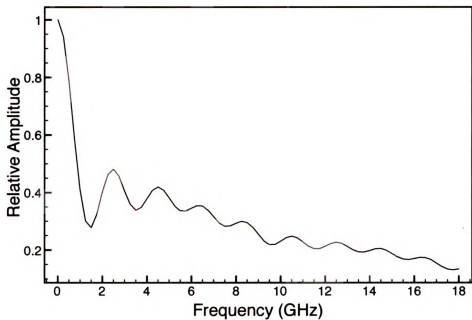


Figure 5.4: Spectrum of the generated pulse.

Although the antennas are positioned as close to one another as possible to simulate a monostatic set up, there still exists a bistatic angle of $\Theta_b = 14.2^\circ$. The position of the antennas with respect to the target is shown in Figure 5.5.

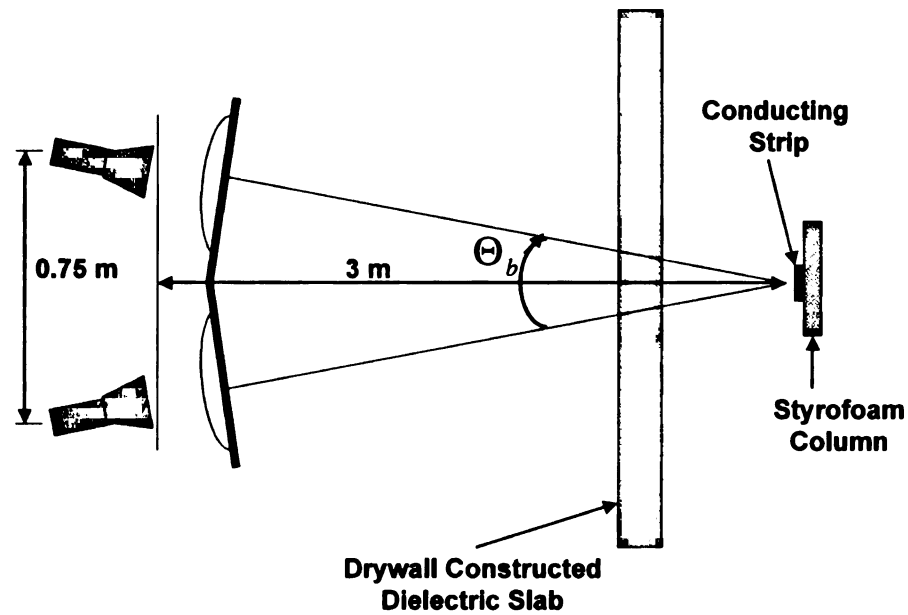


Figure 5.5: Location of transmitting and receiving antennas.

Channel 4 on the HP54753A is used to receive the signal by sampling the incoming voltage. A time window of 10 ns at 1 ns/div is used with 1024 sample points, giving a sample period of about 0.01 ns or an equivalent sample rate of 100 Gs/s. Note that this is significantly faster than the minimum required sample rate of 5 Gs/s identified in the parameter exploration section of this report. The sampled signal is average within the DSO 256 times to increase the SNR. The received signal is stored in a memory location in the DSO. Clutter is eliminated by also storing a measured background signal with no barrier or target present, which is subsequently subtracted from the target signal.

Target data was measured for 21 equally spaced barrier positions spread over a distance of 1.77 m, as shown in Figure 5.6.

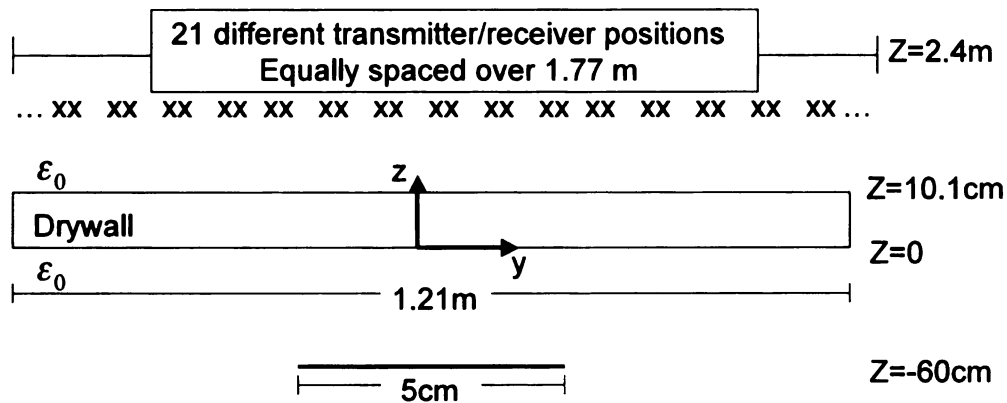


Figure 5.6: Experimental setup.

It is important to note that thermal drift of the instruments can disturb the results. Therefore, the equipment should warm up for a minimum of one hour before measurements are taken. Also, the equipment is vulnerable to electrostatic discharge. To eliminate this concern, one should always be grounded while taking measurements.

5.2 Experiment Calibration

The scattering measurements stored in the DSO are affected by the transfer functions of the antennas ($H_T(f)$, $H_R(f)$), the lenses ($H_{TL}(f)$, $H_{RL}(f)$), mutual interactions between the antennas ($H_A(f)$), interactions between the target and its surroundings ($H_{SC}(f)$), and arch-range clutter ($H_C(f)$). Therefore, a calibration procedure is necessary to recover the target response. A block diagram of the measurement system [17] is shown in Figure 5.7.

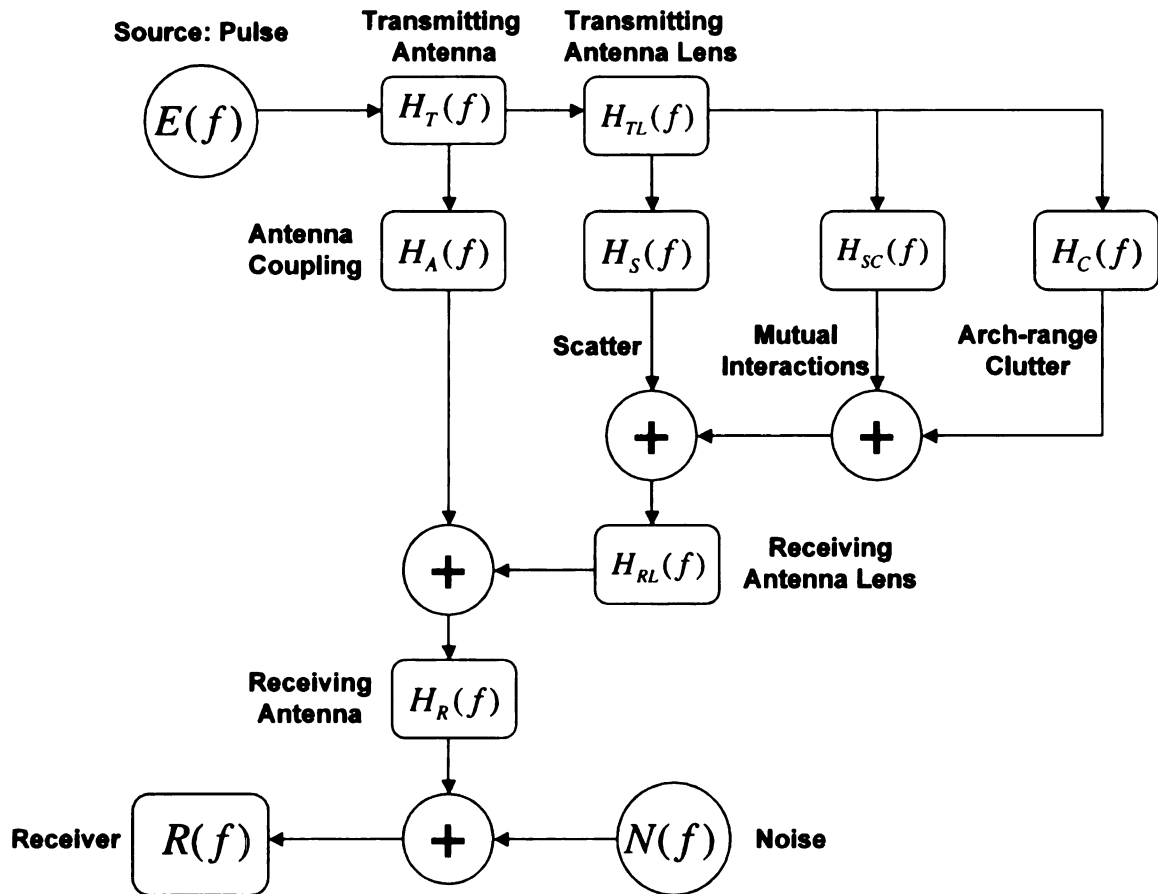


Figure 5.7: Block diagram model of measurement system.

From Figure 5.7 the waveform of an unknown target is formulated as

$$\begin{aligned}
 R_t(f) = E(f)H_T(f)H_R(f) & \left\{ H_A(f) \right. \\
 & \left. + H_{TL}(f)H_{RL}(f) \left[H_S^t(f) + H_{SC}(f) + H_C(f) \right] \right\} + N(f) \quad (5.1)
 \end{aligned}$$

where $H_S^t(f)$ is the system transfer function being solved for and $N(f)$ is the environment noise. A second measurement is done to find the background response (with the target absent) which is used to obtain $H_S^t(f)$. The background measurement is subtracted from the unknown target response. When the time between these mea-

surements is long, the subtraction process will worsen from small changes in the test environment. The formulated response for the background is

$$R_b(f) = E(f)H_T(f)H_R(f) \{H_A(f) + H_{TL}(f)H_{RL}(f)H_C(f)\} + N(f). \quad (5.2)$$

Subtracting the background response from the target response thus gives

$$R_{t-b}(f) = S(f) \left[H_S^t(f) + H_{SC}(f) \right], \quad (5.3)$$

where $S(f)$ is the system transfer function given by

$$S(f) = E(f)H_T(f)H_R(f)H_{TL}(f)H_{RL}(f). \quad (5.4)$$

With this system transfer function the unknown target response can be found. A theoretically known response is measured to determine $S(f)$. A conducting plate is chosen as the known target (calibrator) because its theoretical response is -1 [9]. The background-subtracted plate response is given as

$$R_{C-b}(f) = S(f) \left[H_S^C(f) + H_{SC}(f) \right] \quad (5.5)$$

where $H_S^C(f) = -1$ is the theoretical response of the plate. Absorbers have been placed around the targets in the reflectivity arch range to reduce the mutual interactions. Therefore, the mutual interaction term $H_{SC}(f)$ can be assumed to be negligible or can be eliminated using time gating. The system transfer function is then found to be

$$S(f) = \frac{R_{C-b}(f)}{H_S^C(f)}, \quad (5.6)$$

and the unknown target response is found using

$$H_S^t(f) = \frac{R_{t-b}(f)}{S(f)}. \quad (5.7)$$

Substituting (5.6) into (5.7) results in

$$H_S^t(f) = \frac{R_{t-b}(f)H_S^C(f)}{R_{C-b}(f)}. \quad (5.8)$$

To demonstrate the calibration process, the time-domain response of a background subtracted conducting plate is shown in Figure 5.8.

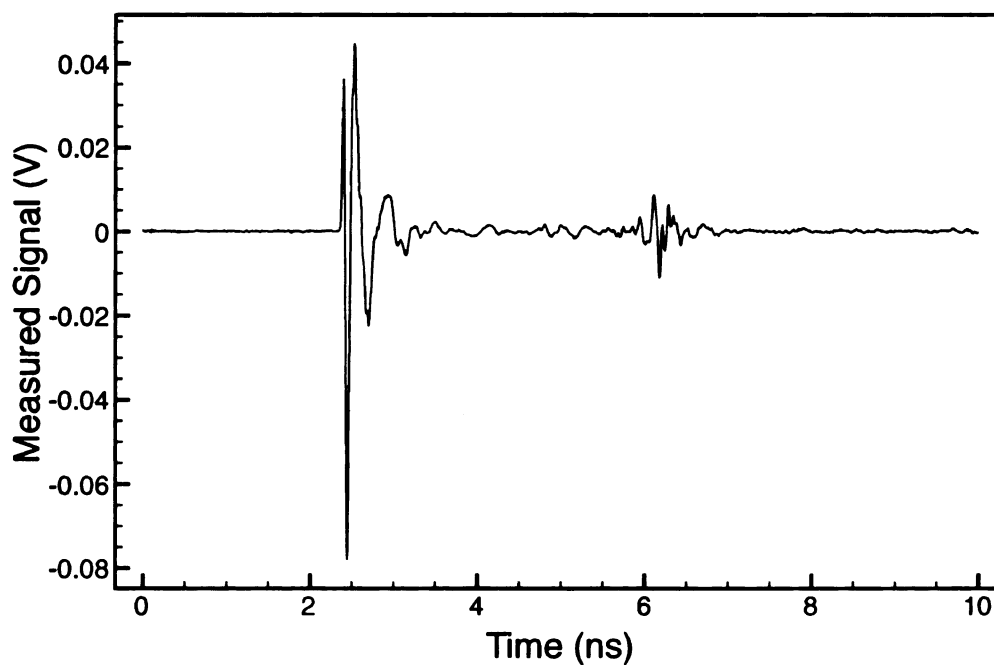


Figure 5.8: Raw measured waveform for a conducting plate.

First, this signal is transformed into the frequency domain using a Fourier transform and truncated between 2.0 – 18 GHz, which is the band specification of the antennas. This spectrum is then divided by the theoretical plate response of -1 , and the resulting system transfer function is shown in Figure 5.9.

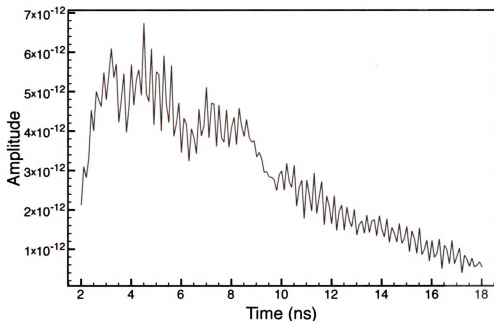


Figure 5.9: System transfer function.

With the system transfer function obtained, the target response is found by applying (5.7). A gaussian modulated cosine is used to window the function with a width of $\tau = 0.12ns$ and centered at 10 GHz. Then, to complete the calibration process the results are transformed back into the time domain.

5.3 Experiment Results

The image created using the experimental data is shown in Figure 5.10 . From this figure it can be seen that the barrier has an approximate width of .1 m and the conducting strip is located at about .6 m from the back of the barrier.

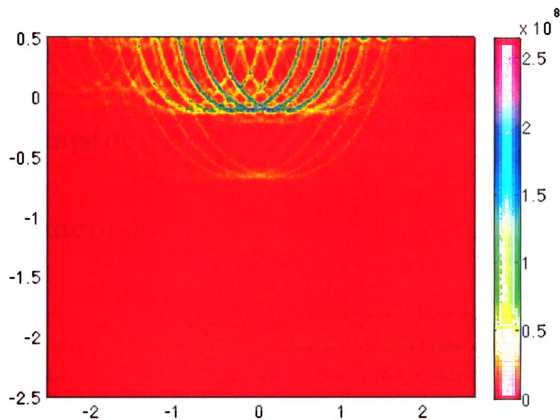


Figure 5.10: Image of barrier and strip created using time-domain response at responses measured at 21 different transmitter/receiver positions.

The image radius of this experimental image is 2.61 cm. Comparing this result to those simulated with the FORTRAN program shows a promising concentration of conducting strip intensities. This suggests that the time domain imaging system can provide accurate images of a target located behind a lossy barrier, validating the simulations results.

Chapter 6

Conclusion

In this thesis, a two-dimensional canonical problem is established that allows the affects of various radar parameters on an ultra-wide band short-pulse and a stepped frequency radar system to be studied. The canonical problem consists of a line source positioned above a lossy dielectric slab and a target located behind the slab. The interrogation cylindrical waves produced by the line source impinge on the barrier and interact with targets placed behind the barrier. The resulting scattered field is analyzed in the frequency domain at specific discrete frequencies. The simulated data acquired is similar to data resulting form a UWB stepped frequency radar system. A time-domain system is established by using an inverse Fourier transform to convert the data into the time domain.

Analyzing the performance of these two radar systems is achieved by comparing images which are constructed using a simple scattering-center technique. Factors such as pulse width, sampling rate, number of bits, and SNR are examined in the time domain to determine their affect on the quality of the image. Bandwidth, sampling rate, SNR, and number of bits are examined in the frequency domain. In addition, a laboratory time-domain radar system was constructed using instrumentation to allow a validation of the simulation results.

Tables 6.1 and 6.2 reveal the dependence of target image on various important parameters. These results can be summarized by providing a set of minimal requirements for producing a good image, and these can be useful for designing an actual radar system. It must be emphasized that these requirements are subjective, since they depend on the desired image quality, and are relative to the barrier and target parameters used in the simulation.

<u>Pulse Width</u>	<u>Sampling Rate</u>	<u>SNR</u>	<u>Digitization</u>
≤ 0.10 ns	≥ 5 Gs/s	≥ 15 dB	≥ 6 Bits

Table 6.1: Minimum system requirements for a time domain radar system.

<u>Bandwidth</u>	<u>Frequency Stepsize</u>	<u>SNR</u>	<u>Digitization</u>
≥ 36.75 %	≤ 40 MHz	≥ 40 dB	≥ 6 Bits

Table 6.2: Minimum system requirements for a frequency domain radar system.

In chapter 5, the theory was verified using experimental results. An actual transient pulse with a 2-18 GHz bandwidth was used for measurements to simulate a realistic time domain radar system. From the results of the measurements, it is confirmed that given certain radar parameters, a target can be imaged behind a lossy barrier.

6.1 Topics for further study

Possible follow-studies include the analysis of different targets behind a dielectric slab. An in-depth look at different shaped objects would be useful in designing a radar system with optimized system parameters. In addition to examining different objects, an increase in the number of targets located behind the barrier would provide

further insight into system performance. Next, a method for quantifying the signal-to-clutter ratio and the ghosting which results from the multiple reflections from the barrier and target could prove useful. Finally, with the time domain system it would be helpful to look at the affects of time-jitter, and to alter the number of transmitter/receiver positions, on the image radius.

Appendix A: Fortran Code for Scattered Electric Field

```
PROGRAM Electric_Field_Scattered

!*****
! For Dielectric Slab
! Scattering by a strip using MoM- TM
! Then Sending the wave back through slab      *
!*****
!
!DECLARING VARIABLES TYPES

IMPLICIT REAL*8 (A-H,O-Z)

PARAMETER (MATSIZE=512)

PARAMETER (LIMIT=4096,LENW=4*LIMIT,KEY=4)

PARAMETER (TEST=1.D-13)

COMPLEX*16 Amn(MATSIZE,MATSIZE) , Bm(MATSIZE) , DIAG(MATSIZE)

COMPLEX*16 J, K, X

INTEGER IPVT(MATSIZE) , IFLAG, NN, MM, M, N, I, II , AA

REAL*8 GAMMA, PI, MU, EPS0, EPSR, EPS, FREQ, W, K0, Y

REAL*8 OMEGA, A, B, RK, Z, H, T, SIG, ZS, Yobs, Zobs, YS

REAL*8 DELTA, YM, YN, ANS1, ANS2, ANS3, ANS4, ANS5, ANS6

REAL*8 ANS7, ANS8, Emag, Ephase, ANST1, ANST2, ANST5

REAL*8 ANST6, ANST8, ANST7, WORK(LENW) , FINTR
```

```

REAL*8 FINTI, FINT, AINTR1, AINTR2, AINTI1, AINTI2

INTEGER IWORK(LIMIT)

EXTERNAL FINTR, FINTI, FINT, AINTR1, AINTR2, AINTI1, AINTI2

COMPLEX*16 ZINT, Umm, Vmm, Ben, d1, d2, CURR, ESUM

REAL WALL, OBS-Y, OBS-Z, SOURCE-Y, SOURCE-Z, STRIP, WIDTH

REAL PARTIS, POINTS, ENDFREQ, FREQ-STEP

!COMMON TO ALL OF PROGRAM

COMMON /NAME1/YM, DELTA, M, N

COMMON /NAME2/K0, K, OMEGA, CURR, MU, PI, J

COMMON /NAME3/ Z, H, T, ZS, YS, Y

COMMON /NAME4/ ECURR, Yobs, Zobs

!DECLARING VARIABLES

PI=3.14159265358979323846D0

J = DCMPLEX(0.D0,1.D0)

MU = 4.D0*PI*1.D-7

EPS0 = 8.854D-12

W = .075D0

        WIDTH = W

T = .1524D0

        WALL = T

ZS = -.8D0

```

```

        STRIP = ZS

YS = 0.01D0

        SOURCE.Y = YS

Zobs = .6524d0

        OBS.Z = Zobs - T

Yobs = -0.00d0

        OBS.Y = Yobs

EPSR = 6.D0

EPS = EPS0*EPSR

SIG = .001D0

FREQ = 20.d6

OPEN(10,FILE='Electric_Field_Scattered_Job_11.DAT',STATUS='
        UNKNOWN')

OPEN(14,FILE='PARAMETERS.DAT',STATUS='UNKNOWN')

OPEN(13,FILE='Center_Current_big_strip.DAT',STATUS='UNKNOWN')

partis = 20.

DO I=1, 800

        Print *, Freq

                if (2*W*FREQ*20.d0/(3.D8) .LT. 10.d0) then

                        NN=20

                else

                        NN = 2*W*FREQ*20.d0/(3.D8)

                end if

```

DELTA = 2.D0*W/NN

Z = -.8d0

H = .6524d0

SOURCE.Z = H - T

YS = 0.01D0

OMEGA = 2.D0*PI*FREQ

K0 = OMEGA*SQRT(EPS0*MU)

X= DCMPLX(EPSR, -SIG/(OMEGA*EPS0))

K = K0*SQRT(X)

CURR = DCMPLX(1.D0, 0.D0)

ESUM = 0.D0

!DEFINING YM AND CREATING Bm MATRIX

DO M=1, NN

YM = -W + (M*1.D0-.5D0)*DELTA

Y = YM

CALL BENINT (FINTR, 0.d0, 10.d0*K0, ANS1
)

CALL BENINT (FINTI, 0.d0, 10.d0*K0, ANS2
)

Bm(M) = -2.D0*ANS1 - 2.D0*J*ANS2

!CREATING Amn MATRIX

DO N=M, NN

YN = -W + (N*1.D0-.5D0)*DELTA


```
CALL BENINT (AINTR1,0.D0,SQRT(K0),
             ANS3)
```

```
CALL BENINT (AINTI1,0.D0,SQRT(K0),
             ANS4)
```

```
CALL BENINT (AINTR2,0.d0,10.
             d0*k0,ANS5)
```

```
CALL BENINT (AINTI2,0.D0,10.
             d0*k0,ANS6)
```

```
D1 = 2.D0*ANS3+J*2.D0*ANS4
```

```
D2 = 2.D0*J*(ANS5+J*ANS6)
```

```
Vmn = D1 + D2
```

```
a = DELTA/2.D0
```

```
b = (M-N)*DELTA
```

```
rk = K0
```

```
call Intc1 (A,B,RK,ZINT)
```

```
Umn = -((MU*OMEGA)/PI)*ZINT
```

```
Amn(M,N) = Umn + Vmn
```

```
END DO
```

```
END DO
```

```
DO M = 2, NN
```

```
DO N = 1, M-1
```

```
Amn(M,N) = Amn(N,M)
```

```
END DO
```

```
END DO
```

!SOLVING FOR THE CURRENTS

CALL DCOMP (512 ,NN, Amn, IPVT, DIAG)

CALL SOLVEC (512 ,NN, Amn, IPVT, Bm)

!Sending current produced waves back through slab

Y = Yobs

H = T - ZS

Z = T - Zobs

DO M=1, NN

YM = -W + (M*1.D0-.5D0)*DELTA

YS = YM

CURR = DELTA*Bm(M)

CALL BENINT (FINTR, 0.d0, 10.
d0*K0, ANS7)

CALL BENINT (FINTI, 0.d0, 10.
d0*K0, ANS8)

ESUM = ESUM + 2.D0*(ANS7 + J*ANS8)

END DO

o1 = FREQ/1.d9

o2 = DREAL(ESUM)

o3 = DIMAG(ESUM)

WRITE (10,999) o1,o2,o3

999 format (3(1x,e12.5))

PRINT *, 'CENTER CURRENT=', ABS(BM(1.d0+NN/2.d0))

```

        write(13,999) o1, DREAL(BM(1.d0+NN/2.d0)), DIMAG(BM
            (1.d0+NN/2.d0))

        FREQ = FREQ + 20.D6

    END DO

    POINTS = I

    END_FREQ = FREQ

    FREQ_STEP = FREQ/POINTS

    CLOSE (10)

    close (13)

    WRITE(14,*) 'SLAB THICKNESS = ', WALL

    WRITE(14,*) 'POSITION OF OBSERVATION POINT ALONG Y = ', OBS_Y

    WRITE(14,*) 'DISTANCE OF OBSERVATION POINT FROM WALL = ',
        OBS_Z

    WRITE(14,*) 'POSITION OF SOURCE ALONG Y = ', SOURCE_Y

    WRITE(14,*) 'DISTANCE OF SOURCE POINT FROM WALL = ', SOURCE_Z

    WRITE(14,*) 'DISTANCE OF STRIP FROM WALL = ', STRIP

    WRITE(14,*) 'WIDTH OF STRIP = ', WIDTH

    WRITE(14,*) 'NUMBER OF PARTITION POINTS = ', PARTIS

    WRITE(14,*) 'NUMBER OF POINTS = ', POINTS

    WRITE(14,*) 'STOP FREQUENCY = ', END_FREQ

    WRITE(14,*) 'STEP FREQUENCY = ', FREQ_STEP

    close (14)

    END

```

!!

REAL*8 FUNCTION Fintr (KY)

REAL*8 KY

EXTERNAL Fint

COMPLEX*16 Fint

Fintr = DREAL (Fint(KY))

RETURN

END

!!

REAL*8 FUNCTION Finti (KY)

REAL*8 KY

EXTERNAL Fint

COMPLEX*16 Fint

Finti = DIMAG (Fint(KY))

RETURN

END

!!

REAL*8 FUNCTION Aintr1(KY)

REAL*8 KY

EXTERNAL Aint1

COMPLEX*16 Aint1

Aintr1 = DREAL (Aint1(KY))

RETURN

END

!!

REAL*8 FUNCTION Ainti1(KY)

REAL*8 KY

EXTERNAL Aint1

COMPLEX*16 Aint1

Ainti1 = DIMAG (Aint1(KY))

RETURN

END

!!

REAL*8 FUNCTION Aintr2(KY)

REAL*8 KY

EXTERNAL Aint2

COMPLEX*16 Aint2

Aintr2 = DREAL (Aint2(KY))

RETURN

END

!!

REAL*8 FUNCTION Ainti2(KY)

```

REAL*8 KY

EXTERNAL Aint2

COMPLEX*16 Aint2

      Ainti2 = DIMAG (Aint2(KY))

RETURN

END

!!!!!!!!!!!!!!!!!!!!!!!!!!!!!!!!!!!!!!!!!!!!!!!!!!!!!!!!!!!!!!!!!!!!!!!!!!!!

COMPLEX*16 FUNCTION Fint (KY)

COMPLEX*16 P, Q, J, K, CURR

integer M, N

REAL*8 MU, PI, Z, H, T, ZS, Y, OMEGA, KY, K0, YM, DELTA, YS

COMMON /NAME1/YM, DELTA, M, N

COMMON /NAME2/K0, K, OMEGA, CURR, MU, PI, J

COMMON /NAME3/ Z, H, T, ZS, YS, Y

      IF (K0*K0 .LT. KY*KY) THEN

          P = -1.D0*J*SQRT(KY*KY-K0*K0)

      ELSE

          P = SQRT(K0*K0-KY*KY)

      END IF

      Q = SQRT(K*K-KY*KY)

      IF (DREAL (Q) .LT. 0.D0) THEN

          Q = -1.D0*Q

```

ENDIF

$$F_{int} = -(J * \text{OMEGA} * \text{CURR} * \text{MU} / (2. \text{d}0 * \text{PI})) * (\text{COS}(\text{KY} * (\text{Y} - \text{YS}))) * \text{EXP}(J * \text{P} * (\text{Z} - \text{H} + \text{T})) / ((- \text{P} * \text{P} / \text{Q}) * \text{SIN}(\text{Q} * \text{T}) - \text{Q} * \text{SIN}(\text{Q} * \text{T}) + 2. \text{D}0 * \text{J} * \text{P} * \text{COS}(\text{Q} * \text{T}))$$

RETURN

END

!!

COMPLEX*16 FUNCTION Aint1 (TAU)

COMPLEX*16 P, Q, J, K, R, CURR

integer M, N

REAL*8 MU, PI, Z, H, T, ZS, OMEGA, KY, K0, TAU, DELTA, RAT,
YM, Y, YS

COMMON /NAME1/YM, DELTA, M, N

COMMON /NAME2/K0, K, OMEGA, CURR, MU, PI, J

COMMON /NAME3/ Z, H, T, ZS, YS, Y

KY=K0-TAU*TAU

IF (K0*K0 .LT. KY*KY) THEN

P = -J*SQRT(KY*KY-K0*K0)

ELSE

P = SQRT(K0*K0-KY*KY)

END IF

Q = SQRT(K*K-KY*KY)

IF (DREAL (Q) .LT. 0.D0) THEN

Q = -1.D0*Q

ENDIF

IF (KY .EQ. 0.D0) THEN

RAT = 1.D0

ELSE

RAT = SIN(KY*DELTA/2.D0)/(KY*DELTA/2.D0)

END IF

R = ((-P*P/Q)*SIN(Q*T)+Q*SIN(Q*T))/((-P*P/Q)*
SIN(Q*T)-Q*SIN(Q*T)+2.d0*J*P*COS(Q*T))

Aint1 = -(MU*OMEGA*DELTA/(2.D0*PI))*(COS(KY*(
M-N)*DELTA)*RAT*R*EXP(J*2.D0*P*ZS))/(SQRT(
K0+KY))

RETURN

END

!!

COMPLEX*16 FUNCTION Aint2 (TAU)

COMPLEX*16 P, Q, J, K, R, CURR

integer M, N

REAL*8 MU, PI, Z, H, T, ZS, OMEGA, KY, K0, TAU, DELTA, RAT,
YM, Y, YS

COMMON /NAME1/YM, DELTA, M, N

COMMON /NAME2/K0, K, OMEGA, CURR, MU, PI, J

COMMON /NAME3/ Z, H, T, ZS, YS, Y

KY=TAU*TAU+K0

IF (K0*K0 .LT. KY*KY) THEN


```

        P = -J*SQRT(KY*KY-K0*K0)

ELSE

        P = SQRT(K0*K0-KY*KY)

END IF

Q = SQRT(K*K-KY*KY)

IF (DREAL (Q) .LT. 0.D0) THEN

        Q = -1.D0*Q

ENDIF

IF (KY .EQ. 0.D0) THEN

        RAT = 1.D0

ELSE

        RAT = SIN (KY*DELTA/2.D0)/(KY*DELTA/2.D0)

END IF

R = (Q*Q-P*P)/(-(P*P+Q*Q) - 2.D0*P*Q*((1.D0+EXP
(-J*2.D0*Q*T))/(1.D0-EXP(-J*2.D0*Q*T))))

Aint2 = -(MU*OMEGA*DELTA/(2.D0*PI))*(COS(KY*(
M-N)*DELTA)*RAT*R*EXP(J*2.D0*P*ZS))/(SQRT(
KY+K0))

RETURN

END

!!!!!!!!!!!!!!!!!!!!!!!!!!!!!!!!!!!!!!!!!!!!!!!!!!!!!!!!!!!!!!!!!!!!!!!!!!!!

subroutine benint (Func,DOWN,UP,ans)

implicit real*8 (a-h,o-z)

```

```

parameter (limit=4096,lenw=4*limit ,key=5)

parameter(pi=3.14159265358979323846d0)

parameter (test=1.d-18)

real*8 work(lenw), K0

integer iwork(limit)

external Func

      call DQAG (Func, down, up, 1.d-200, test, KEY, res0,
                ABSERR, NEVAL, IER, LIMIT, LENW, LAST, IWORK, WORK
                )

      ans = RES0

return

end

!!!!!!!!!!!!!!!!!!!!!!!!!!!!!!!!!!!!!!!!!!!!!!!!!!!!!!!!!!!!!!!!!!!!!!!!!!!!

subroutine Intc1 (a,b1,rk ,zint)

! computes integral from 0 to infinity of the function
! sin(ax)cos(bx)/(x*sqrt(rk^2-x^2))

implicit real*8 (a-h,o-z)

parameter (limit=4096,lenw=4*limit ,key=4)

parameter(pi=3.14159265358979323846d0)

parameter (test=1.d-8)

real*8 work(lenw)

real*8 IA,IB,IC,I1 ,I2

complex*16 zint

```

```

integer iwork(limit)

external Fint1 ,Fintg ,Fintgb

common /IC1/ aa ,bb

common /IC2/ beta

common /IC3/ rrk

! upfact determines upper limit of integration
!   for I2

upfact = 6.d0

b = abs(b1)

beta = rk

aa = a

bb = b

rrk = rk

! compute IB

arg1 = (a+b)*beta

f1 = exp(-arg1)*Ei(arg1) + exp(arg1)*E1(arg1)

arg2 = abs(a-b)*beta

f2 = exp(-arg2)*Ei(arg2) + exp(arg2)*E1(arg2)

if ((a-b) .lt. 0.d0) f2 = -f2

IB = (1.d0/(4.d0*beta))*(f1+f2)

! compute IC

down = 0.d0

up = rk

```

```

call DQAG (Fint1, down, up, 1.d-200, test, KEY, res0, ABSERR,
          NEVAL, IER, LIMIT, LENW, LAST, IWORK, WORK)

IC = res0

! compute IA

IA = IB-IC

! compute I1

down = 0.d0

up = sqrt(rk)

call DQAG (Fintg, down, up, 1.d-200, test, KEY, res0, ABSERR,
          NEVAL, IER, LIMIT, LENW, LAST, IWORK, WORK)

I1 = 2.d0*res0

! compute I2

down = 0.d0

up = upfact*rk

call DQAG (Fintgb, down, up, 1.d-200, test, KEY, res0, ABSERR
          , NEVAL, IER, LIMIT, LENW, LAST, IWORK, WORK)

I2 = 2.d0*res0 + IA

zint = dcplx(I1, I2)

return

end

real*8 function Fint1(x)

implicit real*8 (a-h,o-z)

common /IC1/ a,b

```

```

common /IC2/ beta

Fint1 = sin(a*x)*cos(b*x)/(beta*beta+x*x)

return

end

real*8 function Fintg(t)
implicit real*8 (a-h,o-z)
common /IC1/ a,b
common /IC3/ rk
x = rk-t*t
if (x .ne. 0.d0) then
    Fintg = sin(a*x)*cos(b*x)/(x*sqrt(rk+x))
else
    Fintg = a/sqrt(rk)
end if
return
end

real*8 function Fintgb(t)
implicit real*8 (a-h,o-z)
common /IC1/ a,b
common /IC2/ beta
common /IC3/ rk
x = rk+t*t

```

```
Fintgb = sin(a*x)*cos(b*x)*(1.d0/x - (sqrt(x*x-rk*rk)/(x*x+
  beta*beta)))/sqrt(x+rk)
```

```
return
```

```
end
```

```
Real*8 function E1(X)
```

```
!
! =====
! Purpose: Compute exponential integral E1(x)
! Input : x  — Argument of E1(x)
! Output: E1 — E1(x) ( x > 0 )
! =====
```

```
IMPLICIT DOUBLE PRECISION (A-H,O-Z)
```

```
IF (X.EQ.0.0) THEN
```

```
    E1=1.0D+300
```

```
ELSE IF (X.LE.1.0) THEN
```

```
    E1=-DLOG(X) + (((1.07857D-3*X-9.76004D-3)*X+5.519968D
      -2)*X-0.24991055D0)*X+0.99999193D0)*X-0.57721566D0
```

```
ELSE
```

```
    ES1=(((X+8.5733287401D0)*X+18.059016973D0)*X
      +8.6347608925D0)*X+0.2677737343D0
```

```
    ES2=(((X+9.5733223454D0)*X+25.6329561486D0)*X
      +21.0996530827D0)*X+3.9584969228D0
```

```
    E1=DEXP(-X)/X*ES1/ES2
```

```
ENDIF
```

```
RETURN
```

```
END
```

```
real*8 function EI(X)
```

```

!
!
! Purpose: Compute exponential integral Ei(x)
! Input : x  — Argument of Ei(x)
! Output: EI — Ei(x) ( x > 0 )
!
!

```

```

IMPLICIT DOUBLE PRECISION (A-H,O-Z)

```

```

IF (X.EQ.0.0) THEN

```

```

    EI=-1.0D+300

```

```

ELSE IF (X.LE.40.0) THEN

```

```

    EI=1.0D0

```

```

    R=1.0D0

```

```

    DO 15 K=1,100

```

```

        R=R*K*X/(K+1.0D0)**2

```

```

        EI=EI+R

```

```

        IF (DABS(R/EI) .LE. 1.0D-15) GO TO 20

```

```

15      CONTINUE

```

```

20      GA=0.5772156649015328D0

```

```

        EI=GA+DLOG(X)+X*EI

```

```

ELSE

```

```

    EI=1.0D0

```

```

    R=1.0D0

```

```

    DO 25 K=1,20

```

```

        R=R*K/X

```

```

25      EI=EI+R

```

EI=DEXP(X)/X*EI

ENDIF

RETURN

END

!*****

SUBROUTINE DCOMPC (nbig ,N,A,IPVT,DIAG)

! DECOMPOSES MATRIX A TO TRIANGULAR FORM

!

! **** COMPLEX VERSION ****

!

! FROM: LINEAR ALGEBRA BY GILBERT STRANG

INTEGER N,IPVT(nbig)

INTEGER NM1,I , J,K,KP1,M

COMPLEX*16 A(nbig ,nbig) ,DIAG(nbig)

COMPLEX*16 P,T

!

IPVT(N) = 1

IF (N .EQ. 1) GO TO 70

NM1 = N-1

DO 60 K=1,NM1

KP1 = K+1

! FIND PIVOT P

M = K

DO 10 I=KP1,N

10 IF (ABS(A(I,K)) .GT. ABS(A(M,K))) M=I

IPVT(K) = M


```

IF (M .NE. K) IPVT(N) = -IPVT(N)

P      = A(M,K)

A(M,K) = A(K,K)

A(K,K) = P

DIAG(K) = P

IF (P .EQ. 0.0) GO TO 60

! COMPUTE MULTIPLIERS

20    DO 30 I=KP1,N

30    A(I ,K) = -A(I ,K)/P

! INTERCHANGE ROWS AND COLUMNS

DO 50 J=KP1,N

T      = A(M, J)

A(M, J) = A(K, J)

A(K, J) = T

IF (T .EQ. 0.0) GO TO 50

DO 40 I=KP1,N

A(I , J) = A(I , J) + A(I ,K)*T

40    CONTINUE

50    CONTINUE

60    CONTINUE

70    DIAG(N) = A(N,N)*IPVT(N)

RETURN

```

END

!*****

SUBROUTINE SOLVEC (nbig ,N,A,IPVT ,B)

! SOLVES MATRIX EQN AX=B WITH A DECOMPOSED BY DCOMP

INTEGER N,IPVT(nbig)

INTEGER NM1,K,KB,KP1,KM1,M, I

COMPLEX*16 A(nbig ,nbig) ,B(nbig)

COMPLEX*16 S

! FORWARD ELIMINATION

IF (N .EQ. 1) GO TO 30

NM1 = N-1

DO 10 K=1,NM1

KP1 = K+1

M = IPVT(K)

S = B(M)

B(M) = B(K)

B(K) = S

DO 10 I=KP1,N

10 B(I) = B(I) + A(I,K)*S

! BACK SUBSTITUTION

DO 20 KB=1,NM1

KM1 = N-KB

K = KM1+1

B(K) = B(K)/A(K,K)

S = -B(K)

DO 20 I=1,KM1

20 B(I) = B(I) + A(I,K)*S

30 B(1) = B(1)/A(1,1)

RETURN

END

Appendix B: Fortran Code for Incident Electric Field

```
PROGRAM Electric_Field_Incident

!*****
! For Dielectric Slab
! Scattering by a strip using MoM- TM
! Then Sending the wave back through slab      *
!*****

!DECLARING VARIABLES TYPES

IMPLICIT REAL*8 (A-H,O-Z)

PARAMETER (MATSIZE=512)

PARAMETER (LIMIT=4096,LENW=4*LIMIT,KEY=4)

PARAMETER (TEST=1.D-13)

COMPLEX*16 Amn(MATSIZE,MATSIZE) , Bm(MATSIZE) , DIAG(MATSIZE)

COMPLEX*16 J, K, X

INTEGER IPVT(MATSIZE) , IFLAG, NN, MM, M, N, I, II , AA

REAL*8 GAMMA, PI, MU, EPS0, EPSR, EPS, FREQ, W, K0, OMEGA

REAL*8 A, B, RK, Z, H, T, SIG, ZS, Yobs, Zobs, YS, Y

REAL*8 DELTA, YM, YN, ANS1, ANS2, ANS3, ANS4, ANS5, ANS6

REAL*8 ANS7, ANS8, ANS9, ANS10, ANS11, ANS12, Emag, Ephase
```

```
REAL*8 WORK(LENW) , IINTR1, IINTI1 , IINT1 , IINTR2, IINTI2 ,  
IINT2
```

```
INTEGER IWORK(LIMIT)
```

```
EXTERNAL IINTR1, IINTI1 , IINT1 , IINTR2, IINTI2 , IINT2
```

```
COMPLEX*16 ZINT, Umn, Vmn, Ben, d1, d2, CURR, ESUM, TOTAL,  
TOTAL1, TOTAL2
```

```
real*4 o1 ,o2 ,o3
```

```
!COMMON TO ALL OF PROGRAM
```

```
COMMON /NAME1/YM, DELTA, M, N
```

```
COMMON /NAME2/K0, K, OMEGA, CURR, MU, PI, J
```

```
COMMON /NAME3/ Z, H, T, ZS, YS, Y
```

```
COMMON /NAME4/ ECURR, Yobs, Zobs
```

```
!DECLARING VARIABLES
```

```
PI=3.14159265358979323846D0
```

```
J = DCMPLX(0.D0,1.D0)
```

```
MU = 4.D0*PI*1.D-7
```

```
EPS0 = 8.854D-12
```

```
W = .075D0
```

```
ZS = -.8D0
```

```
YS = 0.01D0
```

```
T = .1524D0
```

```
Zobs = .6524d0
```

```
Yobs = -0.00d0
```

```

EPSR = 6.D0

EPS = EPS0*EPSR

SIG = .001D0

FREQ = 20.d6

OPEN(10,FILE='Electric_Field_Incident_Job_11.DAT',STATUS='
  UNKNOWN')

DO I=1, 800

  Print *, Freq

      if (2*W*FREQ*40.d0/(3.D8) .LT. 10.d0) then

          NN=20

      else

          NN = 2*W*FREQ*20.d0/(3.D8)

      end if

  DELTA = 2.D0*W/NN

  Z = Zobs

  H = .6524d0

  YS = 0.01D0

  Y = Yobs

  OMEGA = 2.D0*PI*FREQ

  K0 = OMEGA*SQRT(EPS0*MU)

  X= DCMLPX(EPSR,-SIG/(OMEGA*EPS0))

  K = K0*SQRT(X)

  CURR = DCMLPX(1.D0,0.D0)

```

```

total = 0.D0

CALL BENINT (IINTR1,0.D0,SQRT(K0),ANS11)

CALL BENINT (IINTI1,0.D0,SQRT(K0),ANS12)

      CALL BENINT (IINTR2,0.d0,10.D0*K0,ANS9)

      CALL BENINT (IINTI2,0.D0,10.D0*K0,ANS10)

            TOTAL1 = 2.D0*(ANS11+J*ANS12)

            TOTAL2 = 2.D0*J*(ANS9+J*ANS10)

            TOTAL = TOTAL1 + TOTAL2

o1 = FREQ/1.d9

o2 = DREAL(TOTAL)

o3 = DIMAG(TOTAL)

      WRITE (10,999) o1,o2,o3
999          format (3(1x,e12.5))

      FREQ = FREQ + 20.D6

END DO

CLOSE (10)

close (11)

END

!!!!!!!!!!!!!!!!!!!!!!!!!!!!!!!!!!!!!!!!!!!!!!!!!!!!!!!!!!!!!!!!!!!!!!!!!!!!

REAL*8 FUNCTION Iintr1 (KY)

REAL*8 KY

EXTERNAL Iint1

```

```
COMPLEX*16 Iint1
```

```
Iintr1 = DREAL (Iint1(KY))
```

```
RETURN
```

```
END
```

```
!!!!!!!!!!!!!!!!!!!!!!!!!!!!!!!!!!!!!!!!!!!!!!!!!!!!!!!!!!!!!!!!!!!!!!!!!!!!!!!!!!!!!!!!!!!!!!!!!!!!!!!!!!!!!!!!!!!!!!!!
```

```
REAL*8 FUNCTION Iint1 (KY)
```

```
REAL*8 KY
```

```
EXTERNAL Iint1
```

```
COMPLEX*16 Iint1
```

```
Iint1 = DIMAG (Iint1(KY))
```

```
RETURN
```

```
END
```

```
!!!!!!!!!!!!!!!!!!!!!!!!!!!!!!!!!!!!!!!!!!!!!!!!!!!!!!!!!!!!!!!!!!!!!!!!!!!!!!!!!!!!!!!!!!!!!!!!!!!!!!!!!!!!!!!!!!!!!!!!
```

```
REAL*8 FUNCTION Iintr2 (KY)
```

```
REAL*8 KY
```

```
EXTERNAL Iint2
```

```
COMPLEX*16 Iint2
```

```
Iintr2 = DREAL (Iint2(KY))
```

```
RETURN
```

```
END
```

```
!!!!!!!!!!!!!!!!!!!!!!!!!!!!!!!!!!!!!!!!!!!!!!!!!!!!!!!!!!!!!!!!!!!!!!!!!!!!!!!!!!!!!!!!!!!!!!!!!!!!!!!!!!!!!!!!!!!!!!!!
```



```

REAL*8 FUNCTION Iinti2 (KY)

REAL*8 KY

EXTERNAL Iint2

COMPLEX*16 Iint2

      Iinti2 = DIMAG (Iint2(KY))

RETURN

END

!!!!!!!!!!!!!!!!!!!!!!!!!!!!!!!!!!!!!!!!!!!!!!!!!!!!!!!!!!!!!!!!!!!!!!!!!!!!

COMPLEX*16 FUNCTION Iint1 (TAU)

COMPLEX*16 P, Q, J, K, CURR, R

integer M, N

REAL*8 MU, PI, Z, H, T, ZS, Y, OMEGA, TAU, KY, K0, YM, DELTA,
      YS

COMMON /NAME1/YM, DELTA, M, N

COMMON /NAME2/K0, K, OMEGA, CURR, MU, PI, J

COMMON /NAME3/ Z, H, T, ZS, YS, Y

KY=K0-TAU*TAU

      IF (K0*K0 .LT. KY*KY) THEN

          P = -1.D0*J*SQRT(KY*KY-K0*K0)

      ELSE

          P = SQRT(K0*K0-KY*KY)

      END IF

      Q = SQRT(K*K-KY*KY)

```

```

IF (DREAL (Q) .LT. 0.D0) THEN

      Q = -1.D0*Q

ENDIF

R = (Q*Q-P*P)/((-P*P+Q*Q)-2.D0*P*Q*((1.D0+EXP
(-J*2.D0*Q*T))/(1.D0-EXP(-J*2.D0*Q*T))))

Iint1 = -(CURR*MU*OMEGA/(2.D0*PI))*COS(KY*(Y-
YS))*(EXP(-J*P*ABS(Z-H))+R*EXP(-J*P*(Z+H
-2.D0*T)))/(SQRT(K0+KY))

RETURN

END

!!!!!!!!!!!!!!!!!!!!!!!!!!!!!!!!!!!!!!!!!!!!!!!!!!!!!!!!!!!!!!!!!!!!

COMPLEX*16 FUNCTION Iint2 (TAU)

COMPLEX*16 P, Q, J, K, CURR, R

integer M, N

REAL*8 MU, PI, Z, H, T, ZS, Y, OMEGA, TAU, KY, K0, YM, DELTA,
YS

COMMON /NAME1/YM, DELTA, M, N

COMMON /NAME2/K0, K, OMEGA, CURR, MU, PI, J

COMMON /NAME3/ Z, H, T, ZS, YS, Y

KY=TAU*TAU+K0

      IF (K0*K0 .LT. KY*KY) THEN
            P = -1.D0*J*SQRT(KY*KY-K0*K0)
      ELSE
            P = SQRT(K0*K0-KY*KY)
      END IF

      Q = SQRT(K*K-KY*KY)

```

```
IF (DREAL (Q) .LT. 0.D0) THEN
```

```
    Q = -1.D0*Q
```

```
ENDIF
```

```
    R = (Q*Q-P*P)/(-(P*P+Q*Q)-2.D0*P*Q  
      *((1.D0+EXP(-J*2.D0*Q*T))/(1.D0-  
      EXP(-J*2.D0*Q*T))))
```

```
    Iint2 = -(CURR*MU*OMEGA/(2.D0*PI))*  
      COS(KY*(Y-YS))*(EXP(-J*P*ABS(Z-H))  
      +R*EXP(-J*P*(Z+H-2.D0*T)))/(SQRT(  
      K0+KY))
```

```
RETURN
```

```
END
```

```
!!!!!!!!!!!!!!!!!!!!!!!!!!!!!!!!!!!!!!!!!!!!!!!!!!!!!!!!!!!!!!!!!!!!!!!!!!!!
```

```
subroutine benint (Func,DOWN,UP,ans)
```

```
implicit real*8 (a-h,o-z)
```

```
parameter (limit=4096,lenw=4*limit ,key=5)
```

```
parameter(pi=3.14159265358979323846d0)
```

```
parameter (test=1.d-15)
```

```
real*8 work(lenw), K0
```

```
integer iwork(limit)
```

```
external Func
```

```
    call DQAG (Func, down, up, 1.d-200, test, KEY, res0,  
      ABSERR, NEVAL, IER, LIMIT, LENW, LAST, IWORK, WORK  
      )
```

```
    ans = RES0
```

return

end

Appendix C: Matlab Imaging Code

```
clear all

%%%%%%%%%%%%%%%%%%%%%%%%%%%%%%%%%%%%%%%%%%%%%%%%%%%%%%%%%%%%%%%%%%%%%%%%%%%%%%
%Loading Files into Matrix %
%%%%%%%%%%%%%%%%%%%%%%%%%%%%%%%%%%%%%%%%%%%%%%%%%%%%%%%%%%%%%%%%%%%%%%%%%%%%%%

%Tau from wavecalc

    tau = 0.12;

%Engery

    Eng = 1/tau;

load Electric_Field_Scattered_Job_01.dat;
load Electric_Field_Scattered_Job_02.dat;
load Electric_Field_Scattered_Job_03.dat;
load Electric_Field_Scattered_Job_04.dat;
load Electric_Field_Scattered_Job_05.dat;
load Electric_Field_Scattered_Job_06.dat;
load Electric_Field_Scattered_Job_07.dat;
load Electric_Field_Scattered_Job_08.dat;
load Electric_Field_Scattered_Job_09.dat;
load Electric_Field_Scattered_Job_10.dat;
load Electric_Field_Scattered_Job_11.dat;
```

```
load Electric_Field_Scattered_Job_12.dat;
load Electric_Field_Scattered_Job_13.dat;
load Electric_Field_Scattered_Job_14.dat;
load Electric_Field_Scattered_Job_15.dat;
load Electric_Field_Scattered_Job_16.dat;
load Electric_Field_Scattered_Job_17.dat;
load Electric_Field_Scattered_Job_18.dat;
load Electric_Field_Scattered_Job_19.dat;
load Electric_Field_Scattered_Job_20.dat;
load Electric_Field_Scattered_Job_21.dat;
load Electric_Field_Incident_Job_allT.dat;

ES(:,1) = Electric_Field_Scattered_Job_01(:,2)/Eng;
ES(:,2) = Electric_Field_Scattered_Job_02(:,2)/Eng;
ES(:,3) = Electric_Field_Scattered_Job_03(:,2)/Eng;
ES(:,4) = Electric_Field_Scattered_Job_04(:,2)/Eng;
ES(:,5) = Electric_Field_Scattered_Job_05(:,2)/Eng;
ES(:,6) = Electric_Field_Scattered_Job_06(:,2)/Eng;
ES(:,7) = Electric_Field_Scattered_Job_07(:,2)/Eng;
ES(:,8) = Electric_Field_Scattered_Job_08(:,2)/Eng;
ES(:,9) = Electric_Field_Scattered_Job_09(:,2)/Eng;
ES(:,10) = Electric_Field_Scattered_Job_10(:,2)/Eng;
ES(:,11) = Electric_Field_Scattered_Job_11(:,2)/Eng;
```

ES(:,12) = Electric_Field_Scattered_Job_12(:,2)/Eng;
ES(:,13) = Electric_Field_Scattered_Job_13(:,2)/Eng;
ES(:,14) = Electric_Field_Scattered_Job_14(:,2)/Eng;
ES(:,15) = Electric_Field_Scattered_Job_15(:,2)/Eng;
ES(:,16) = Electric_Field_Scattered_Job_16(:,2)/Eng;
ES(:,17) = Electric_Field_Scattered_Job_17(:,2)/Eng;
ES(:,18) = Electric_Field_Scattered_Job_18(:,2)/Eng;
ES(:,19) = Electric_Field_Scattered_Job_19(:,2)/Eng;
ES(:,20) = Electric_Field_Scattered_Job_20(:,2)/Eng;
ES(:,21) = Electric_Field_Scattered_Job_21(:,2)/Eng;
EI(:,1) = Electric_Field_Incident_Job_allT(:,2)/Eng;
EI(:,2) = Electric_Field_Incident_Job_allT(:,2)/Eng;
EI(:,3) = Electric_Field_Incident_Job_allT(:,2)/Eng;
EI(:,4) = Electric_Field_Incident_Job_allT(:,2)/Eng;
EI(:,5) = Electric_Field_Incident_Job_allT(:,2)/Eng;
EI(:,6) = Electric_Field_Incident_Job_allT(:,2)/Eng;
EI(:,7) = Electric_Field_Incident_Job_allT(:,2)/Eng;
EI(:,8) = Electric_Field_Incident_Job_allT(:,2)/Eng;
EI(:,9) = Electric_Field_Incident_Job_allT(:,2)/Eng;
EI(:,10) = Electric_Field_Incident_Job_allT(:,2)/Eng;
EI(:,11) = Electric_Field_Incident_Job_allT(:,2)/Eng;
EI(:,12) = Electric_Field_Incident_Job_allT(:,2)/Eng;
EI(:,13) = Electric_Field_Incident_Job_allT(:,2)/Eng;

```

EI(:,14) = Electric_Field_Incident_Job_allT(:,2)/Eng;
EI(:,15) = Electric_Field_Incident_Job_allT(:,2)/Eng;
EI(:,16) = Electric_Field_Incident_Job_allT(:,2)/Eng;
EI(:,17) = Electric_Field_Incident_Job_allT(:,2)/Eng;
EI(:,18) = Electric_Field_Incident_Job_allT(:,2)/Eng;
EI(:,19) = Electric_Field_Incident_Job_allT(:,2)/Eng;
EI(:,20) = Electric_Field_Incident_Job_allT(:,2)/Eng;
EI(:,21) = Electric_Field_Incident_Job_allT(:,2)/Eng;

%%%%%%%%%%%%%%%%%%%%%%%%%%%%%%%%%%%%%%%%%%%%%%%%%%%%%%%%%%%%%%%%%%%%%%%%%%%%%%
%Initialize
%%%%%%%%%%%%%%%%%%%%%%%%%%%%%%%%%%%%%%%%%%%%%%%%%%%%%%%%%%%%%%%%%%%%%%%%%%%%%%
%speed of light

    c=3E8;

%speed of wave in wall

    v=c/sqrt(6);

%Time shift

    shift = 1E-9;

%End of file

    last=32768;

%Time step from E-file

    delta_t=1.52E-12;

%Number of points at end of file to shift

    Ns = shift/delta_t;

    Ns = round(Ns);

```



```

%position in the z-direction of the transmitters
    z=.65;

%determines the gride size
    delta=.01;

%Front side of wall in z-direction
    wall_ZA=.1524;

%Back side of wall in z-direction
    wall_ZB=0;

%size of display window in z-direction
    zp_low=-2;
    zp_high=.5;

%size of display window in y-direction
    yp_low=-2.6;
    yp_high=2.6;

%Number of gride Points in z and y direction
    zp_delta=((zp_high-zp_low)/delta)+1;
    yp_delta=((yp_high-yp_low)/delta)+1;

%First position of transmitter from E-field file
    y_start=-2.5;

%Incrementing size of transmitter position from E-Field file
    y_delta=.25;

%number of transmitter positions

```

```

    num_files=21;

%position somewhere between wall and object

    threshold_dist=-.5;

%Position of sources to front of wall for thresholding

    threshold_dist2=.2;

%incrementing size of the threshold

    threshold_delta_z=((threshold_dist-zp_low)/delta)+1;

%number of gride points for the threshold positions

    threshold_delta_z2=((threshold_dist2-zp_low)/delta)+1;

%Fixing Es and Ei files to include shift

for m=1:1:num_files;

    for i=1:1:Ns;

        ES0(i,m) = ES(last-Ns+i,m);

    end

    for i=Ns+1:1:last;

        ES0(i,m)=ES(i-Ns,m);

    end

    for i=1:1:Ns;

        EI0(i,m) = EI(last-Ns+i,m);

    end

    for i=Ns+1:1:last;

        EI0(i,m)=EI(i-Ns,m);

    end
end

```

```

end

%initializing value

for n=1:1:zp_delta*yp_delta;

    value(n)=0;

end

%%%%%%%%%%%%%%%%%%%%%%%%%%%%%%%%%%%%%%%%%%%%%%%%%%%%%%%%%%%%%%%%%%%%%%%%%%%%%%
%Scattered                                                                    %
%%%%%%%%%%%%%%%%%%%%%%%%%%%%%%%%%%%%%%%%%%%%%%%%%%%%%%%%%%%%%%%%%%%%%%%%%%%%%%

y=y_start;

n=1;

for m=1:1:num_files;

    for zp=zp_low:delta:zp_high;

        for yp=yp_low:delta:yp_high;

            dist=sqrt((y-yp)^2+(z-zp)^2);

            if (zp < wall_ZB)

                theta=asin((abs(zp-z))/dist);

                dist_A=abs(wall_ZA-z)/sin(theta);

                dist_B=abs(wall_ZB-wall_ZA)/sin(theta);

                dist_C=abs(zp-wall_ZB)/sin(theta);

                time = (2*dist_A/c)+(2*dist_B/v)+(2*dist_C/c)+
                    shift;

            elseif (zp < wall_ZA)

                theta=asin((abs(zp-z))/dist);

                dist_A=abs(wall_ZA-z)/sin(theta);

```

```

        dist_B=abs(zp-wall_ZA)/sin(theta);
        time = (2*dist_A/c)+(2*dist_B/v)+shift;
    else
        time=2*dist/c+shift;
    end
    p=time/delta_t;
    post=round(p)+2;
    post_low=round(p-delta/c)+2;
    post_high=round(p+delta/c)+2;
    if (post_low >= last)
        A=ES0(last,m);
    else
        A=[ES0(post_high,m),ES0(post_low,m),ES0(post,m)];
    end
    E=max(abs(A));
    value(n)=value(n)+abs(E);
    n=n+1;
end
end
y=y+y_delta;
n=1;
end

```

```

%%%%%%%%%%%%%%%%%%%%%%%%%%%%%%%%%%%%%%%%%%%%%%%%%%%%%%%%%%%%%%%%%%%%%%%%%%%%%%
%Incident                                                                    %
%%%%%%%%%%%%%%%%%%%%%%%%%%%%%%%%%%%%%%%%%%%%%%%%%%%%%%%%%%%%%%%%%%%%%%%%%%%%%%

y=y_start;

n=1;

for m=1:1:num_files;

    for zp=zp_low:delta:zp_high;

        for yp=yp_low:delta:yp_high;

            dist=sqrt((y-yp)^2+(z-zp)^2);

            if (zp < wall_ZB)

                theta=asin((abs(zp-z))/dist);

                dist_A=abs(wall_ZA-z)/sin(theta);

                dist_B=abs(wall_ZB-wall_ZA)/sin(theta);

                dist_C=abs(zp-wall_ZB)/sin(theta);

                time = (2*dist_A/c)+(2*dist_B/v)+(2*dist_C/c)+
                    shift;

            elseif (zp < wall_ZA)

                theta=asin((abs(zp-z))/dist);

                dist_A=abs(wall_ZA-z)/sin(theta);

                dist_B=abs(zp-wall_ZA)/sin(theta);

                time = (2*dist_A/c)+(2*dist_B/v)+shift;

            else

                time=2*dist/c+shift;

            end

        end

    end

end

```

```

    p=time/delta_t;

    post=round(p)+2;

    post_low=round(p-delta/c)+2;

    post_high=round(p+delta/c)+2;

    if (post_low >= last)

        A=EI0(last,m);

    else
        A=[EI0(post_high,m),EI0(post_low,m),EI0(post,m)];
    end

    E=max(abs(A));

    value(n)=value(n)+abs(E);

    n=n+1;

    end

end

y=y+y_delta;

n=1;

end

%%%%%%%%%%%%%%%%%%%%%%%%%%%%%%%%%%%%%%%%%%%%%%%%%%%%%%%%%%%%%%%%%%%%%%%%%%
%Quantification %
%%%%%%%%%%%%%%%%%%%%%%%%%%%%%%%%%%%%%%%%%%%%%%%%%%%%%%%%%%%%%%%%%%%%%%%%%%

Nback=10;

fac=1.5;

Int=0;

box_z_end=-.65;

```

```

box_y_start = -.23;

box_z_start = -.95;

box_y_end = .23;

box_area = (abs(box_y_end - box_y_start)) * (abs(box_z_end -
    box_z_start));

grid_z_start = (abs(zp_low - box_z_start) / delta) + 1;

grid_z_end = (abs(zp_low - box_z_end) / delta) + 1;

grid_y_start = (abs(yp_low - box_y_start) / delta) + 1;

grid_y_end = (abs(yp_low - box_y_end) / delta) + 1;

n = zp_delta * (grid_z_start - 1) + grid_y_start;

i = 1;

for z = grid_z_start : 1 : grid_z_end
    for y = grid_y_start : 1 : grid_y_end
        Box1(i) = value((z - 1) * yp_delta + y);

        zi(i) = floor((i - 1) / (grid_y_end - grid_y_start + 1)) + 1;

        yi(i) = i - (zi(i) - 1) * (grid_y_end - grid_y_start + 1);

        i = i + 1;
    end
end

Box2 = sort(Box1, 'descend');

iend = i - 1;

sum_y = 0;

sum_z = 0;

```

```

sum_f=0;

sum_R=0;

sum_A=0;

for i=1:iend;

    sum_y=sum_y+Box1(i)*yi(i);

    sum_z=sum_z+Box1(i)*zi(i);

    sum_f=sum_f+Box1(i);

    y_0=sum_y/sum_f;

    z_0=sum_z/sum_f;

end

thresh=0.5*Box2(1);

for i=1:iend;

    Di(i)=sqrt((yi(i)-y_0)*(yi(i)-y_0)+(zi(i)-z_0)*(zi(i)-z_0));

    Ai(i)=abs((yi(i)-y_0)*(zi(i)-z_0));

    if (Box1(i)>thresh)

        sum_R=sum_R+Box1(i)*Di(i);

        sum_A=sum_A+Box1(i)*Ai(i);

    end

end

Radius=sum_R/sum_f;

Area=sum_A/sum_f;

v=sqrt(var(Box1));

```



```

fract1=0.99;

num1=0;

for i=1:iend
    if (Box2(i) > fract1*mean(Box2))
        num1=num1+1;
    end
end

Box_roth=0;

for i=1:10
    Box_roth=Box_roth+Box2(i);
end

Rothwell=Box_roth/10

num1/iend

figure(2)

plot(Box2);

%%%%%%%%%%%%%%%%%%%%%%%%%%%%%%%%%%%%%%%%%%%%%%%%%%%%%%%%%%%%%%%%%%%%%%%%%%%%%%
%Thresholding                                                                    %
%%%%%%%%%%%%%%%%%%%%%%%%%%%%%%%%%%%%%%%%%%%%%%%%%%%%%%%%%%%%%%%%%%%%%%%%%%%%%%

%for the stip

for n=1:1:threshold_delta_z*yp_delta;

    threshold=0;

    if (value(n) < threshold)

        value(n)=0;

    end
end

```

```

end

%for the slab

for n=round(threshold_delta_z*yp_delta)+1:1:round(
    threshold_delta_z2*yp_delta);

    threshold=0;

    if (value(n) < threshold)

        value(n)=0;

    end

end

%for above slab

for n=round(threshold_delta_z2*yp_delta)+1:1:yp_delta*
    zp_delta

    threshold=0;

    if (value(n) < threshold)

        value(n)=0;

    end

end

end

%%%%%%%%%%%%%%%%%%%%%%%%%%%%%%%%%%%%%%%%%%%%%%%%%%%%%%%%%%%%%%%%%%%%%%%%%%%%%%
%Graphing                                                                    %
%%%%%%%%%%%%%%%%%%%%%%%%%%%%%%%%%%%%%%%%%%%%%%%%%%%%%%%%%%%%%%%%%%%%%%%%%%%%%%

for z=1:1:zp_delta;

    for y=1:1:yp_delta;

        F(z,y) = value(y+yp_delta*(z-1));

    end

end

```

```
end

[y,z] = meshgrid(1:1:yp_delta,1:1:zp_delta);

figure(1)

pcolor(yp_low+delta*(y-1),zp_low+delta*(z-1),F(:,,:));

colorbar;

shading interp;

colormap hsv;
```

Bibliography

- [1] Ferris Jr., D. D. and N. C. Curris, *A survey of current technologies for through-the-wall surveillance (TWS)*, proceeding SPIE, Vol. 3577, 6272, Jan. 1999.
- [2] Ahmad, F. and M. Amin, *A non coherent approach to through-the-wall radar imaging*, Proceedings of the 8th International Symposium on Signal Processing and Its Applications, Vol. 2, 28 31, 2005.
- [3] Taylor, J. D., *Introduction to Ultra-wideband Radar Systems*, CRC Press, 1995.
- [4] Chen, F. C. and W. C. Chew, *Time-domain ultra-wideband microwave imaging radar system*, Journal of Electromagnetic Waves and Applications, Vol. 17, No. 2, 313331, 2003.
- [5] Maaref, N., Millot, P., and X. Ferrière, *Electromagnetic Imaging Method Based on Time Reversal Processing Applied to Through-the-Wall Target Localization*, Progress In Electromagnetics Research M, Vol. 1, 5967, 2008.
- [6] Soumekh, M., *Synthetic Aperture Radar Signal Processing*, John Wiley and sons, Inc., New York, NY, 1999.
- [7] Chan, Y. K. and V. C Koo, *An introduction to synthetic aperture radar (SAR)*, Progress In Electromagnetics Research B, Vol. 2, 2760, 2008.
- [8] Charvat, G.L., *A Low-Power Radar Imaging System*, Ph.D. Thesis, Michigan State University, 2007.
- [9] D.K. Cheng, *Field and Wave Electromagnetics* Addison-Wesley Publishing Company, Inc, 1992.
- [10] E.J. Rothwell and M.J. Cloud, *Electromagnetics, Second Edition*, CRC Press, Boca Raton, Florida, 2009.
- [11] R. Piessens, et. al., *Quadpack: a subroutine package for automatic integration*, Springer-Verlag, Berlin, 1983.
- [12] W. Press, B. Flannery, S. Teukolsky, and W. Vetterling, *Numerical Recipes, Cambridge University Press*, Cambridge, 1986.

- [13] N. Kinayman and M.I. Aksun, *Comparative study of acceleration techniques for integrals and series in electromagnetic problems*, Antennas and Propagation Society International Symposium, 1995.
- [14] J Davis, Y Huang, SG Millard, and JH Bungey, *Determination of dielectric properties of insitu concrete at radar frequencies*, International Symposium (NDT-CE 2003), Non-Destructive Testing in Civil Engineering, 2003.
- [15] <http://netlib.org/quadpack/index.html>.
- [16] A. Kizilay, *A perturbation method for transient multipath analysis of electromagnetic scattering from targets above periodic surfaces*, Ph.D. Thesis, Michigan State University, 2000.
- [17] J. E. Ross, III, *Application of transient electromagnetic fields to radar target discrimination*, Ph.D. Thesis, Michigan State University, 1992.